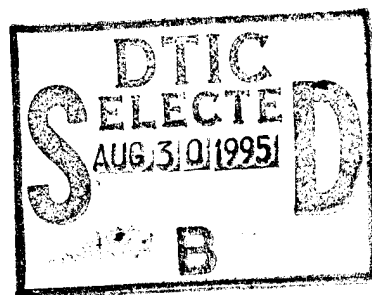


NPS-ME-95-001

NAVAL POSTGRADUATE SCHOOL MONTEREY, CALIFORNIA



**MULTIMATERIAL EULERIAN
AND COUPLED LAGRANGIAN-EULERIAN
FINITE ELEMENT ANALYSIS OF
UNDERWATER SHOCK PROBLEMS**

by

LCDR J.E. Chisum, USN
Professor Y.S. Shin, Principal Investigator

October 1, 1994 - August 1, 1995

Approved for public release; distribution is unlimited.

Prepared for: Defense Nuclear Agency
Alexandria, VA 20311

Naval Postgraduate School
Monterey, CA 93943

19950829 039

DTIC QUALITY INSPECTED 8


**Naval Postgraduate School
Monterey, California**

Rear Admiral T.A. Mercer
Superintendent

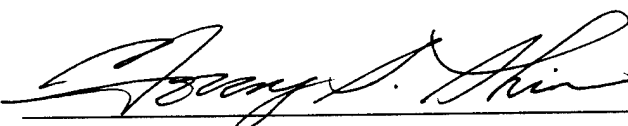
R. Elster
Provost

This report was prepared for and fully funded by both the Defense Nuclear Agency, Alexandria, VA 20311 and the Naval Postgraduate School, Monterey, CA 93943.

This report was prepared by:



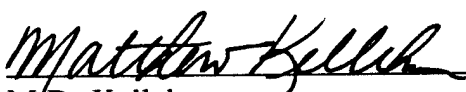
J.E. Chisum
LCDR, USN



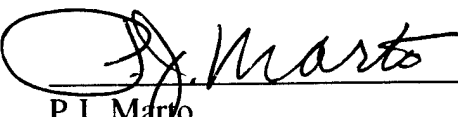
Y.S. Shin
Professor of Mechanical Engineering

Reviewed by:

Released by:



M.D. Kelleher
Chairman
Dept. of Mechanical Eng.



P.J. Maro
Dean of Research

REPORT DOCUMENTATION PAGE			Form Approved OMB No. 0704-0188	
Public reporting burden for this collection of information is estimated to average 1 hour per response, including the time for reviewing instruction, searching existing data sources, gathering and maintaining the data needed, and completing and reviewing the collection of information. Send comments regarding this burden estimate or any other aspect of this collection of information, including suggestions for reducing this burden, to Washington Headquarters Services, Directorate for Information Operations and Reports, 1215 Jefferson Davis Highway, Suite 1204, Arlington, VA 22202-4302, and to the Office of Management and Budget, Paperwork Reduction Project (0704-0188) Washington DC 20503.				
1. AGENCY USE ONLY (Leave blank)		2. REPORT DATE August 1, 1995		3. REPORT TYPE AND DATES COVERED Progress Report from October 1, 1994 to August 1, 1995
4. TITLE AND SUBTITLE Multimaterial Eulerian and Coupled Lagrangian-Eulerian Finite Element Analysis of Underwater Shock Problems			5. FUNDING NUMBERS	
6. AUTHOR(S) J.E. Chisum and Y.S. Shin				
7. PERFORMING ORGANIZATION NAME(S) AND ADDRESS(ES) Naval Postgraduate School Monterey CA 93943-5000			8. PERFORMING ORGANIZATION REPORT NUMBER NPS-ME-95-001	
9. SPONSORING/MONITORING AGENCY NAME(S) AND ADDRESS(ES) Defense Nuclear Agency Alexandria, VA 20311			10. SPONSORING/MONITORING AGENCY REPORT NUMBER	
11. SUPPLEMENTARY NOTES The views expressed in this report are those of the authors and do not reflect the official policy or position of the Department of Defense or the U.S. Government.				
12a. DISTRIBUTION/AVAILABILITY STATEMENT Approved for public release; distribution is unlimited.			12b. DISTRIBUTION CODE	
13. ABSTRACT (maximum 200 words) The application of coupled Lagrangian-Eulerian and multimaterial Eulerian finite element analysis to problems of interest in underwater shock research was investigated. Analyses were conducted for the classical problems of a spherical shell and an infinite cylinder loaded by a plane acoustic step wave, and for the expansion and collapse of explosion generated gas bubbles in deep water. Results for the elastic response of a spherical shell and an infinite cylinder were found to be in excellent agreement with the analytical solution results, and results for the expansion and collapse of a deep explosion generated gas bubble in the absence of nearby boundary surfaces were found to agree well with experimental results. Several analyses were conducted with explosive charges detonated at various distances from a rigid wall; results from these analyses were in qualitative agreement with what is known about this case, and serve to characterize the behavior of the resulting bubble in terms of the distance to the wall.				
14. SUBJECT TERMS Coupled Analysis, Multimaterial Analysis, Bubble, Lagrangian, Eulerian, Shock			15. NUMBER OF PAGES 132	
			16. PRICE CODE	
17. SECURITY CLASSIFI- CATION OF REPORT Unclassified	18. SECURITY CLASSIFI- CATION OF THIS PAGE Unclassified	19. SECURITY CLASSIFI- CATION OF ABSTRACT Unclassified	20. LIMITATION OF ABSTRACT UL	

ABSTRACT

The application of coupled Lagrangian-Eulerian and multimaterial Eulerian finite element analysis to problems of interest in underwater shock research was investigated. Analyses were conducted for the classical problems of a spherical shell and an infinite cylinder loaded by a plane acoustic step wave, and for the expansion and collapse of explosion generated gas bubbles in deep water. Results for the elastic response of a spherical shell and an infinite cylinder were found to be in excellent agreement with the analytical solution results, and results for the expansion and collapse of a deep explosion generated gas bubble in the absence of nearby boundary surfaces were found to agree well with experimental results. Several analyses were conducted with explosive charges detonated at various distances from a rigid wall; results from these analyses were in qualitative agreement with what is known about this case, and serve to characterize the behavior of the resulting bubble in terms of the distance to the wall.

Accession For	
NTIS GRA&I	<input checked="" type="checkbox"/>
DTIC TAB	<input type="checkbox"/>
Unannounced	<input type="checkbox"/>
Justification	
By	
Distribution/Avail	
Availability Codes	
Dist	Avail and/or Special
A-1	

TABLE OF CONTENTS

I. INTRODUCTION	1
II. NUMERICAL COMPUTER CODE	3
III. COUPLED ANALYSIS OF CLASSICAL PROBLEMS	7
A. SPHERICAL SHELL/PLANE STEP WAVE	7
B. INFINITE CYLINDER/PLANE STEP WAVE	13
IV. MULTIMATERIAL EULERIAN ANALYSIS OF BUBBLES	21
A. DEEP SPHERICAL BUBBLE	21
B. BUBBLES NEAR RIGID BOUNDARIES	29
V. CONCLUSION	53
APPENDIX A: SPHERICAL SHELL/PLANE STEP WAVE INPUT	55
APPENDIX B: INFINITE CYLINDER/PLANE STEP WAVE INPUT ...	59
APPENDIX C: A POLYNOMIAL STATE EQUATION FOR SEAWATER	61
APPENDIX D: DEEP SPHERICAL BUBBLE INPUT	65
APPENDIX E: BUBBLES NEAR RIGID BOUNDARIES-SHAPES	69
APPENDIX F: BUBBLES NEAR RIGID BOUNDARIES-INPUT	97
LIST OF REFERENCES	115
INITIAL DISTRIBUTION LIST	118

LIST OF FIGURES

Figure 1.	Eulerian Element Control Volume Changes Due to Presence of Coupling Surface With "General Coupling" Method	4
Figure 2.	Blending of Eulerian Elements to Prevent Small Element From Controlling Stable Time Step Size When Using "General Coupling" Method	5
Figure 3.	Comparison Between Eulerian Mesh With "General Coupling" and "ALE Coupling" Methods	6
Figure 4.	Spherical Shell/Plane Step Wave Problem Geometry	8
Figure 5.	Steel Shell Elements, Dummy Elements, and Resulting Closed Coupling Surface for Spherical Shell/Plane Step Wave Problem	9
Figure 6.	Fluid Mesh for Spherical Shell/Plane Step Wave Problem . . .	11
Figure 7.	Size and Position of Spherical Shell Relative to Eulerian Fluid for Spherical Shell/Plane Step Wave Problem	12
Figure 8.	Non-Dimensional Incident Pressure Independent Radial Velocity Versus Non-Dimensional Time for Spherical Shell/Plane Step Wave Problem	14
Figure 9.	Infinite Cylinder/Plane Step Wave Problem Geometry	15
Figure 10.	Structural and Dummy Elements in Finite Element Model for Infinite Cylinder/Plane Step Wave Problem	16
Figure 11.	Fluid Mesh for Infinite Cylinder/Plane Step Wave Problem . .	18
Figure 12.	Size and Position of Infinite Cylinder Relative to Eulerian Fluid for Infinite Cylinder/Plane Step Wave Problem	19

Figure 13.	Non-Dimensional Incident Pressure Independent Radial Velocity Versus Non-Dimensional Time for Infinite Cylinder/Plane Step Wave Problem	20
Figure 14.	Deep Spherical Bubble Problem Geometry	22
Figure 15.	Finite Element Model for Deep Spherical Bubble Problem . .	26
Figure 16.	Radius Versus Time Behavior for Deep Spherical Bubble Problem (0.2990 kg TNT Charge at 178.6 m Depth in Seawater)	27
Figure 17.	Geometry of Bubble Near Rigid Boundary Problems	30
Figure 18.	Overall Model Geometry for Quarter Symmetry Axisymmetric Finite Element Model For Free-Field Analysis	32
Figure 19.	Quarter Symmetry Axisymmetric Finite Element Model for Free-Field Analysis	33
Figure 20.	Close Up View of Finite Element Model in Area Near Charge for Free-Field Analysis	35
Figure 21.	Finite Element Model Geometry for Rigid Wall at 1.000 Free-Field Radii From Center of Charge	36
Figure 22.	Close Up View of Finite Element Model in Area Near Charge for Rigid Wall at 1.000 Free-Field Radii From Center of Charge	37
Figure 23.	Finite Element Model Geometry for Rigid Wall at 4.015 Free-Field Radii From Center of Charge	39
Figure 24.	Finite Element Model for Rigid Wall at 4.015 Free-Field Radii From Center of Charge	40
Figure 25.	Close up View of Finite Element Model in Area Near Charge for Rigid Wall at 4.015 Free-Field Radii From Center of Charge	41

Figure 26.	Equivalent Spherical Radius vs Time for Explosion Gas Bubbles Near a Rigid Wall	43
Figure 27.	Non-Dimensional First Oscillation Period vs (Non-Dimensional Standoff Distance From Rigid Wall) ⁻¹	44
Figure 28.	Displacement of Center of Mass vs Time for Explosion Gas Bubbles Near a Rigid Wall	46
Figure 29.	Maximum and Minimum Equivalent Spherical Radii Versus (Non-Dimensional Standoff Distance From Rigid Wall) ⁻¹ . . .	50
Figure 30.	Displacement of Bubble Center of Mass at First Minimum and Peak Bubble Velocity Versus (Non-Dimensional Standoff Distance) ⁻¹	51
Figure 31.	Bubble Shape for Rigid Wall at $h^*=4.015$ at Time $t=0.50T$. .	69
Figure 32.	Bubble Shape for Rigid Wall at $h^*=4.015$ at Time $t=0.80T$. .	70
Figure 33.	Bubble Shape for Rigid Wall at $h^*=4.015$ at Time $t=0.90T$. .	71
Figure 34.	Bubble Shape for Rigid Wall at $h^*=4.015$ at Time $t=0.95T$. .	72
Figure 35.	Bubble Shape for Rigid Wall at $h^*=4.015$ at Time $t=0.98T$. .	73
Figure 36.	Bubble Shape for Rigid Wall at $h^*=4.015$ at Time $t=0.99T$. .	74
Figure 37.	Bubble Shape for Rigid Wall at $h^*=4.015$ at Time $t=1.00T$. .	75
Figure 38.	Bubble Shape for Rigid Wall at $h^*=2.008$ at Time $t=0.50T$. .	76
Figure 39.	Bubble Shape for Rigid Wall at $h^*=2.008$ at Time $t=0.80T$. .	77
Figure 40.	Bubble Shape for Rigid Wall at $h^*=2.008$ at Time $t=0.90T$. .	78
Figure 41.	Bubble Shape for Rigid Wall at $h^*=2.008$ at Time $t=0.95T$. .	79
Figure 42.	Bubble Shape for Rigid Wall at $h^*=2.008$ at Time $t=0.98T$. .	80
Figure 43.	Bubble Shape for Rigid Wall at $h^*=2.008$ at Time $t=0.99T$. .	81
Figure 44.	Bubble Shape for Rigid Wall at $h^*=2.008$ at Time $t=1.00T$. .	82
Figure 45.	Bubble Shape for Rigid Wall at $h^*=1.374$ at Time $t=0.50T$. .	83
Figure 46.	Bubble Shape for Rigid Wall at $h^*=1.374$ at Time $t=0.80T$. .	84

Figure 47.	Bubble Shape for Rigid Wall at $h^*=1.374$ at Time $t=0.90T$. .	85
Figure 48.	Bubble Shape for Rigid Wall at $h^*=1.374$ at Time $t=0.95T$. .	86
Figure 49.	Bubble Shape for Rigid Wall at $h^*=1.374$ at Time $t=0.98T$. .	87
Figure 50.	Bubble Shape for Rigid Wall at $h^*=1.374$ at Time $t=0.99T$. .	88
Figure 51.	Bubble Shape for Rigid Wall at $h^*=1.374$ at Time $t=1.00T$. .	89
Figure 52.	Bubble Shape for Rigid Wall at $h^*=1.000$ at Time $t=0.50T$. .	90
Figure 53.	Bubble Shape for Rigid Wall at $h^*=1.000$ at Time $t=0.80T$. .	91
Figure 54.	Bubble Shape for Rigid Wall at $h^*=1.000$ at Time $t=0.90T$. .	92
Figure 55.	Bubble Shape for Rigid Wall at $h^*=1.000$ at Time $t=0.95T$. .	93
Figure 56.	Bubble Shape for Rigid Wall at $h^*=1.000$ at Time $t=0.98T$. .	94
Figure 57.	Bubble Shape for Rigid Wall at $h^*=1.000$ at Time $t=0.99T$. .	95
Figure 58.	Bubble Shape for Rigid Wall at $h^*=1.000$ at Time $t=1.00T$. .	96

I. INTRODUCTION

This report describes work ongoing at the Naval Postgraduate School to apply coupled Lagrangian-Eulerian and multimaterial Eulerian finite element analysis techniques to problems in underwater shock research. Previous underwater shock research at the Naval Postgraduate School has concentrated on experimentation, e.g. by Jones and Shin [Ref. 1], and doubly asymptotic approximation boundary element techniques, sometimes combined with experimentation, e.g. by Fox et. al [Ref. 2], Nelson et. al. [Ref. 3], Kwon et. al [Ref. 4], and Chisum [Ref. 5].

However, for certain types of problems doubly asymptotic approximation boundary element techniques have not been advanced to the point that they can provide useful results. This is true in particular for problems involving the oscillation of gas bubbles generated by underwater explosions. This area is of considerable interest, as the pressure pulsations produced by such bubbles can under certain circumstances produce significant whipping of nearby marine or submarine structures.

In addition, there are certain practical constraints on the ability to conduct experimentation to determine structural responses. Full scale experimentation is extremely expensive, and certain physical phenomena related to explosion gas bubbles cannot be scaled in a practical experimental setup.

In light of these factors, and taking into consideration the ongoing advances in computer capabilities and the recent availability of advanced finite element programs which can efficiently calculate the fluid-structure interaction between Eulerian and Lagrangian materials and are capable of dealing with several different Eulerian materials in the same problem, a more basic approach might allow

solution of heretofore unsolvable problems. In this approach, each of the materials in an underwater shock problem are modeled in the most advantageous way for that class of material; fluid media and explosives using Eulerian elements, and structural materials using Lagrangian elements.

One advantage of this approach is that there are few approximations involved; the resulting solution can essentially be made as accurate as the discretization allowed by the available computational resources and the certainty with which the properties of the materials involved are known will permit.

This approach also overcomes the problems involved with modeling all of the material in a problem with Lagrangian elements, which in an underwater shock problem quickly become so distorted that the stable time step size approaches zero and the time to compute a solution out to near steady state approaches infinity. Nor is the approach of modeling all of the material in an underwater shock problem using Eulerian materials generally practical, as this approach requires that an extremely large number of Eulerian elements be used in order to accurately capture the response of structural materials in the problem, which is usually the primary item of interest.

By using a finite element code which contains both Lagrangian and Eulerian processors and a method for computing the fluid-structure interaction at the interface between Lagrangian and Eulerian materials, the advantages of both types of analysis are realized and the shortcomings associated with attempting to use one or the other alone are eliminated. This is the approach we have chosen to pursue. Initial results from this approach have been very promising [Ref. 6].

II. NUMERICAL COMPUTER CODE

The finite element program used for the results described in this report is MSC/DYTRAN [Ref. 7], a three dimensional finite element program available from the MacNeal-Schwendler Corporation. This program was developed by combining and extending two other computer programs, MSC/DYNA [Ref. 8] and MSC/PISCES [Ref. 9]. Both of these programs have a proven record for the analysis areas for which they were developed.

Like MSC/DYNA, MSC/DYTRAN is capable of handling non-linear, large strain structural response problems. MSC/DYTRAN is also capable of solving problems involving Lagrangian-Lagrangian two surface (contact-impact) and single surface (folding) problems. A complete constitutive model can be defined in terms of an equation of state, a shear model, a yield model, a failure model, and a spall model.

Multimaterial Eulerian processors in MSC/DYTRAN allow for up to 9 different eulerian materials to be present in a given problem. In addition, two different methods are available to provide for calculation of the fluid-structure interaction between Lagrangian and Eulerian materials.

In the "General Coupling" method, the Lagrangian and Eulerian meshes are geometrically independent, and interact via a coupling surface attached to the Lagrangian structure. This method requires that the coupling surface form a closed, simply connected volume, on one side (inside or outside) of which the Eulerian elements are "void" (contain no material). The deformable coupling surface "cuts across" Eulerian elements, changing their control volume and surface areas. This is illustrated in Figure 1, for two dimensional Eulerian elements. To prevent the

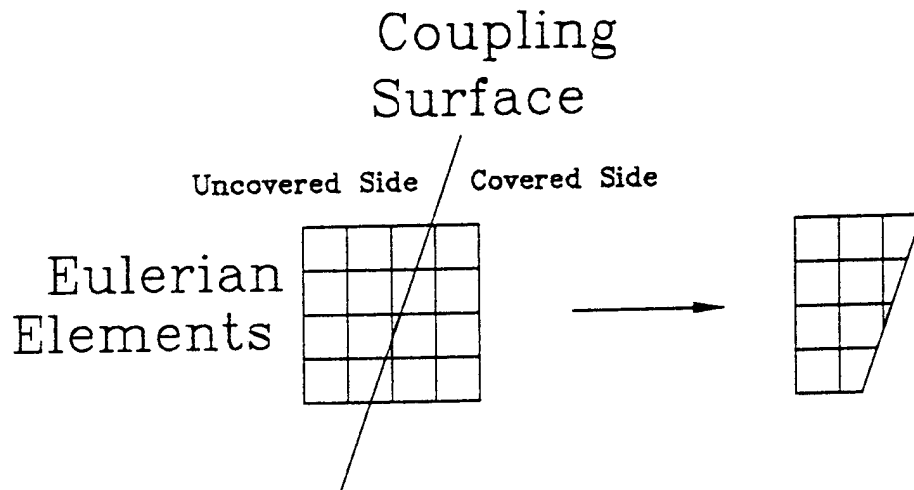


Figure 1. Eulerian Element Control Volume Changes Due to Presence of Coupling Surface With "General Coupling" Method

stable time step size from being controlled by very small Eulerian control volumes formed by the coupling surface, elements for which the ratio between the "covered" (void) volume fraction and the initial volume is less than a user modifiable "blend" parameter are combined with adjacent elements to form larger elements; this is illustrated in Figure 2.

The other method provided by MSC/DYTRAN for coupling of Lagrangian and Eulerian materials is "Arbitrary Lagrange-Euler" (ALE) coupling. In this method, the fluid and structural mesh geometries are not independent. Instead, the interface surface between the Lagrangian and Eulerian elements is actually composed of the union of the faces of these elements. As this interface is deformed during deformation of the Lagrangian structure, Eulerian grid points which are attached to this also move. To keep the geometry of the Eulerian mesh relatively "nice", other Eulerian grid points away from the coupling surface can be allowed to move, e.g. towards the center of their nearest neighbors. Note that in

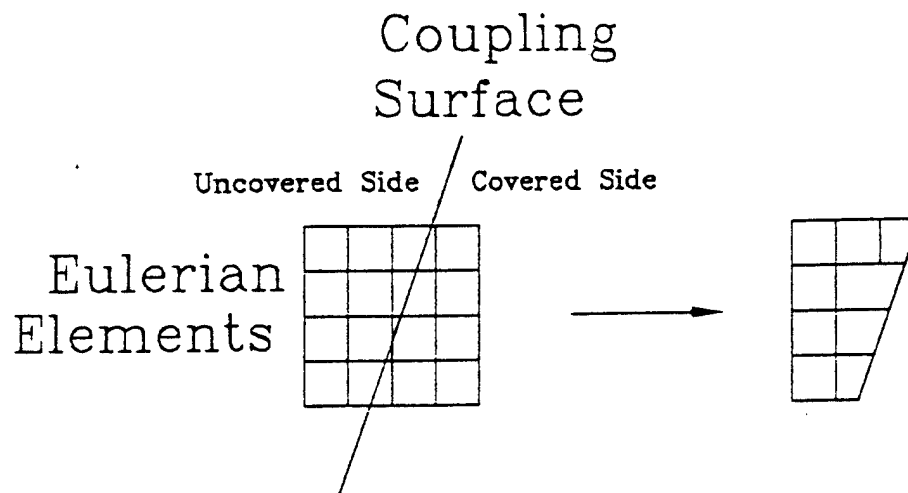


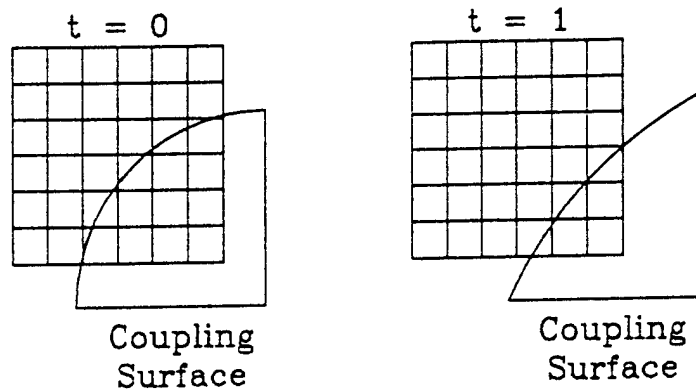
Figure 2. Blending of Eulerian Elements to Prevent Small Element From Controlling Stable Time Step Size When Using "General Coupling" Method

this method, the Eulerian mesh is not stationary. However, the motion of the Eulerian mesh is purely geometrical; the velocity of material through this mesh is independent of the motion of the mesh.

Figure 3 illustrates the difference between these two fluid-structure coupling methods, in two dimensions.

General Coupling

(Eulerian mesh doesn't change)



ALE Coupling

(Eulerian mesh deforms with structure)

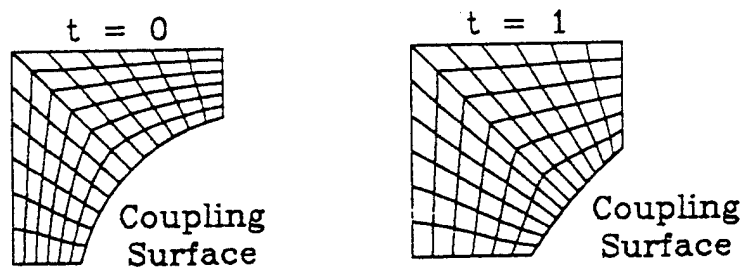


Figure 3. Comparison Between Eulerian Mesh With "General Coupling" and "ALE Coupling" Methods

III. COUPLED ANALYSIS OF CLASSICAL PROBLEMS

In order to examine the performance of using coupled Lagrangian-Eulerian finite element analysis for underwater shock problems, two classical problems for which analytical solution data is available were analyzed. These analyses examined the elastic response of a spherical shell and an infinite cylinder to loading from a plane step wave propagating through an acoustic media.

Huang has solved these problems analytically, using a direct inverse Laplace transform of a finite number of terms of the infinite series expansion of the equations for the respective shells [Refs. 10 and 11]. For our finite element analyses, the same material properties, parameters, and non-dimensionalization procedures used by Huang in his analyses were used.

A. SPHERICAL SHELL/PLANE STEP WAVE

Figure 4 shows the geometry of the spherical shell/plane step wave problem. The material properties and parameters used for this problem were:

Shell Material:	Steel
Young's Modulus for Steel:	30×10^6 psi
Poisson's Ratio for Steel:	0.3
Density of Steel:	486 lbm/ft ³
Shell Thickness to Radius Ratio:	0.02
Fluid:	Water
Water Density:	62.4 lbm/ft ³
Water Acoustic Wave Speed:	4794 ft/s

The problem was non-dimensionalized using the radius of the sphere as the characteristic length, the time for an acoustic wave to transit one radius as the characteristic time, and the bulk modulus of water as the characteristic pressure. A bulk modulus equation of state was used to model the water in this problem, and

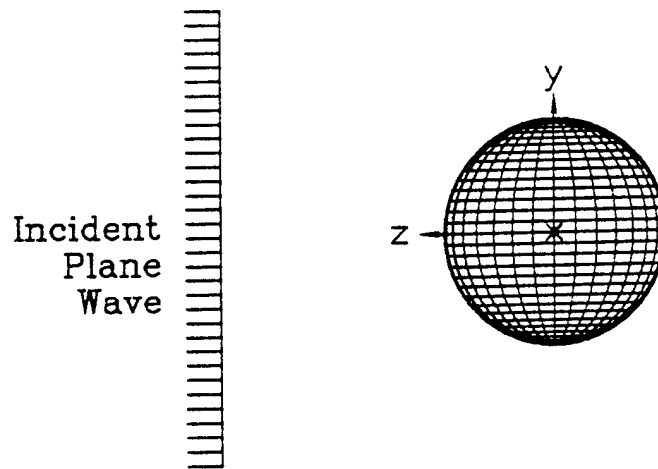


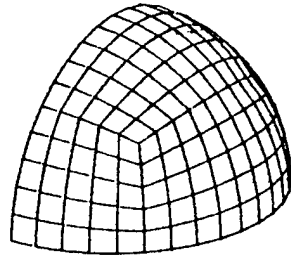
Figure 4. Spherical Shell/Plane Step Wave Problem Geometry

a small incident pressure wave magnitude (1×10^{-3} bulk modulus units) was used to keep deformations small enough for the elastic assumption to be valid.

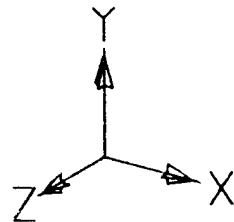
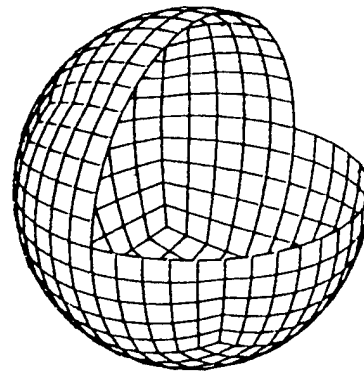
For our finite element model, a quarter symmetry model was used. An elastic material model consisting of 150 quadrilateral Lagrangian shell elements was used to model one quarter of the spherical steel shell. A single constraint set was used to constrain the appropriate translational and rotational degrees of freedom of grid points lying on symmetry planes.

MSC/DYTRAN's "General Coupling" fluid-structure interaction method, in which the Lagrangian and Eulerian meshes are independent and interact via a coupling surface, was used for this problem. This method requires that the coupling surface form a closed, simply connected volume; for simplicity, this closed volume was generated by using 450 dummy elements in addition to the 150 Lagrangian shell elements used to model the steel shell. The Lagrangian (steel) shell elements, the dummy elements, and the resulting closed coupling surface are illustrated in Figure 5.

Steel Shell Elements



Dummy Elements



Closed Coupling Surface

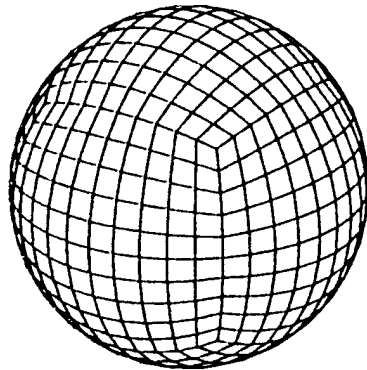


Figure 5. Steel Shell Elements, Dummy Elements, and Resulting Closed Coupling Surface for Spherical Shell/Plane Step Wave Problem

Because only a finite volume of fluid material can be modeled using this approach, it was decided to construct a model for which the solution would be unaffected by reflection from the boundaries of the fluid volume for times less than six radius transit times. The block of water modeled is thus a rectangle bounded by the planes $x=0$ and $x=4$, $y=0$ and $y=4$, and $z=4$ and $z=-4$, where the point $(0,0,0)$ represents the center of the sphere and units are in terms of the radius of the sphere. Every point on the shell is thus at least three radii away from a boundary, and since acoustic waves travel one shell radius per radius transit time, no boundary reflection reaches the shell for six radius transit times. The fluid mesh used consists of 65,536 cubical Eulerian elements; the length of each side of each element is $1/8$ radii. Figure 6 shows the fluid mesh used for this problem.

All boundaries of this fluid volume were left with a default "wall" boundary condition except the boundary at $z=4$ radii; this boundary was given a "flow" boundary condition, with a pressure of 0.001 bulk moduli and a particle velocity, determined from the one dimensional wave equation

$$p = \rho c u \quad (1)$$

of 0.001 times the acoustic wave speed in water, in the $-z$ direction. Initial conditions were imposed on all of the Eulerian elements such that all elements between the $z=4$ radii and $z=1$ radii planes had an initial pressure of 0.001 bulk moduli and a particle velocity of 0.001 times the acoustic wave speed in water in the $-z$ direction, and all elements between the $z=1$ and $z=-4$ radii planes had zero initial pressure and particle velocity. Time $t=0$ for the finite element analysis thus corresponds to the instant when the plane step wave first touches the sphere, at the point $(0,0,1)$.

The relationship between the size of the spherical shell and the fluid volume modeled in this problem is illustrated in Figure 7, from two different viewpoints.

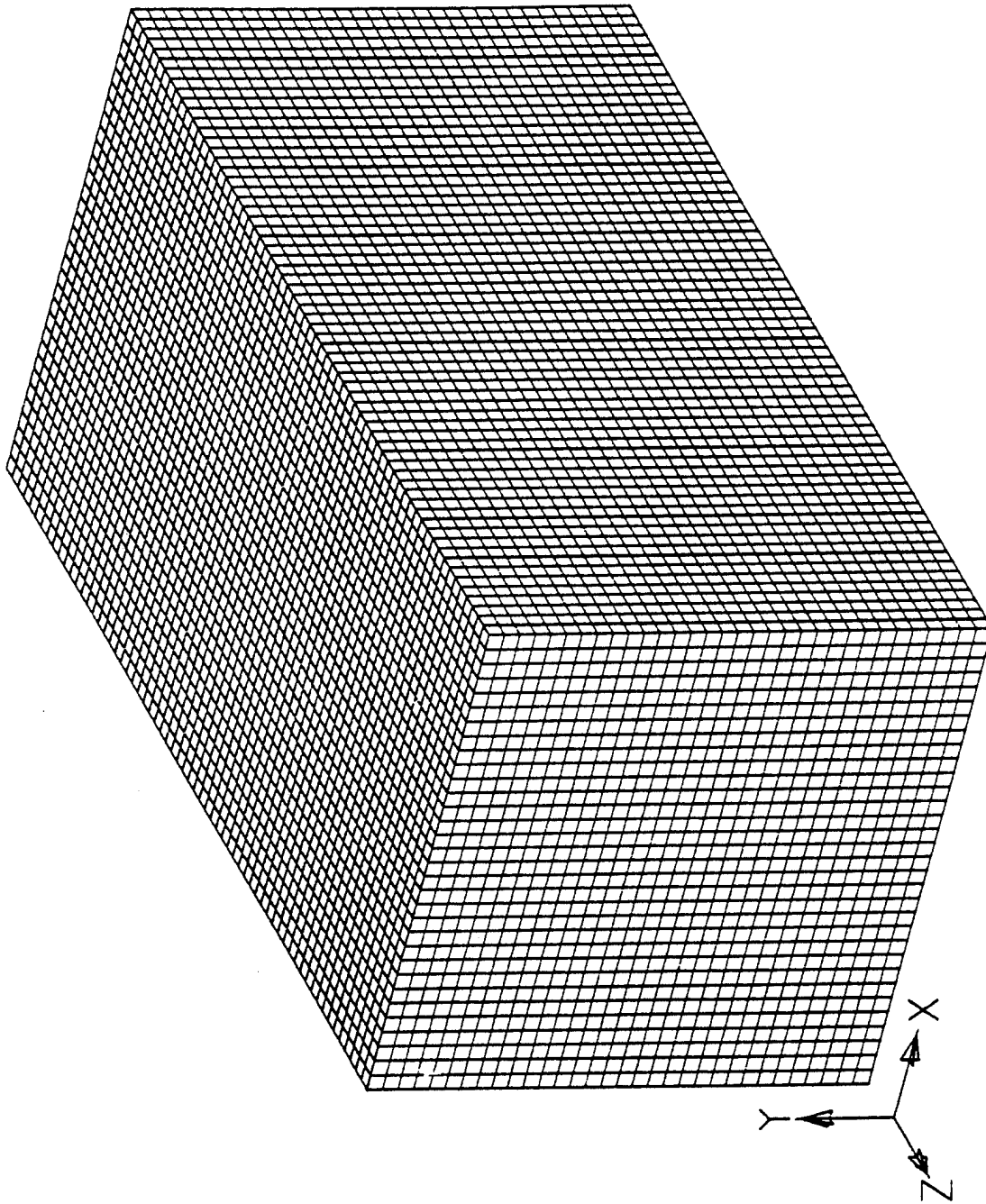


Figure 6. Fluid Mesh for Spherical Shell/Plane Step Wave Problem

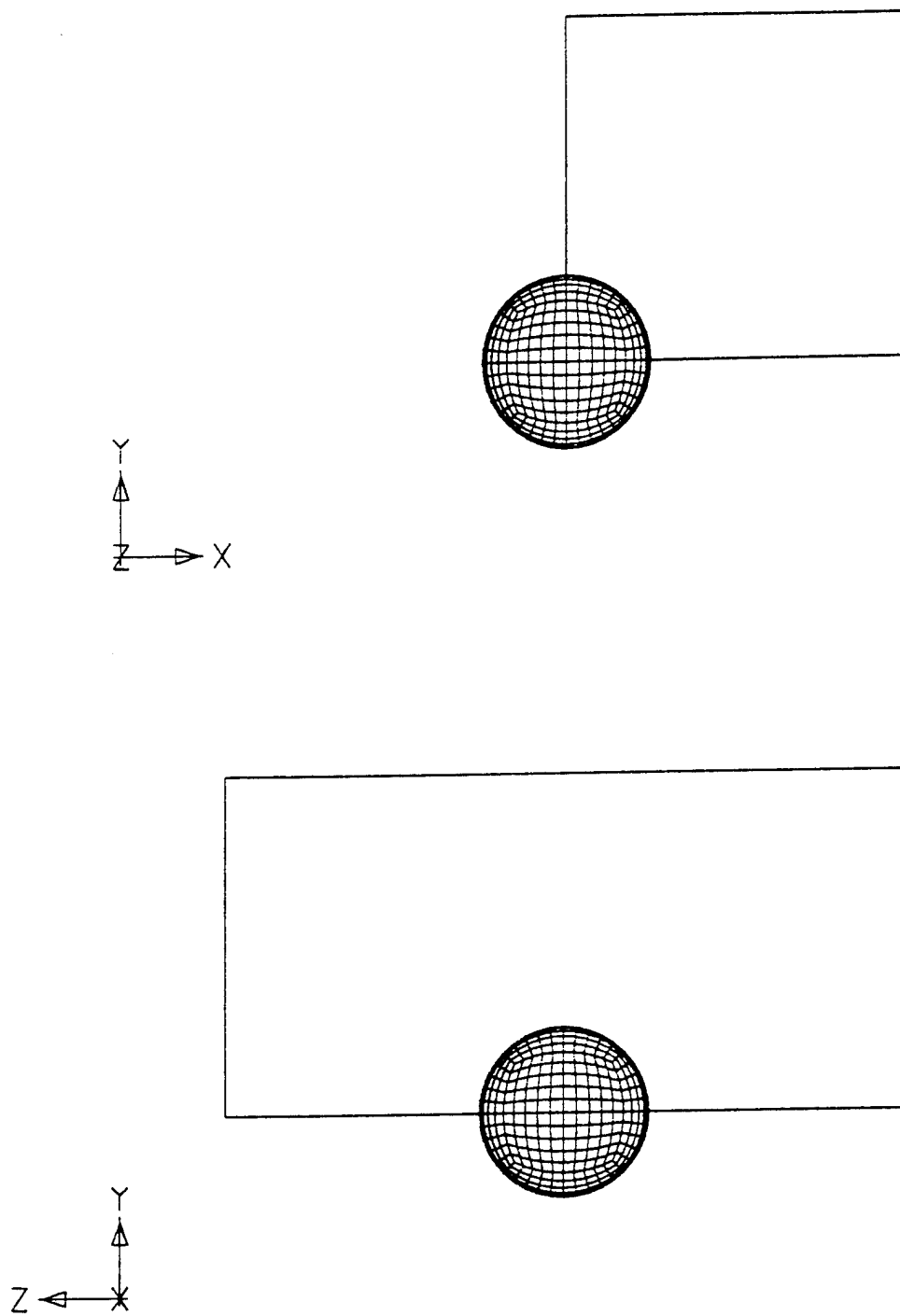


Figure 7. Size and Position of Spherical Shell Relative to Eulerian Fluid for Spherical Shell/Plane Step Wave Problem

For clarity, only the outline of the fluid block that was modeled is shown.

The steel shell element, dummy element, and fluid element geometry for this problem were all created using the finite element preprocessing program LS-INGRID [Ref. 12]. A small FORTRAN translating program was then used to convert the output files from LS-INGRID to NASTRAN compatible format files, which were then read into MSC/XL [Ref. 13]. Symmetry constraints, the "flow" boundary condition, and material properties were then added using MSC/XL, and a single "bulk data" file was written out. The LS-INGRID input files, FORTRAN geometry translating program, and MSC/XL input data stream used to create the model for this problem, together with the MSC/DYTRAN input file used to control the analysis, are provided in Appendix A. The information provided in Appendix A is sufficient to duplicate our analysis.

The resulting transient solution for the radial velocity of the shell, at azimuth angles of 0° , 90° , and 180° (which correspond to the points $(0,0,1)$, $(0,1,0)$, and $(0,0,-1)$, using the coordinate system shown in Figure 1) are shown in Figure 8. Huang's new 70 term Cesaro sum solution [Ref. 14] for these same points is shown for comparison purposes. While our finite element solution shows some overshoot and resulting oscillation for 0° , in general the agreement with Huang's analytical solution is quite good. All velocities in Figure 8 are non-dimensionalized to be independent of the magnitude of the incident pressure wave, by dividing the original non-dimensional velocity by the non-dimensional magnitude of the incident pressure wave.

B. INFINITE CYLINDER/PLANE STEP WAVE

Figure 9 shows the geometry of the infinite cylinder/plane step wave problem. The same material properties, parameters, and non-dimensionalization procedures used in the spherical shell/plane step wave problem were used for this

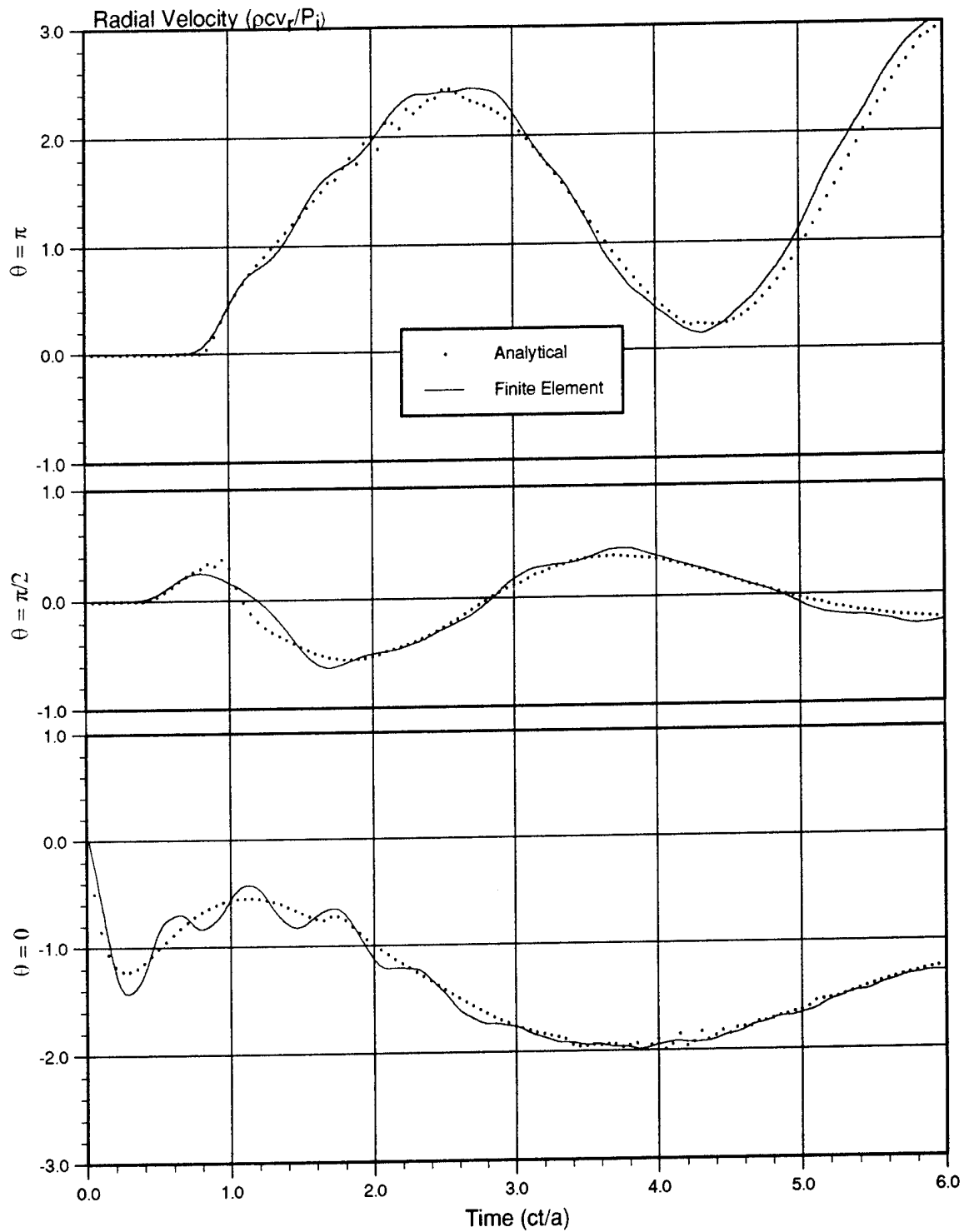


Figure 8. Non-Dimensional Incident Pressure Independent Radial Velocity Versus Non-Dimensional Time for Spherical Shell/Plane Step Wave Problem

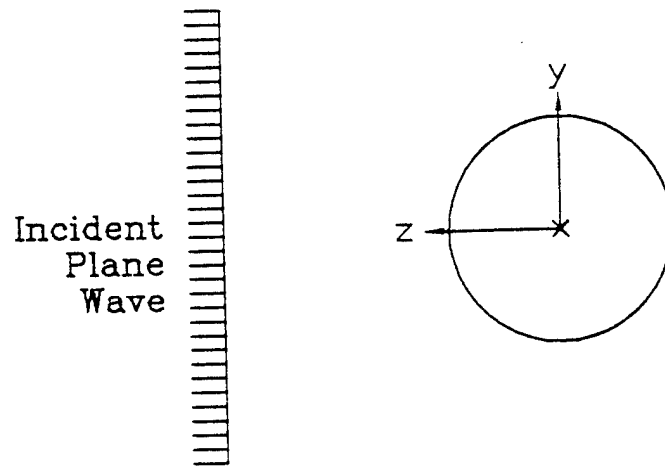


Figure 9. Infinite Cylinder/Plane Step Wave Problem Geometry

problem, except that a shell thickness to radius ratio of 0.029056 was used for this problem.

Because of the symmetry of the problem, only a single 0.1 cylinder radii wide "ring" of the infinite cylinder was modeled for our finite element analysis. In addition, since the problem has symmetry about the plane defined by a point on the axis of the cylinder and the vector normal to the incoming pressure wave front, only one half of this ring was modeled.

The shell was modeled with 36 Lagrangian elements, with appropriate translational and rotational symmetry constraints placed upon the grid points associated with these elements. MSC/DYTRAN's "General Coupling" fluid-structure interaction method was used for this problem; to form the closed volume coupling surface required for this method, 72 dummy triangular and two dummy quadrilateral elements were defined. Figure 10 shows the Lagrangian structural elements and dummy elements used in our finite element model for this problem.

The fluid mesh used for this problem consisted of a thin block of elements,

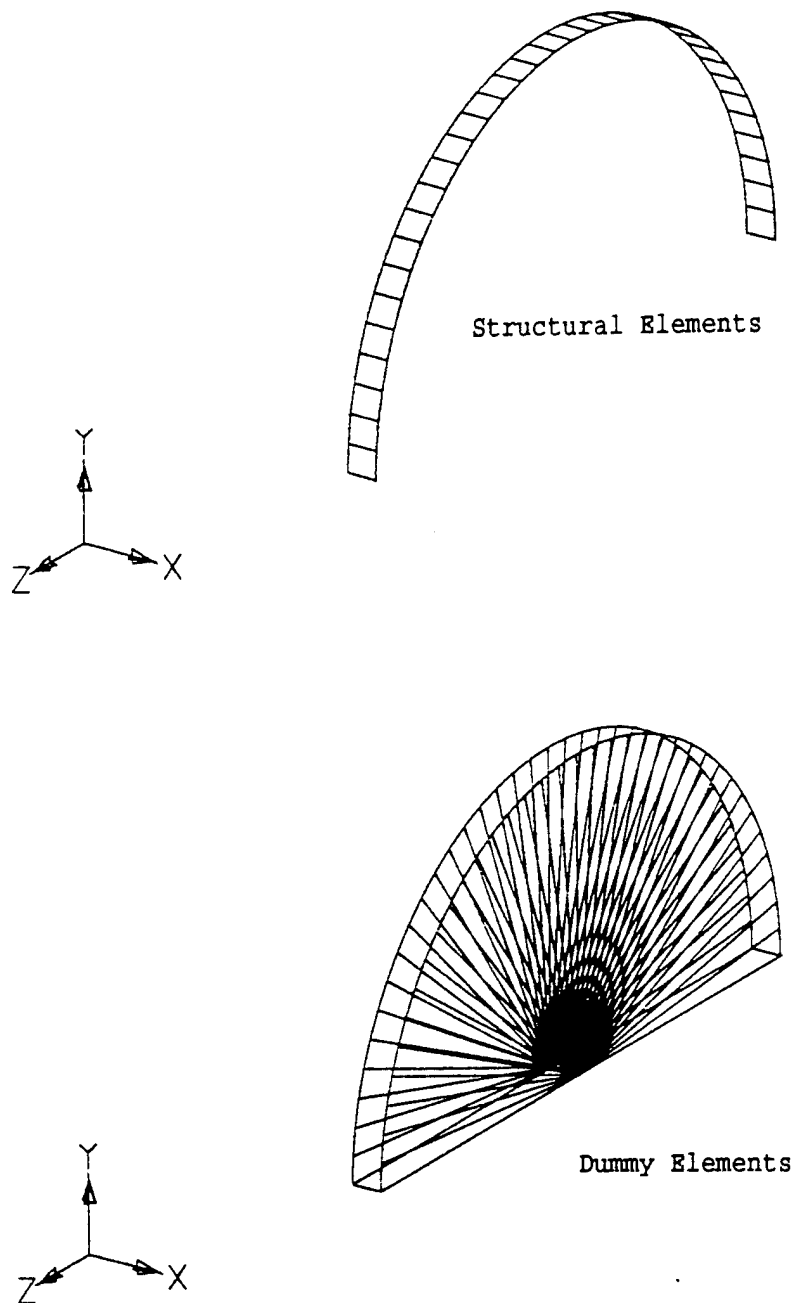


Figure 10. Structural and Dummy Elements in Finite Element Model for Infinite Cylinder/Plane Step Wave Problem

with the dimensions $0.1 \times 4 \times 8$ cylinder radii. This fluid block was meshed with $1 \times 88 \times 176$ hexahedron elements, for a total of 15488 fluid elements. Thus, the length of each element in the y and z directions was $1/11$ cylinder radii. The fluid mesh used is shown in Figure 11. As in the "Spherical Shell/Plane Step Wave" problem, the amount of fluid modeled is sufficient to prevent reflection of acoustic waves from the boundaries from affecting the solution for times less than 6 radius transit times.

All boundary conditions for the fluid mesh shown in Figure 11 were left as default "wall" (no flow) boundaries, except for the boundary at $z=4$ cylinder radii, which was given a "flow" boundary condition with a prescribed pressure of 0.001 bulk moduli and a z direction particle velocity of -0.001 cylinder radii/cylinder radius transit time. Initial conditions were prescribed such that all fluid between the $z=4$ and $z=1$ cylinder radii planes had these same values, and the remaining fluid had zero initial pressure and particle velocity. Thus, time $t=0$ corresponds to the instant when the pressure wave just touches the cylinder, at the point (0,0,1) (using the rectangular coordinates of Figure 9; in cylindrical coordinates this point is at a radius of one cylinder radii from the cylinder axis, at an angle of 0°).

The size and position of the cylinder relative to the fluid volume modeled is illustrated in Figure 12. Only the outline of the fluid volume modeled is shown in this figure.

The entire finite element model for this problem was created using MSC/XL. The MSC/XL input data stream and MSC/DYTRAN run file used for this analysis are provided in Appendix B. These files are sufficient to duplicate our analysis.

Results from our analysis, for the pressure-independent non-dimensional radial velocity of the shell at 0° , 90° , and 180° are compared with the 8-term finite series analytical solution found by Huang [Ref. 11] in Figure 13; again, very good agreement between the finite element and analytical solutions is seen.

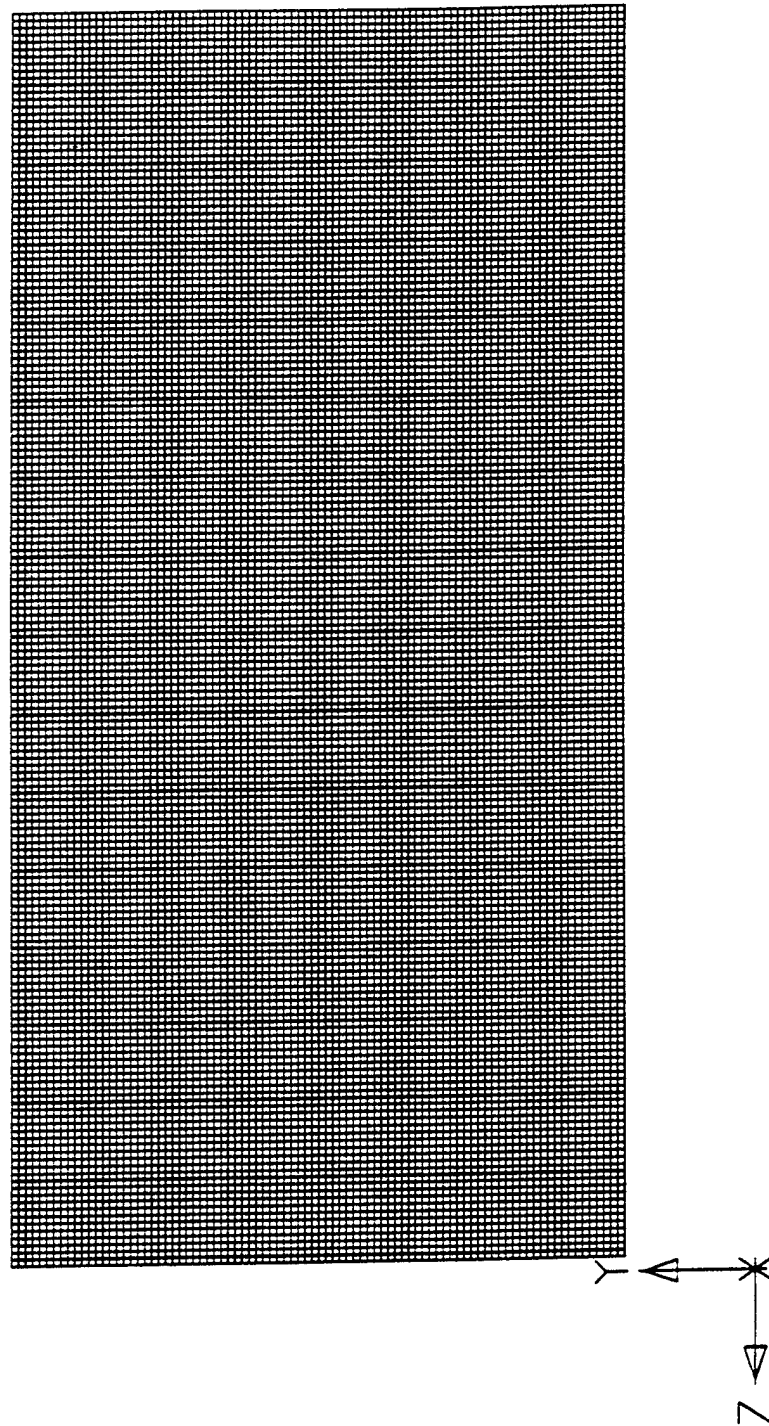


Figure 11. Fluid Mesh for Infinite Cylinder/Plane Step Wave Problem

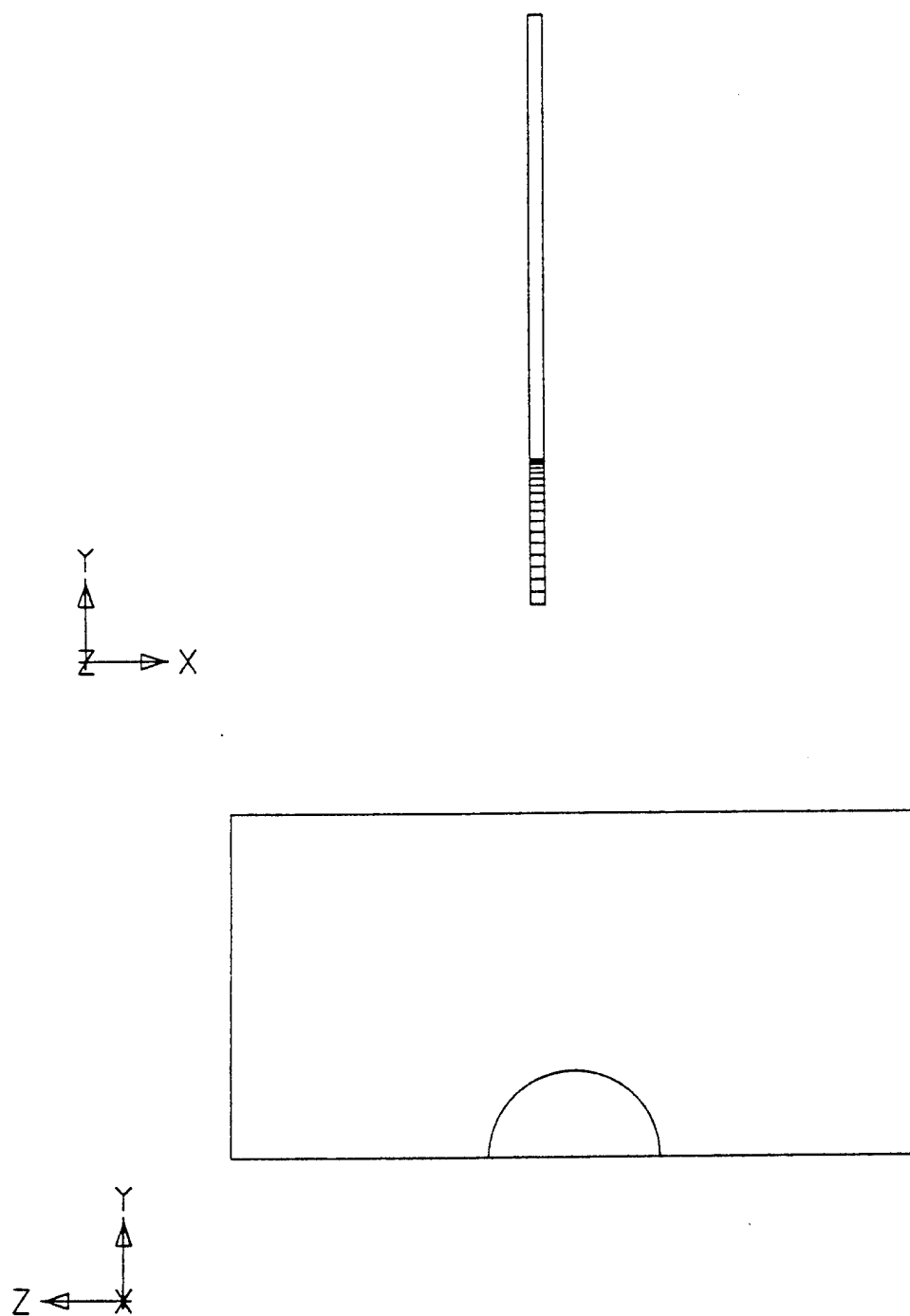


Figure 12. Size and Position of Infinite Cylinder Relative to Eulerian Fluid for Infinite Cylinder/Plane Step Wave Problem

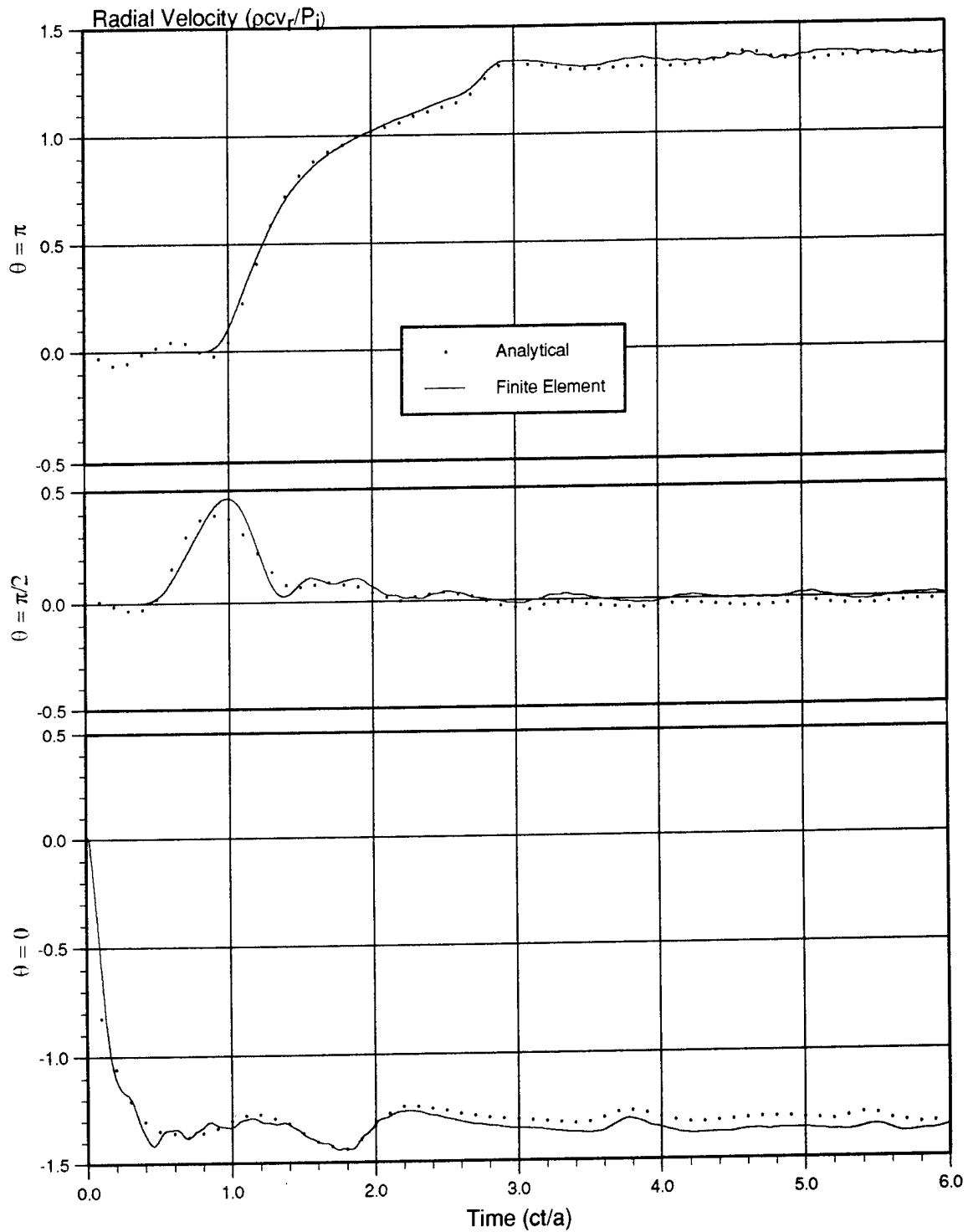


Figure 13. Non-Dimensional Incident Pressure Independent Radial Velocity Versus Non-Dimensional Time for Infinite Cylinder/Plane Step Wave Problem

IV. MULTIMATERIAL EULERIAN ANALYSIS OF BUBBLES

As mentioned in the introduction, the whipping induced on nearby marine and submarine structures due the oscillation of the bubble produced by an underwater explosion is of considerable interest, as the damage due to this phenomena can exceed that due to the primary shock wave. In order to investigate the feasibility of modeling the physics of underwater explosion gas bubbles using a multimaterial Eulerian hydrocode formulation, several finite element analyses were conducted.

A. DEEP SPHERICAL BUBBLE

The first bubble related finite element analysis conducted investigated the detonation of a deeply submerged explosive charge in the absence of nearby boundary surfaces. As deep charges are known to undergo little vertical migration due to gravity [Ref. 15], a quasi one-dimensional finite element model, in which gravity is neglected entirely, was used for this analysis.

The problem thus has spherical symmetry. The particular parameters chosen for this analysis correspond to one of a series of tests conducted during and shortly after World War II at the Woods Hole Oceanographic Institute [Ref. 16], and consist of a 0.299 kg (0.660 lb) TNT charge detonated at a depth of 178.6 m (586 ft). The geometry of this problem is shown in Figure 14.

The TNT in this problem was modeled using a Jones-Wilkins-Lee (JWL) equation of state, with standard equation of state and detonation velocity parameters for TNT [Ref. 17]. With this state equation, the pressure in the "burned fraction" of the explosive material is related to the specific internal energy and the density

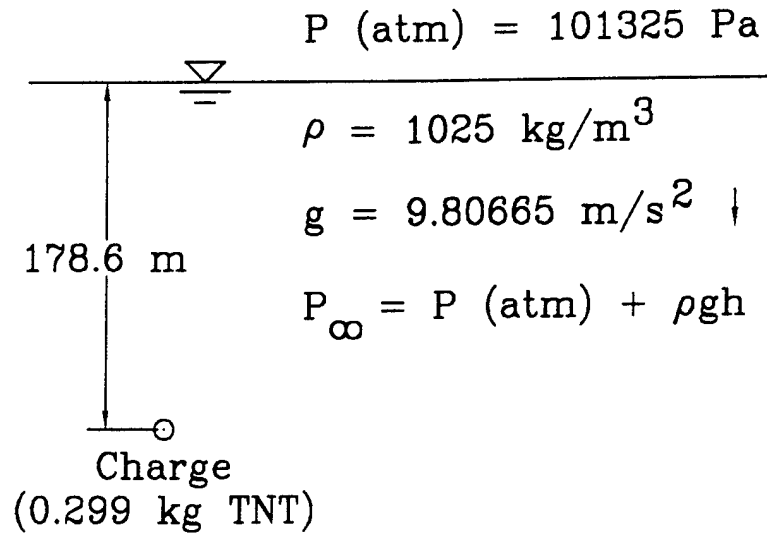


Figure 14. Deep Spherical Bubble Problem Geometry

by:

$$p = A \left(1 - \frac{\omega \eta}{R_1} \right) e^{-\frac{R_1}{\eta}} + B \left(1 - \frac{\omega \eta}{R_1} \right) e^{-\frac{R_2}{\eta}} + \omega \eta \rho_0 E \quad (2)$$

where

$$\eta = \rho / \rho_0$$

ρ_0 = initial density

E = specific internal energy (per unit mass)

A, B, ω, R_1, R_2 are constants for the explosive

The "burned fraction" is just that portion of the explosive contained within the sphere formed by the spherical detonation wave front propagating outward from the detonation point with detonation velocity d . As the nominal 0.660 lb TNT charge size reported for this experiment represents a slight increase over the actual charge size, as calculated by the original researchers to account for the increased energy of the booster and detonator [Ref. 16], the explosive was modeled as a

homogeneous mass of TNT. The equation of state parameters used were [Ref. 17]:

$$\begin{aligned}
 \rho_0 &= 1630 \text{ kg/m}^3 \\
 E &= 4.29 \times 10^6 \text{ J/kg} \\
 A &= 3.712 \times 10^{11} \text{ Pa} \\
 B &= 3.231 \times 10^9 \text{ Pa} \\
 \omega &= 0.30 \\
 R_1 &= 4.15 \\
 R_2 &= 0.95 \\
 d &= 6390 \text{ m/s}
 \end{aligned}$$

In order to model the seawater in which this experiment was conducted, a polynomial equation of state was used. This state equation relates the pressure in the fluid to the acoustic condensation μ and the specific internal energy by:

$$p = a_1 \mu + a_2 \mu^2 + a_3 \mu^3 + (b_0 + b_1 \mu + b_2 \mu^2) \rho_0 E \quad (\mu > 0) \quad (3)$$

$$p = a_1 \mu + (b_0 + b_1 \mu) \rho_0 E \quad (\mu < 0)$$

where

$$\begin{aligned}
 \mu &= (\rho - \rho_0) / \rho_0 \\
 \rho_0 &= \text{initial density} \\
 E &= \text{specific internal energy (per unit mass)} \\
 a_1, a_2, a_3, b_0, b_1, b_2 &\text{ are constants for the fluid}
 \end{aligned}$$

and the upper equation applies to a fluid in a compressed state, while the lower applies to a fluid in an expanded state. Constants for this state equation were determined by using the mathematical calculation program MATHCAD [Ref. 18] to fit available literature equation of state data for fresh water compressed to extreme pressures to the form of equation (3), and then replacing the initial (reference) density and the first (adiabatic bulk modulus) term with the reference density and adiabatic bulk modulus of seawater. This determination of polynomial equation of state constants for seawater is provided in Appendix C. The seawater equation of state parameter values determined by this procedure, appropriate for

condensation values on the order of $\mu < 0.8$, are:

$$\begin{aligned}a_1 &= 2.306 \times 10^9 \text{ Pa} \\a_2 &= 8.432 \times 10^9 \text{ Pa} \\a_3 &= 8.014 \times 10^9 \text{ Pa} \\b_0 &= 0.4934 \\b_1 &= 1.3937 \\b_2 &= 0.0000 \\\rho_0 &= 1025 \text{ kg/m}^3\end{aligned}$$

The initial conditions given to the seawater modeled in this problem were an initial acoustic condensation of zero (initial density of 1025 kg/m^3) and an initial specific internal energy of 3750.4 J/kg . This initial specific internal energy value was determined from equation (3) and the above constants; it represents the specific internal energy necessary to give the seawater an initial pressure equal to standard atmospheric pressure plus the ρgh pressure at a depth of 178.6 m in seawater, using the standard gravitational constant value for g of 9.80665 m/s^2 .

As MSC/DYTRAN is a three-dimensional code, the increasing volume as one moves away from the center of the charge was taken into account in our quasi one-dimensional model by modeling a diverging pyramid shaped region of fluid, with default "wall" (no flow) boundary conditions on all sides. However, the very end of this pyramid shaped volume was modeled using rectangular parallelepiped shaped hexahedron elements with the same volume as the equivalent pyramid. This both avoids the use of a five sided pyramid shaped volume at the point of the pyramid (which is not a standard finite element shape) and keeps the stable time step size, which by the Courant Criterion is proportional to the smallest dimension of an element, from being very small. Rectangular parallelepiped shaped hexahedron elements were used to model the charge, and non-rectangular hexahedron elements, whose top and bottom were parallel but whose sides had a slope of 0.1 , were used to model the fluid. As our primary interest was in the bubble rather than the initial shock wave, only three elements were used to model

the charge. In order to prevent reflection from the far end of the finite volume of fluid modeled for the duration of the analysis, a large volume of fluid was modeled. The radial dimension of the seawater in the model extended to 10,000 times the initial 3.526 cm "radius" (height of rectangular parallelepiped actually modeled was 1/3 this radius) of the charge. To model this large volume of seawater, 996 hexahedron elements with a non-uniform radial mesh spacing were used, with elements becoming larger further away from the charge center (where gradients are smaller). The finite element model used in this analysis is shown from a three-dimensional perspective in Figure 15.

To determine the radius versus time behavior of the explosion gas bubble, the volume of explosive gases at each time step was output. This volume was then converted to a full spherical volume by multiplying by the appropriate geometric factor and then used to calculate the radius of this sphere. The resulting radius versus time curve is shown in Figure 16. Also shown in this figure are the experimentally determined first maximum bubble radius and first bubble oscillation period [Ref. 16]. The finite element analysis and experimental results for these quantities are seen to be in excellent agreement.

As only maximum bubble radii and bubble periods were measured in this set of experiments, it is possible that the finite element analysis radius versus time curve could agree with experimental results at these two points but still have the wrong shape. However, while an analytical solution does not exist for this problem, we can calculate an analytical solution for the simplified problem of a bubble with negligible internal energy expanding and collapsing in an incompressible media. Expressing the total energy associated with radial flow of the fluid in terms of the maximum radius of the bubble (mathematically, this is equivalent to using the maximum radius of the bubble to determine the initial conditions of the problem) and then separating variables gives the relationship

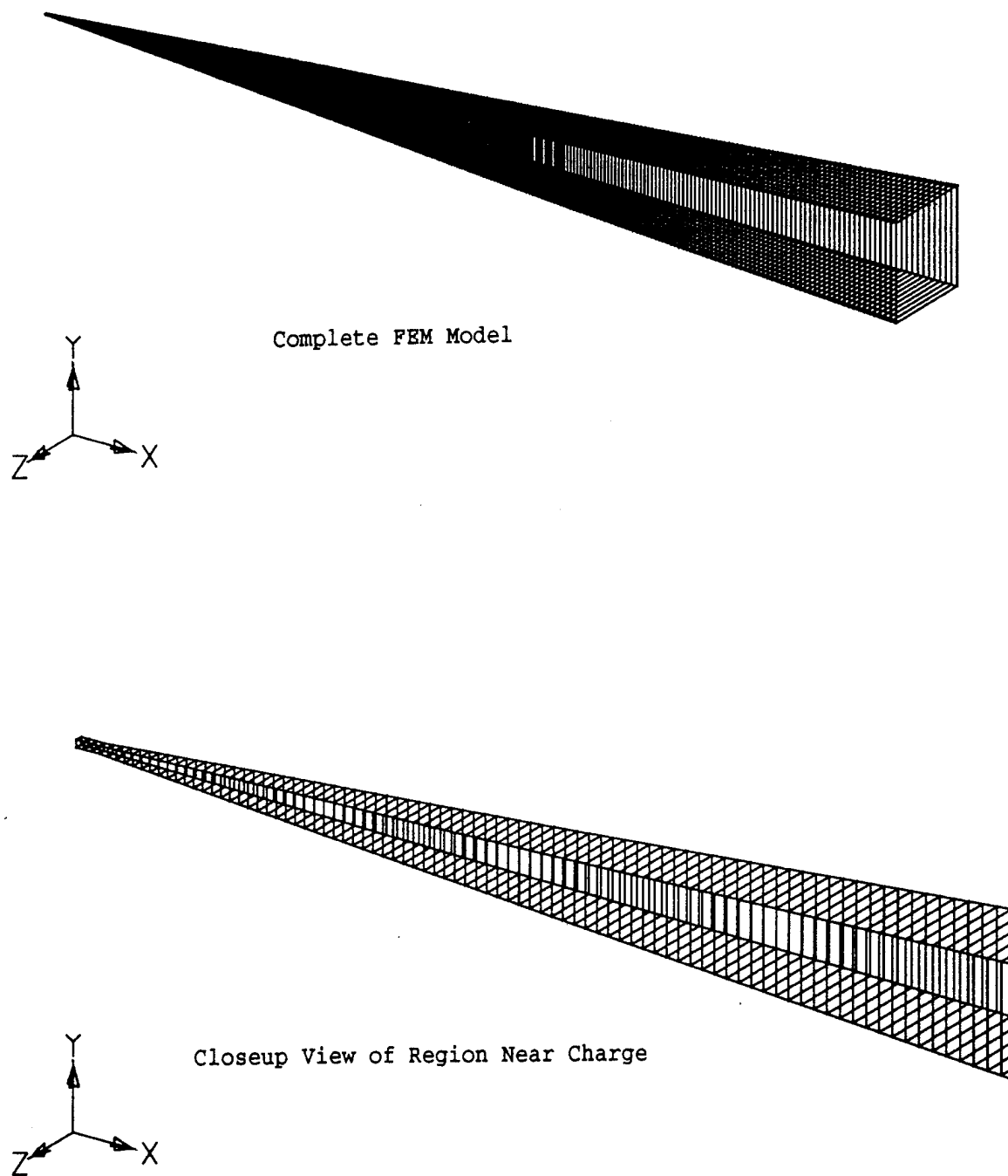


Figure 15. Finite Element Model for Deep Spherical Bubble Problem

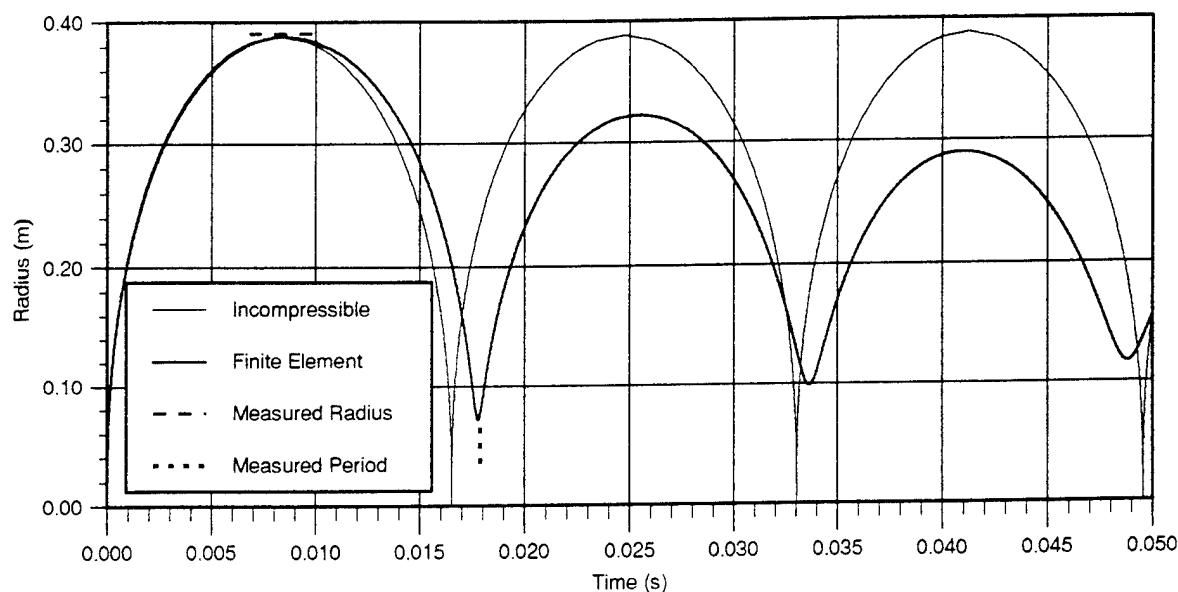


Figure 16. Radius Versus Time Behavior for Deep Spherical Bubble Problem (0.2990 kg TNT Charge at 178.6 m Depth in Seawater)

between the bubble radius and time as [Ref. 19]:

$$t = \left(\frac{3\rho_0}{2P_0} \right)^{1/2} \int_{r_0}^r \frac{da}{[(r_{\max}/a)^3 - 1]^{1/2}} \quad (4)$$

The radius versus time curve obtained by numerically integrating this equation step-by-step, using the seawater density and hydrostatic pressure used in the finite element analysis for this problem, the maximum radius obtained from that analysis, and an initial radius of zero, is also plotted in Figure 16.

Figure 16 thus shows that not only are the maximum bubble radius and bubble period obtained from the finite element analysis for the first bubble oscillation in excellent agreement with the experimental values for these quantities, but the shape of the radius versus time curve is also very similar to that obtained from analytical analysis of the simplified (incompressible/negligible internal energy) problem. Up to the time of the first maximum radius, these curves nearly overlay

one another, while after that time the finite element solution begins lagging the simplified problem analytical solution.

The effects of a more realistic state equation for the seawater and the explosion bubble gases (as opposed to the seawater being incompressible and the internal energy of the bubble gases being zero) are clearly shown in Figure 16. In the more realistic (finite element) analysis, the bubble oscillation is asymmetric about the maximum radius and the bubble period is lengthened. An approximate analysis by Herring [Ref. 19] shows that a "first-order" effect of compressibility is to cause the compression portion of the oscillation cycle to take longer than the expansion portion of the cycle, which is what was observed in the finite element analysis. In addition, the radius versus time behavior for the finite element analysis shows a decreasing maximum radius and period and increasing minimum radius for subsequent oscillations. This is due to the energy loss associated with radiation of an outward traveling pressure wave (the "bubble pulse") when the bubble approaches a radius minimum [Ref. 19].

Up until the time of the first minimum, the results from the finite element analysis are in excellent agreement with both experimental and approximate analytical results. As there is at least a few percent uncertainty in the detonation energy for any particular explosion, the agreement with experimental results is as good as can reasonably be achieved. The maximum bubble radius and bubble period for the second oscillation cycle were also measured in this experiment; the measured value for the second maximum radius was 11.6 inches (about 29.5 cm), and the measured time for the second minimum was 30.85 msec. There thus appears to have been an energy loss when the bubble was near its minimum radius in excess of that attributable to acoustic radiation. It is believed that this energy loss was due to heat transfer. As Hicks has pointed out, deep (non-migrating) bubbles are unstable near their first minimum, and photographs show that numerous

at this time numerous needle-like water jets spray into the gas bubble, significantly cooling the hot bubble gases [Ref. 20]. The energy loss in the gas bubble due to this phenomena has not been accounted for in our finite element analysis.

The input and postprocessing files used in this analysis, as well as the FORTRAN program used to compute the solution to the simplified (incompressible media/negligible internal energy) problem are provided in Appendix D.

B. BUBBLES NEAR RIGID BOUNDARIES

A number of interesting phenomena are associated with the expansion and collapse of gas bubbles generated by underwater explosions in the vicinity of boundaries. These include migration of the bubble towards or away from the boundary and changes in the shape and oscillation period of the bubble. Each of these phenomena can effect the damage done by the bubble on marine or submarine structures.

One of the limiting cases is that in which the boundary behaves as a perfectly rigid wall. This case is of interest because the effect of the wall on the bubble approximates the effect on the bubble of either a hard bottom or a nearby stiff marine or submarine structure. The simplest situation, in which the rigid boundary can be treated as an infinite plane, is appropriate when the explosion takes place near a hard bottom or when the explosion takes place near a stiff structure with a radius of curvature that is large compared with the dimensions of the resultant bubble.

The results discussed in this section are for this situation. The charge modeled is a 10.24 kg cylinder of TNT, 20 cm in diameter and 20 cm high, submerged in seawater at a depth of 1000 m. The first analysis conducted was for the "free-field" case in which the rigid boundary is absent (rigid boundary at infinite distance from center of charge); this analysis yielded a maximum free-field

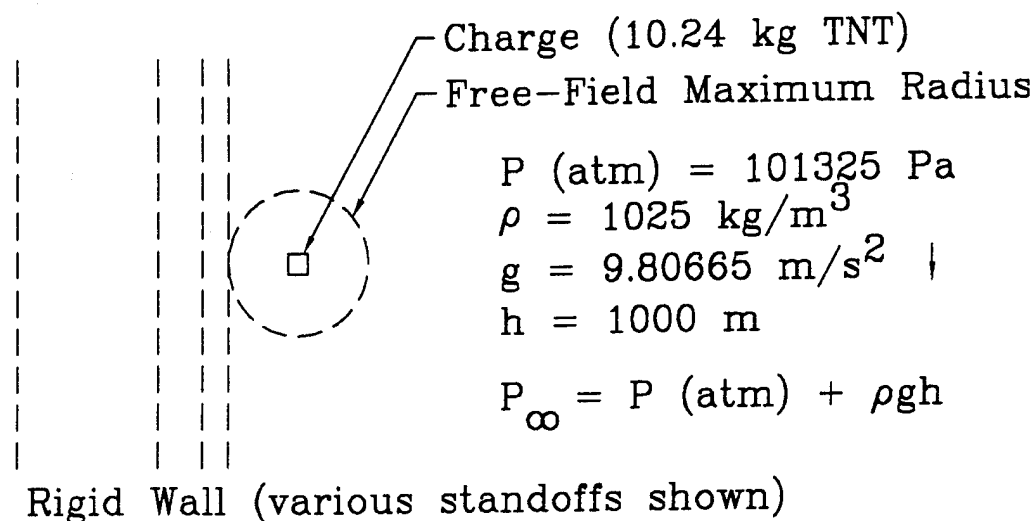


Figure 17. Geometry of Bubble Near Rigid Boundary Problems

bubble radius of 70.98 cm. Subsequent finite element analyses were then conducted with a rigid wall placed at 4.015, 2.008, 1.374, and 1.000 times this distance from the center of the charge.

The geometry of these problems is shown in Figure 17. As in the previous section (the "Deep Spherical Bubble" problem), gravitational effects on the motion of the bubble were neglected, and the gravitational constant was used only to determine the hydrostatic pressure in the seawater surrounding the charge, which is assumed to have a constant value equal to the hydrostatic pressure at the depth of the charge. The problem is then axisymmetric, with the axis of symmetry being the line normal to the rigid wall passing through the axis of the cylindrical charge; the problem could alternatively be made axisymmetric by using a horizontal rigid wall, whose normal is the gravitational vector.

The diverging geometry of the problem was again modeled using geometrically diverging (wedge shaped) finite element models. Quasi two-dimensional models were used. Three different types of finite element models

were used in the analyses. For the free-field analysis, a quarter symmetry axisymmetric model was used; half symmetry axisymmetric models were used for the analyses which involved a nearby rigid wall. The half symmetry axisymmetric models for the cases in which the rigid wall was 4.015, 2.008, and 1.374 maximum free-field radii from the center of the charge were modeled using only Eulerian elements, with the rigid wall being a simple no-flow boundary condition; the fluid media is thus modeled only on one side of the wall. The case in which the rigid wall is at 1.000 free-field radii from the center of the charge was modeled by using a full half symmetric axisymmetric model and a single large Lagrangian steel solid element, with interaction between the Eulerian and Lagrangian materials being accomplished with MSC/DYTRAN's "General Coupling" method. While this is somewhat less efficient than the procedure used for the other rigid wall cases, it is the simplest procedure for locating the rigid wall at precisely 1.000 free-field radii from the center of the charge.

The finite element mesh for these analyses consisted of three different Eulerian "regions." A refined region near the charge, where gradients are highest, was used to ensure reasonable accuracy in capturing the motion of the bubble. Outside of this "central" region a large, less refined region was used to ensure that reflection from the non-rigid wall boundaries did not effect the results during the duration of the analyses. This "outside" region can be thought of as "storing" energy and momentum during bubble expansion, which then effects bubble collapse after the momentum field reverses direction. A "transition" region was used to connect the central and outside regions.

The overall geometry of the finite element model for the quarter symmetry axisymmetric free-field analysis is shown in Figure 18, from a three-dimensional perspective. Figure 19 shows the complete finite element model for this analysis from a two-dimensional perspective. A close up view of the lower left corner of

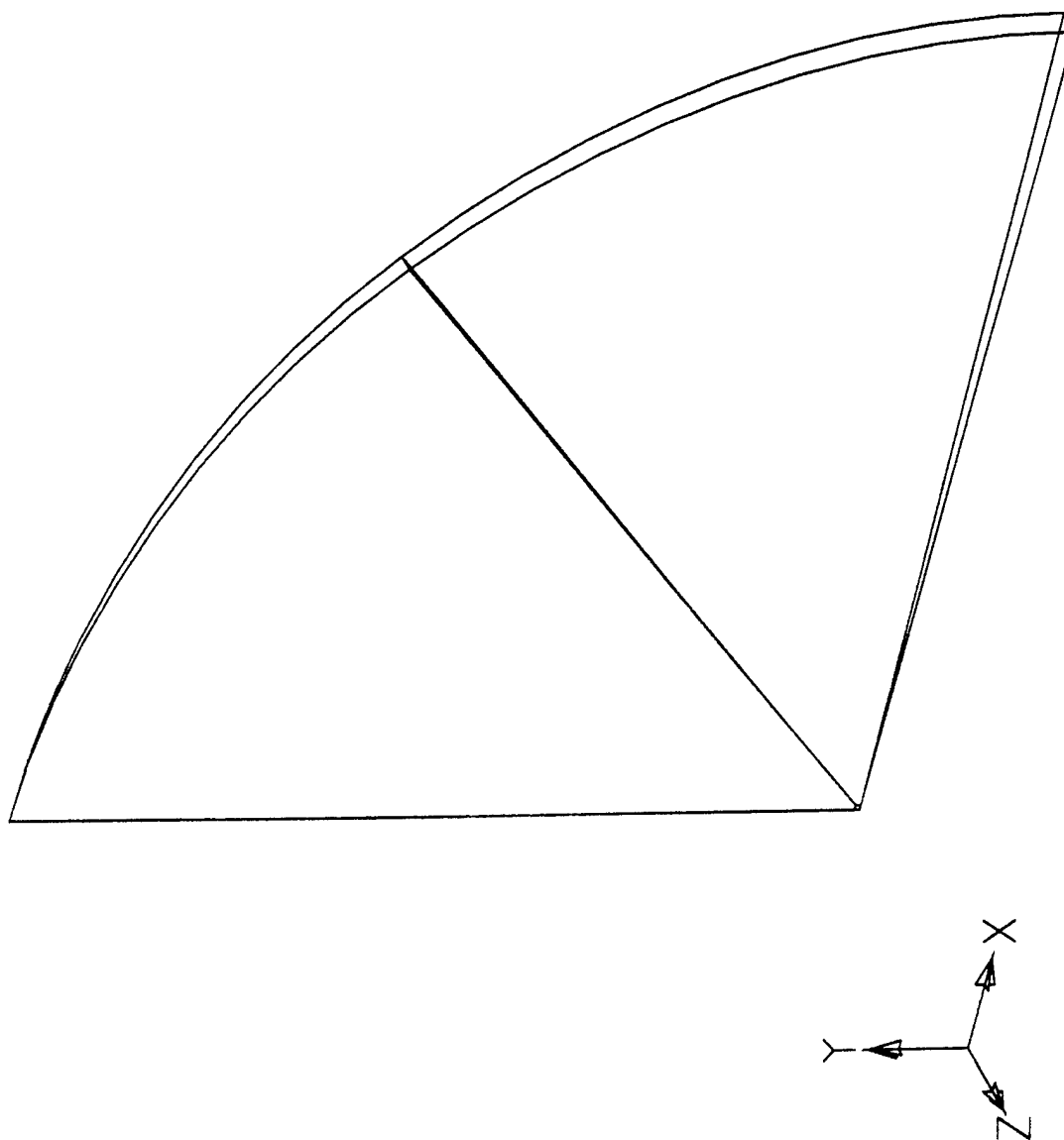


Figure 18. Overall Model Geometry for Quarter Symmetry Axisymmetric Finite Element Model For Free-Field Analysis

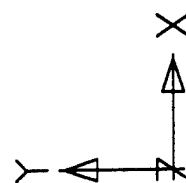
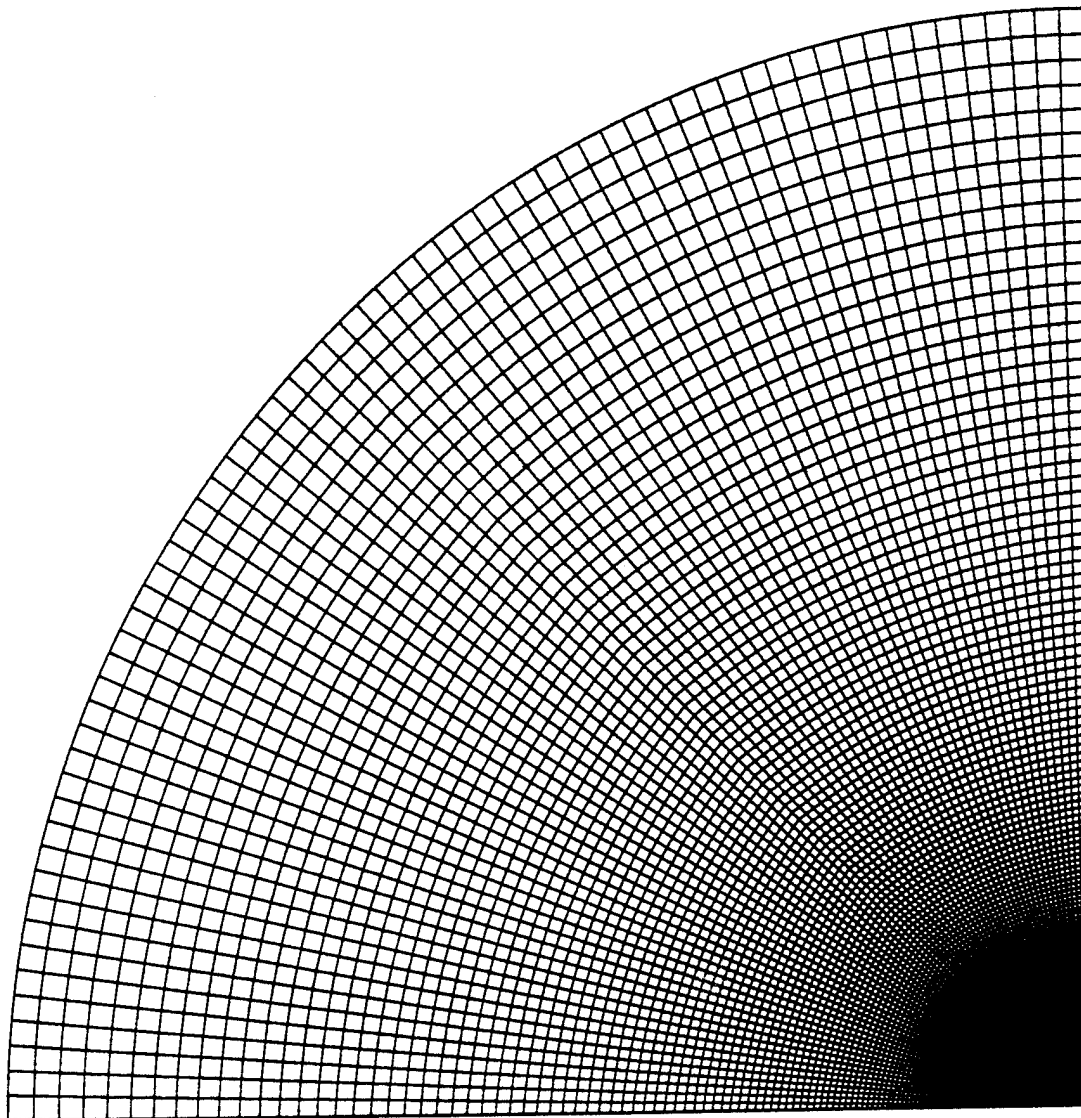


Figure 19. Quarter Symmetry Axisymmetric Finite Element Model for Free-Field Analysis

Figure 19, which includes the "central" and "transition" regions, and a small portion of the "outside" region, is shown in Figure 20. The 4 x 4 element square block (from a two-dimensional perspective) of elements in the lower left corner of this figure are initially filled with TNT; the remaining elements are initially filled with seawater. The axisymmetric symmetry axis in Figures 19 and 20 lies along the left edge in these figures. The quarter symmetry plane, which is normal to and bisects the axis of the charge, lies along the bottom edge in these figures. The central region consists of 9801 Eulerian elements, and the outer region contains 13600 Eulerian elements. The two-dimensional height and width of the elements in the central region is 0.025 m; the overall central region dimensions are 2.475 x 2.475 m. The total "wedge" of fluid modeled is 2° of arc of a solid sphere with a radius of 400 m. The inverted-L shaped transition region, which provides a 3:1 mesh coarsening, is composed of 269 Eulerian elements.

The above described finite element model was used as the basic building block for the models used in the other analyses. For the analysis in which the rigid wall is located at 1.000 maximum free field radius from the center of the charge, the fluid portion of the model was created by reflecting the free-field finite element model about its quarter symmetry plane. The rigid boundary was then created by modeling a single large solid steel Lagrangian element and using MSC/DYTRAN's General Coupling algorithm. The finite element model geometry for this analysis is shown in Figure 21, from a three-dimensional perspective. Figure 22 shows a close up view of the area in which the charge is located, from a two-dimensional perspective; the shaded elements in this figure initially contain TNT, while the remaining elements initially contain seawater.

For the analyses in which the rigid wall was located at 1.374, 2.008, and 4.015 maximum free-field radii from the center of the charge, fluid elements were added to the area between the free-field quarter symmetry plane and the rigid wall

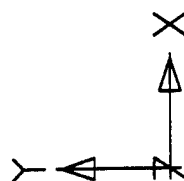
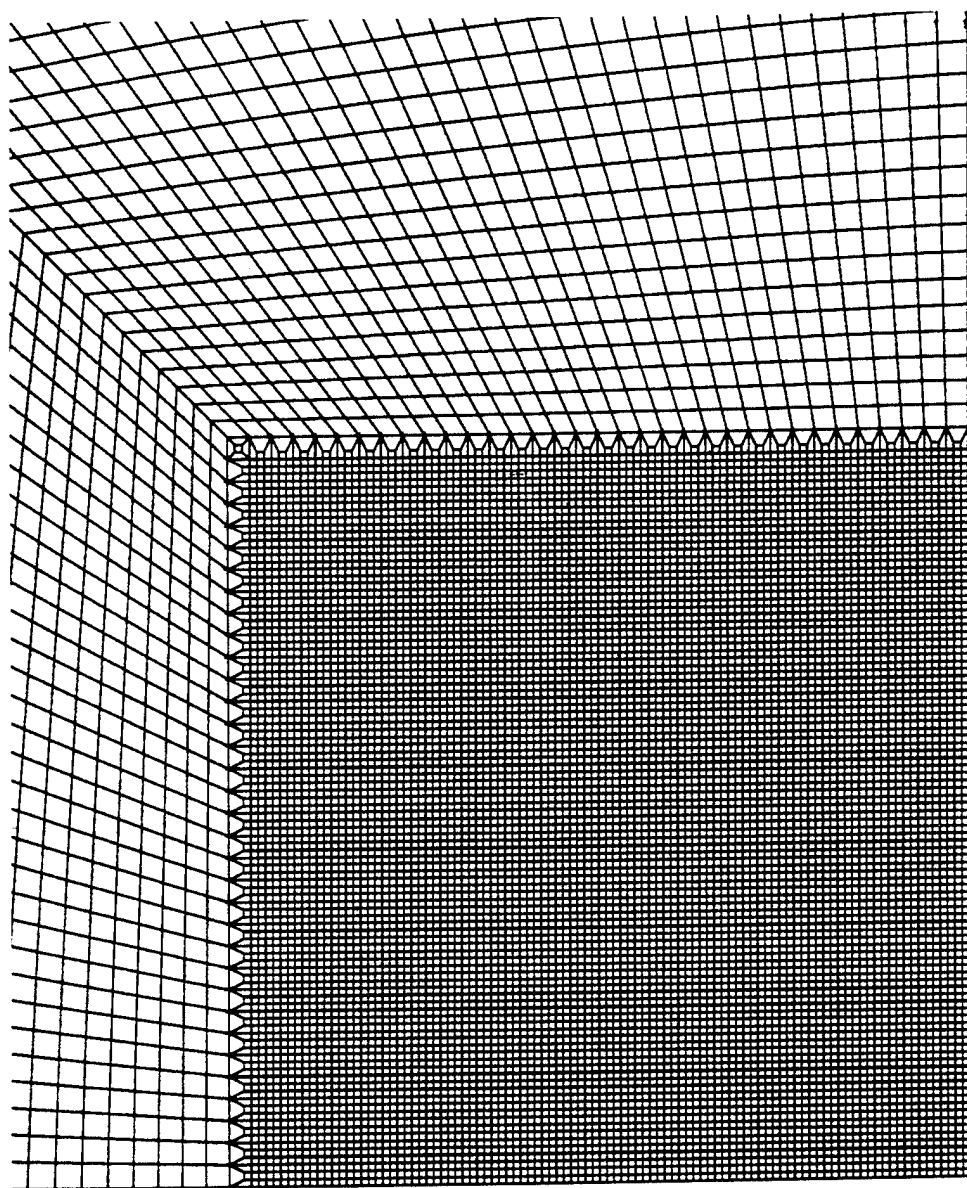


Figure 20. Close Up View of Finite Element Model in Area Near Charge for Free-Field Analysis

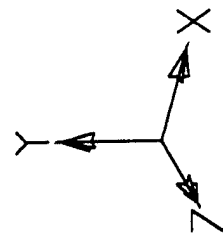
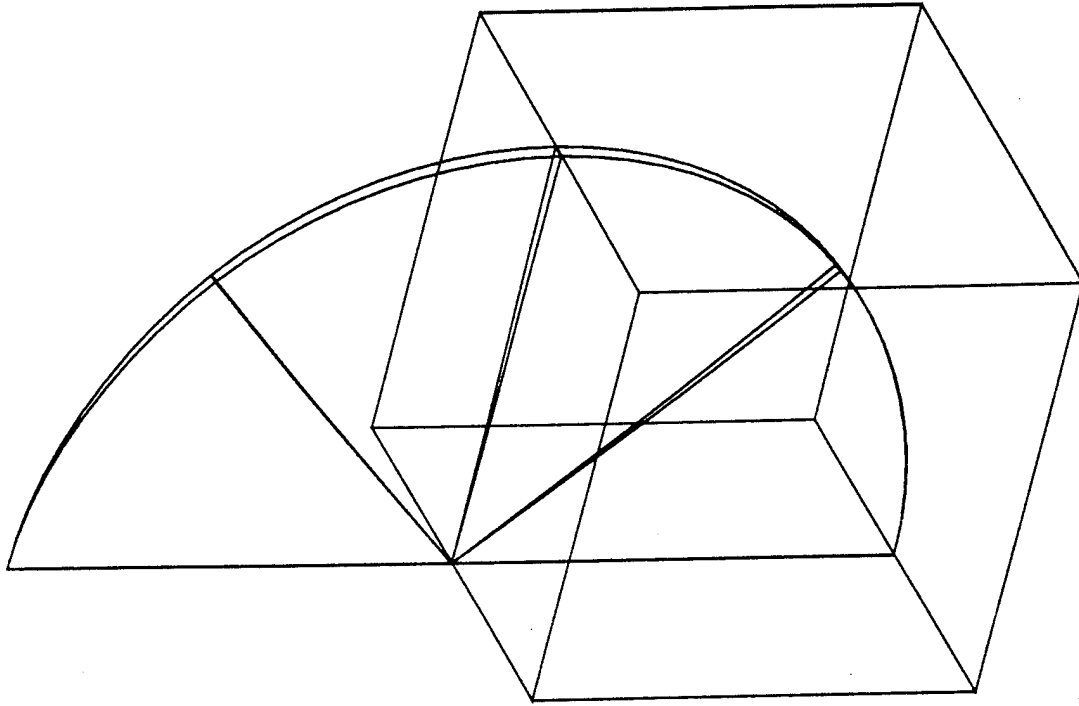


Figure 21. Finite Element Model Geometry for Rigid Wall at 1.000 Free-Field Radii From Center of Charge

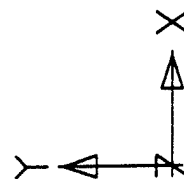
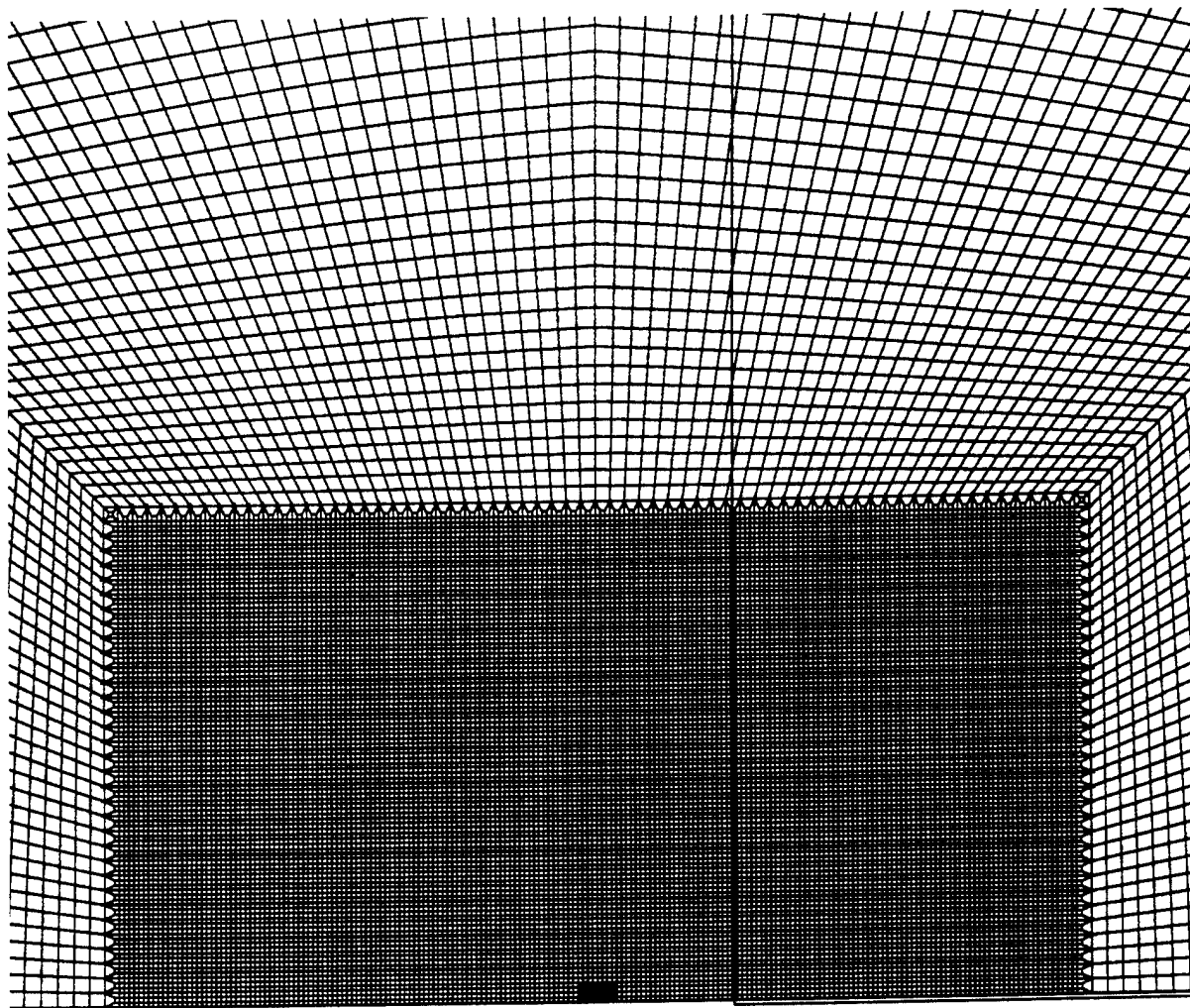


Figure 22. Close Up View of Finite Element Model in Area Near Charge for Rigid Wall at 1.000 Free-Field Radii From Center of Charge

plane. The wall itself was then modeled by just making the boundary condition on the element faces bordering the desired rigid wall location a no-flow boundary condition. Figure 23 shows the finite element model geometry for a typical case (rigid wall at 4.015 free-field radii from center of charge), from a three-dimensional perspective. The complete finite element model for this case is shown in Figure 24, from a two-dimensional perspective. A close up view of this model in the area near the charge is shown in Figure 25. The finite element models for the cases in which the rigid wall is located at 1.374 and 2.008 free-field radii from the center of the charge are similar.

The same state equations for TNT and seawater used in the "Deep Spherical Bubble" analysis were used for these analyses. Detonation was initiated at the center of the TNT charge (midpoint of the axisymmetric axis of the cylindrical charge). The initial density and specific internal energy of seawater at a depth of 1000 m was 1025 kg/m^3 and $20076 \text{ Pa m}^3/\text{kg}$, respectively; these values when used with the previous equation of state coefficients give the correct hydrostatic pressure at a depth of 1000 m.

For simplicity in model generation, the two angled faces in the models which appear to meet at the y axis (see Figures 18, 21, and 23) are actually offset a very small distance ($\pm 5 \text{ }\mu\text{m}$); they thus make an angle of $\pm 1^\circ$ not from the xy plane at $z=0$, but from the xy planes at $z = +5 \text{ }\mu\text{m}$ and $z = -5 \text{ }\mu\text{m}$, respectively. This small offset cannot be seen on any reasonable scale (it is small even in comparison with the other dimensions of the smallest elements), and permits the model to be meshed using only hexahedron elements. Since we are using a three dimensional code to model an axisymmetric two dimensional problem, the stable timestep size safety factor, normally taken as about 0.666, was increase by a factor of about 28.6 ($1/\tan(2^\circ)$), the difference between z-direction and x or y-direction element lengths for elements bordering the axisymmetric symmetry axis. This

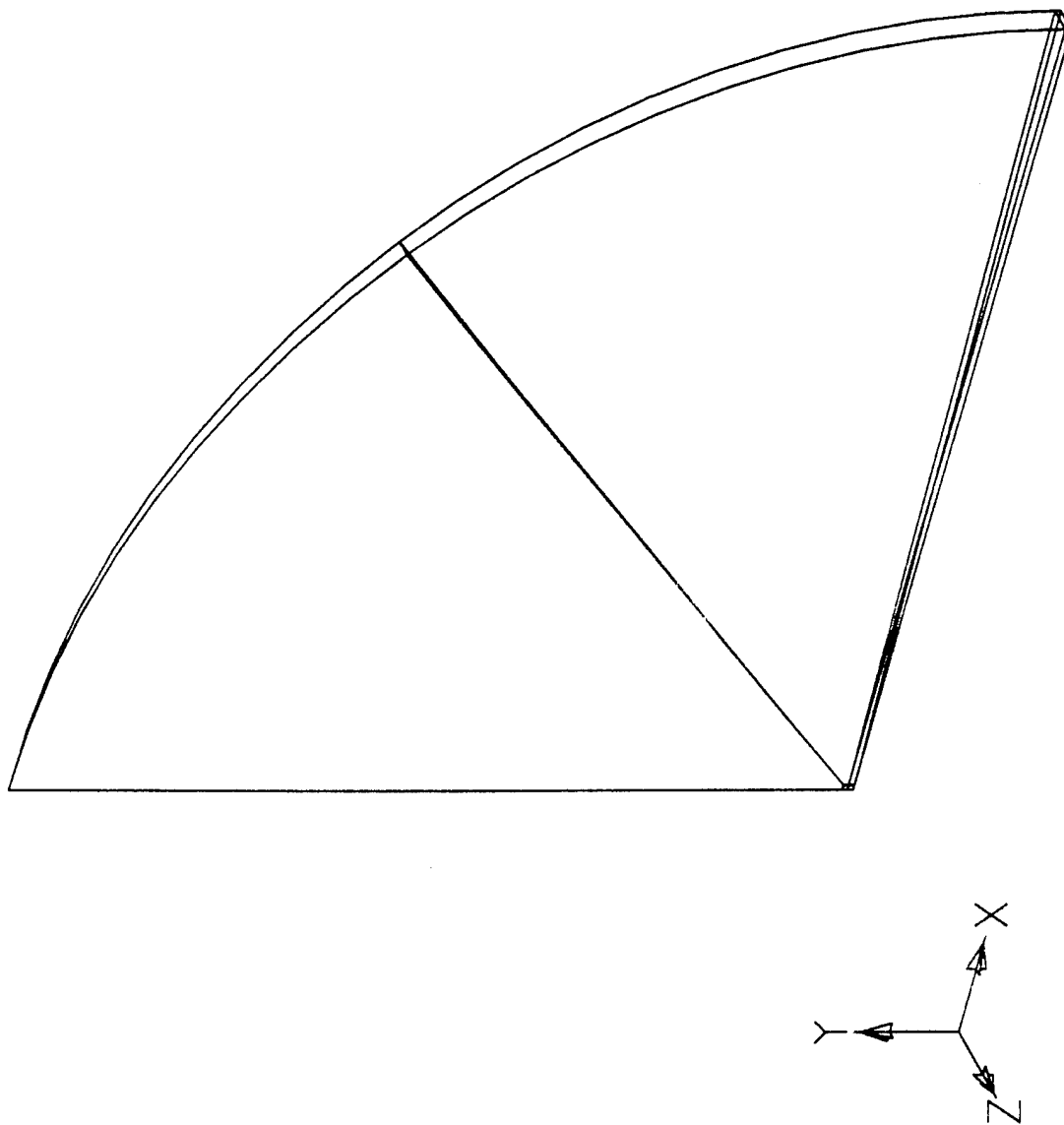


Figure 23. Finite Element Model Geometry for Rigid Wall at 4.0015 Free-Field Radii From Center of Charge

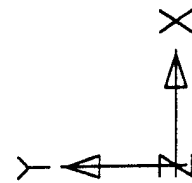
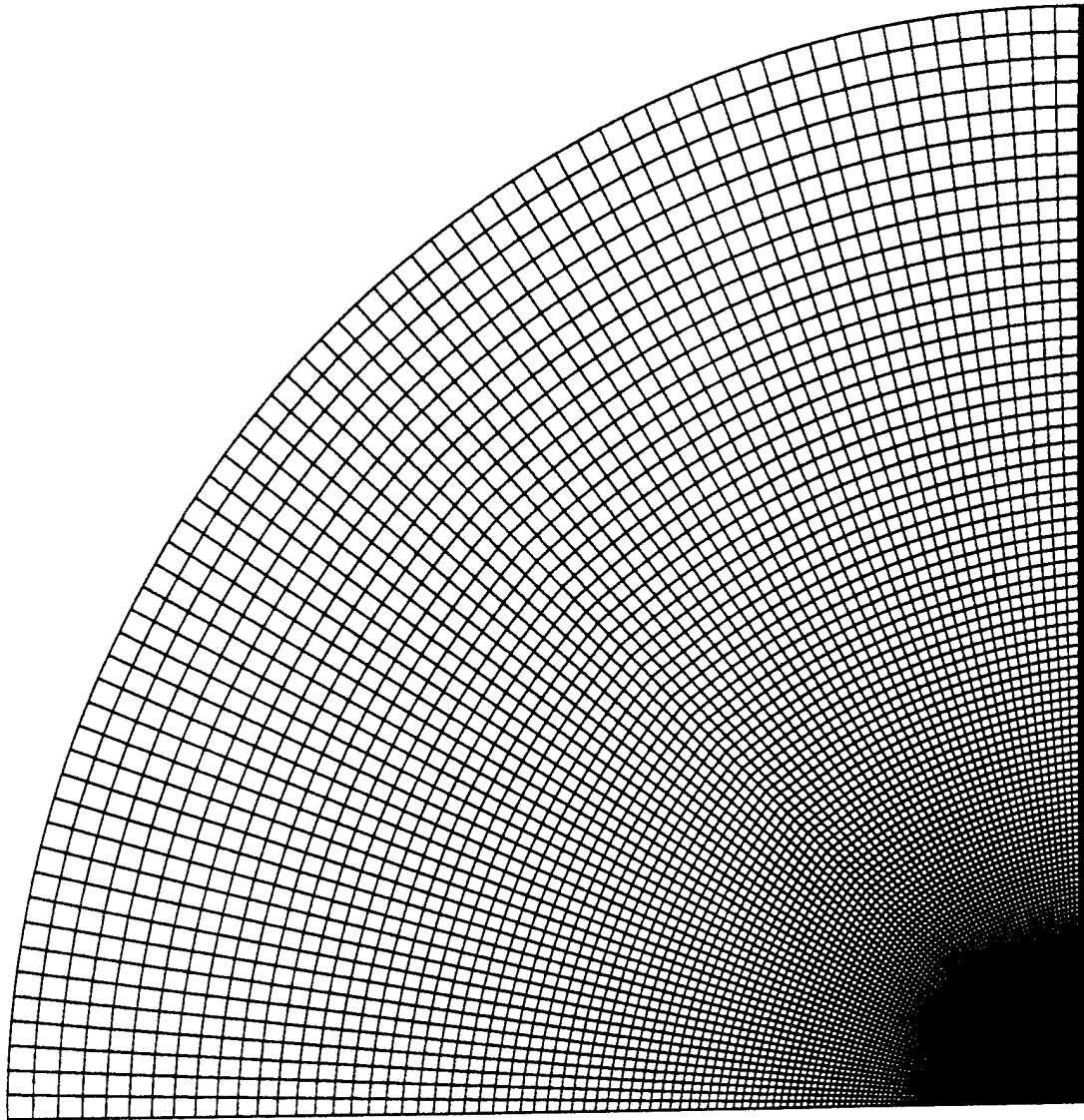


Figure 24. Finite Element Model for Rigid Wall at 4.015 Free-Field Radii From Center of Charge

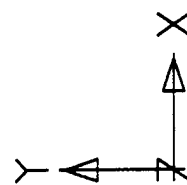
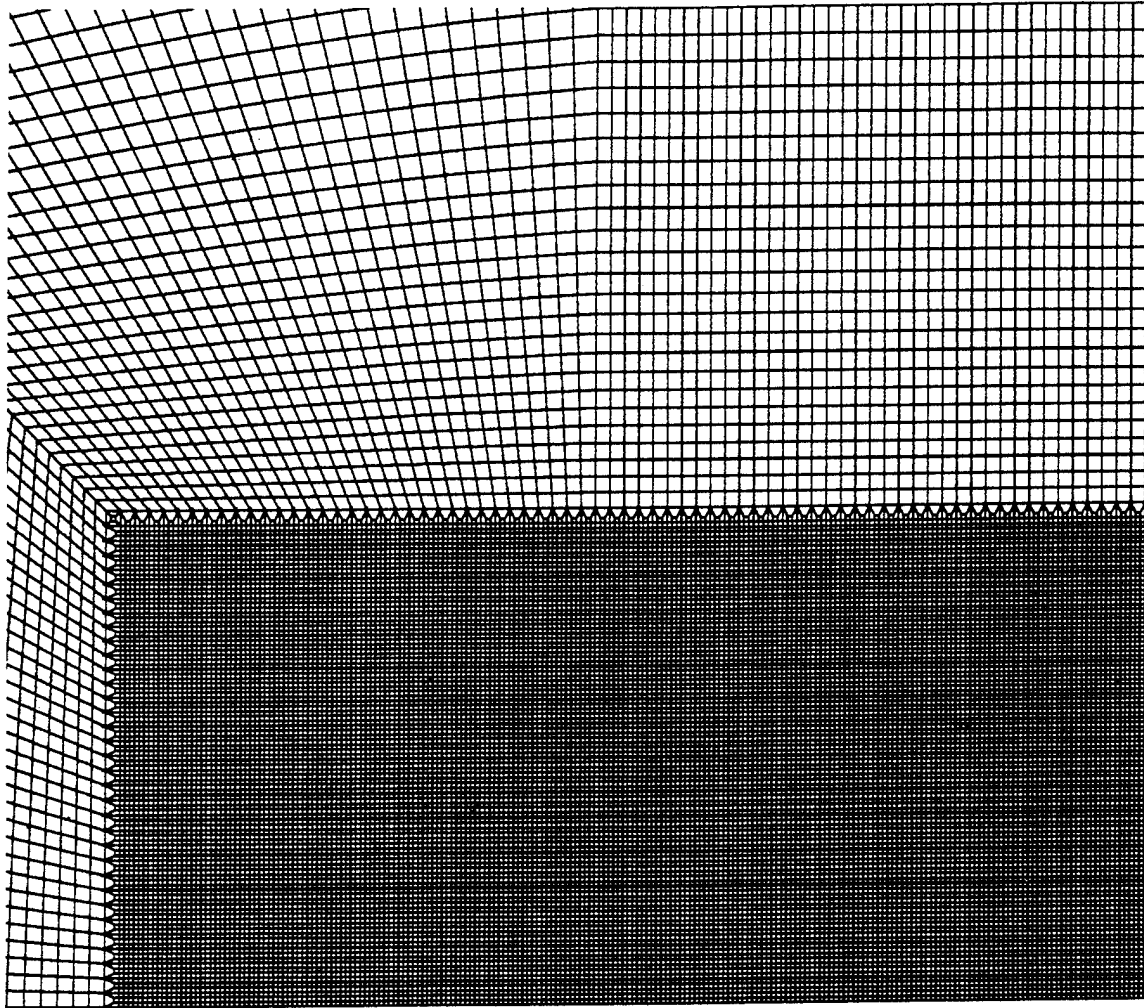


Figure 25. Close up View of Finite Element Model in Area Near Charge for Rigid Wall at 4.015 Free-Field Radii From Center of Charge

immediately reduces the solution time by a factor of 28.6, but has the potential to introduce instability if the fluid in elements far from the axis have a much higher combined wave and partial velocity than that in any elements bordering the axis. Such a situation is unlikely, and no solution instability was seen. Run times of about two hours on a RISC based Unix workstation were obtained.

Analysis results for the "volume-equivalent spherical radius" (radius of a spherical bubble with the same volume as the actual bubble) versus time behavior are plotted in Figure 26. The volume equivalent spherical radius versus time behavior for the free-field case and the cases where the rigid wall is located at 4.015 and 2.008 free-field radii ($h^* = 4.015$ and $h^* = 2.008$) from the center of the charge is shown in the upper graph, while the lower graph shows this same information for the cases in which the rigid wall is located at 1.374 and 1.000 free-field radii from the center of the charge. The $h^* = 2.008$ radius versus time curve is repeated in the lower graph in Figure 26 as a reference. From these graphs, the main effects of the rigid wall are seen to be to increase the period of oscillation, to reduce the maximum volume, and to increase the minimum volume and the amount of time when the bubble is near minimum volume (to "spread out" the minimum).

An approximate analysis by Herring [Ref. 19] for a spherical bubble with negligible internal energy expanding and collapsing in an incompressible fluid in the vicinity of a rigid wall gives the modified oscillation period as

$$T' = T \left[1 + \frac{r_{ave}}{4h} \right] \quad (5)$$

where T' is the period when the wall is present, T is the free-field period, h is the initial distance from the bubble center to the wall, and r_{ave} is the average radius of the bubble over one oscillation in the absence of the wall. Herring's analysis thus

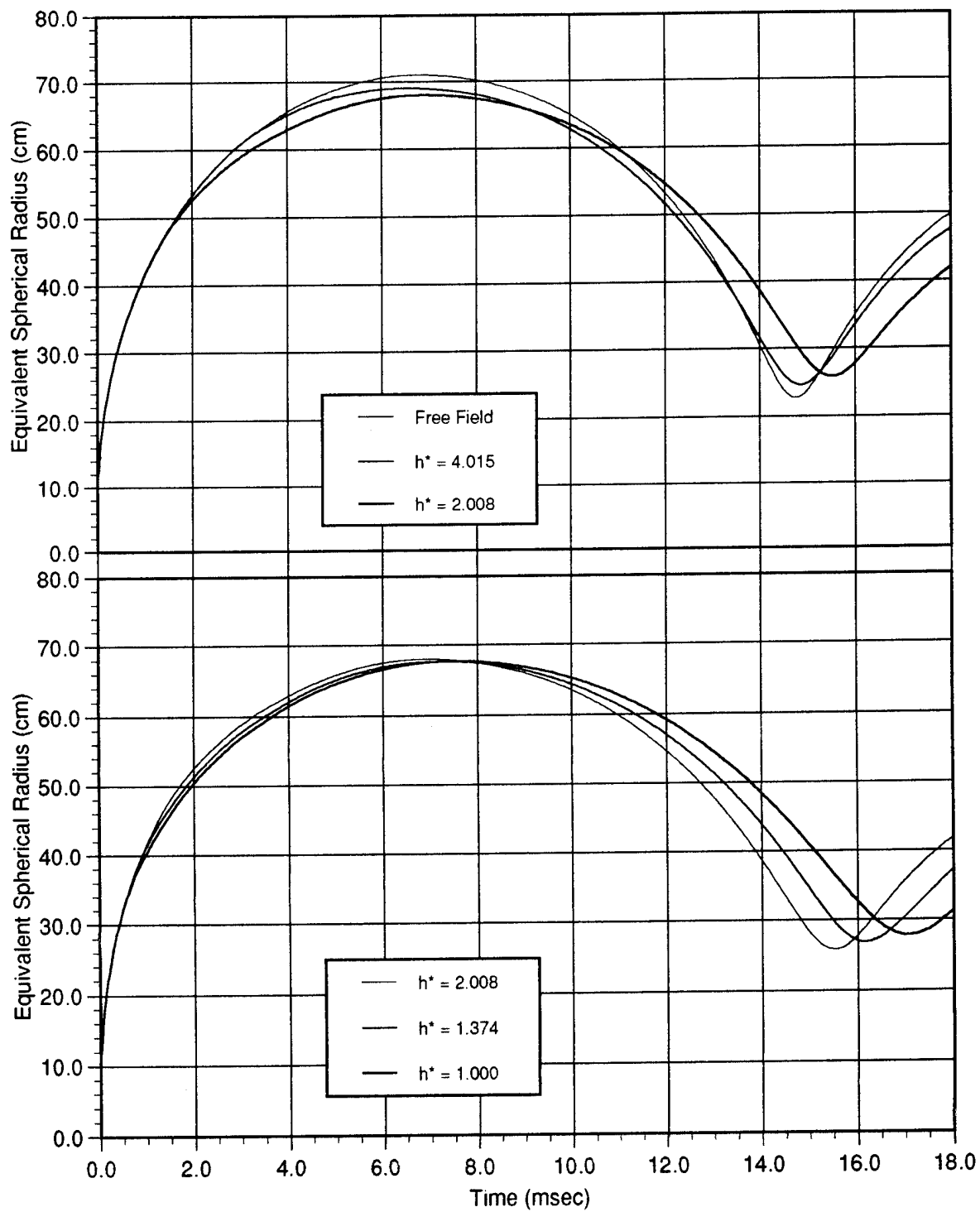


Figure 26. Equivalent Spherical Radius vs Time for Explosion Gas Bubbles Near a Rigid Wall

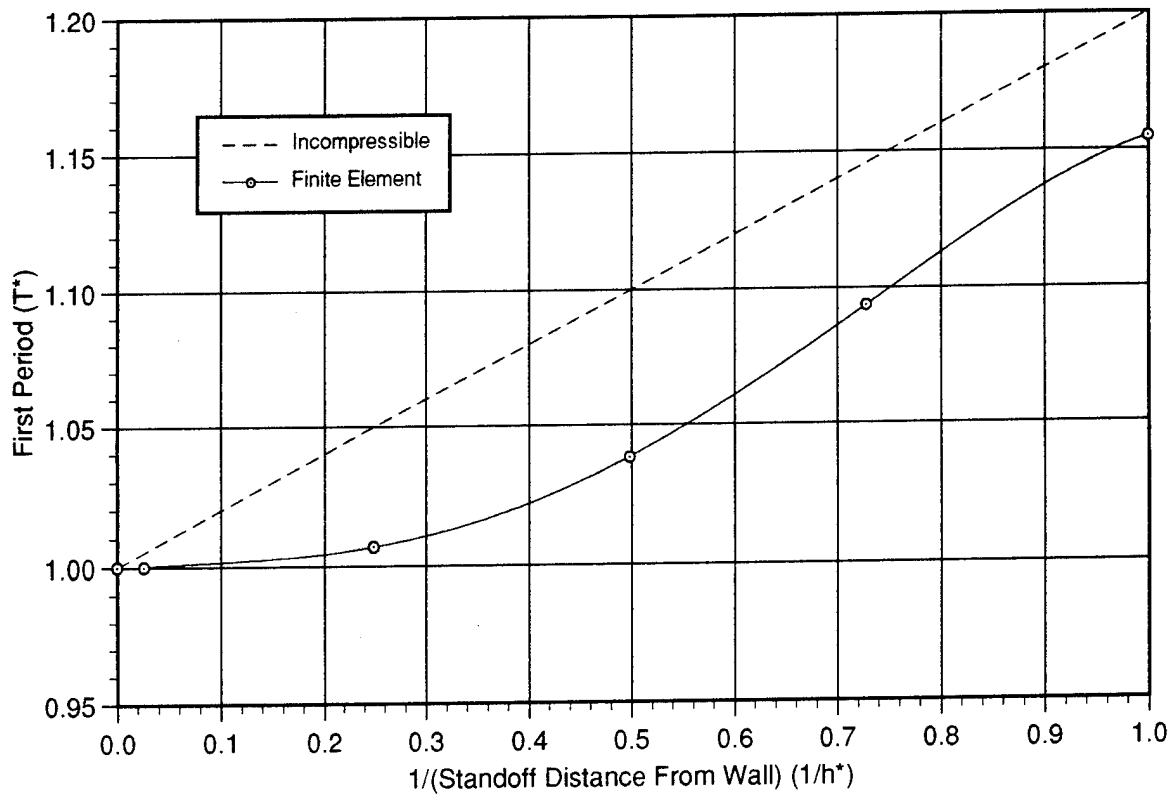


Figure 27. Non-Dimensional First Oscillation Period vs (Non-Dimensional Standoff Distance From Rigid Wall)⁻¹

predicts that the bubble period will increase linearly with the quantity $(1/h)$. While our analyses predict an increase in the bubble oscillation period when a rigid wall is present, results from our analyses indicate that the increase is not linearly proportional to the inverse of the standoff distance between the center of the charge and the wall. Results from our analyses for T^* versus $1/h^*$, where $T^* = T'/T$ is the non-dimensional period and $1/h^*$ is the inverse of the non-dimensional standoff distance (maximum free-field bubble radius divided by the initial standoff distance between the center of the charge and the wall) are plotted in Figure 27. The equivalent non-dimensional quantities predicted by Herring's formula (equation (5)), where the quantity r_{ave} was calculated by numerically integrating the radius

versus time curve from our free-field analysis and dividing that quantity by the period determined from that analysis, is shown for comparison purposes.

Examining Figure 27, it is seen that at standoff distances less than about two free-field radii ($1/h^*$ greater than about 0.5) the periods determined from our analyses increase almost linearly with $1/h^*$, and the T^* versus $1/h^*$ curve has about the same slope as that predicted by Herring's analysis. However, for standoff distances greater than about two free-field radii our analyses indicate that the wall has a smaller effect than that predicted by Herring's analysis. This is due to the compressibility of the fluid media in our analyses. In fact, because of the finite wave speed in a compressible media, there is a finite distance beyond which the wall can have no effect on the bubble within a given time frame. The peak sound speed seen during our analyses was 3733 m/s; in conjunction with the 14.761 msec bubble period from our free-field analysis, the calculated standff distance beyond which the wall can have no effect is at most 38.8 free-field radii. This point is indicated by the second open circle from the left in Figure 27 (and in other subsequent graphs). The remaining open circles each represent a data point from our analyses.

The displacement of the center of mass of the bubble as a function of time was found from results from the finite element analyses by numerically integrating the material velocity time history data. Analysis results for the displacement of the center of mass of the bubble as a function of time are shown in Figure 28. In this figure a positive displacement is a displacement away from the rigid wall, while a negative displacement is a displacement towards the wall; the rigid wall can thus be visualized as lying below the time axis. The upper graph in Figure 28 shows the displacement of the center of mass of the bubble for the cases in which the rigid wall is located at 4.015 and 2.008 maximum free-field radii from the initial position of the center of the charge, and the lower graph shows this quantity for

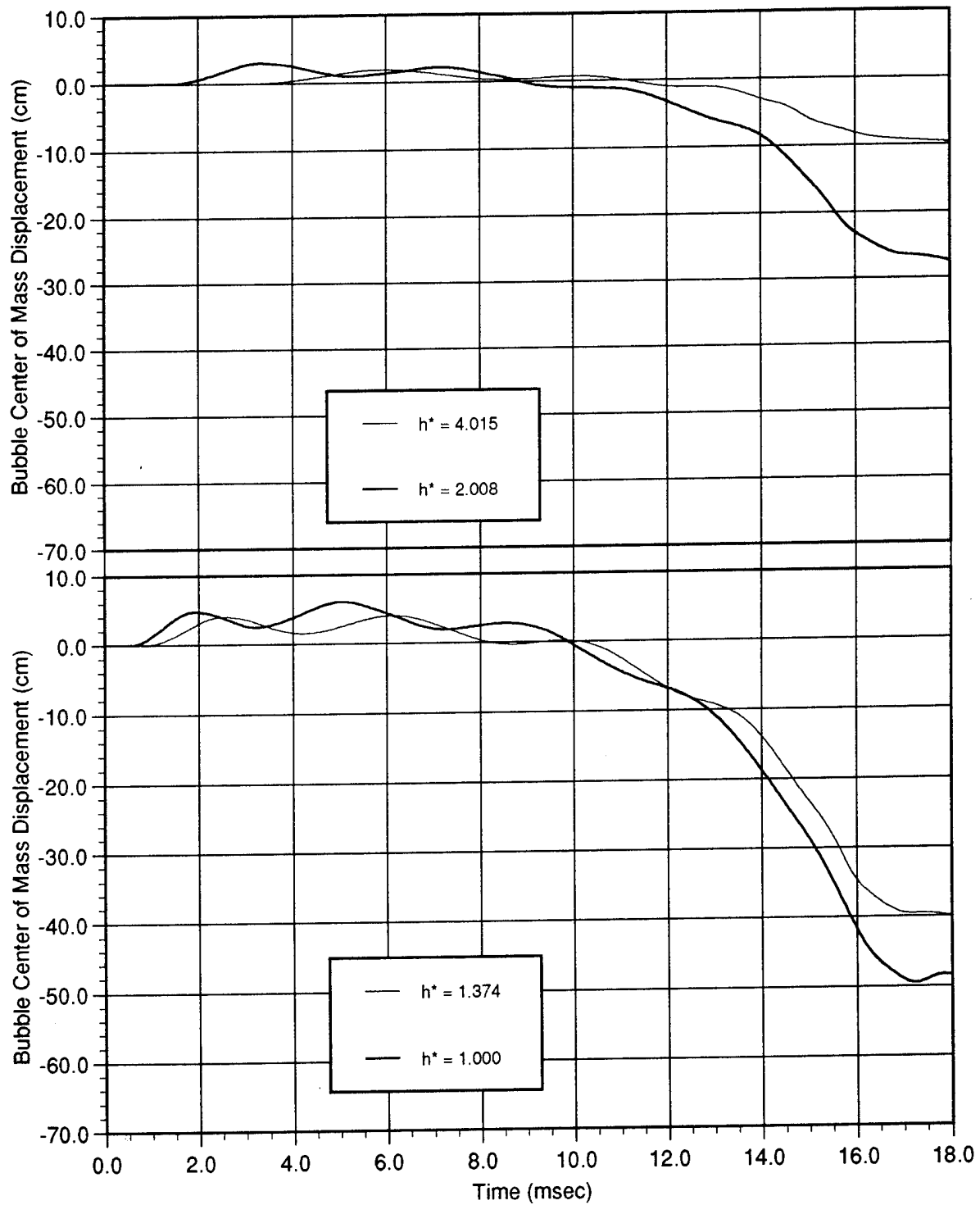


Figure 28. Displacement of Center of Mass vs Time for Explosion Gas Bubbles Near a Rigid Wall

initial standoff distances of 1.374 and 1.000 maximum free-field radii. The general characteristic of these curves is a small initial displacement away from the wall during the earlier portion of the oscillation, and then a much larger motion towards the wall as the bubble nears minimum volume. This general curve shape has been explained by Cole [Ref. 20] in terms of the wall's interference with the flow during expansion and collapse and the resultant momentum field in the fluid:

In the case of a rigid surface, the presence of the boundary interferes with radial flow of water, whether outward or inward, near a spherical surface in its vicinity. Initially, when the pressure in the gas is in excess of the hydrostatic pressure, the water on the bubble surface near the wall is less readily displaced, and the bubble surface moves away from the wall. The effect is relatively small, however, because the net pressure (in excess of hydrostatic) is positive for a short part of the bubble period, and the bubble is small during this time. When the pressure falls below hydrostatic, acceleration of the flow toward the bubble surface does not occur as readily on the side toward the wall, and the flow must be such as to bring the surface nearer to the wall. A considerable amount of momentum is imparted to a large mass of water this way when the bubble is large. As the bubble contracts, the momentum acquired becomes concentrated in a smaller mass of water near the bubble, and the velocity of flow in this region increases. The bubble surface must then move toward the wall with increasing speed as if attracted to it. This effect is so much larger than the repulsion when the pressure exceeds hydrostatic that the dominant motion is an apparent attraction increasing the bubble velocity toward the wall as it contracts, even though the momentum of the flow is decreasing in the most contracted stages.

An approximate analysis by Herring [Ref. 21], in which terms of order higher than $1/h^2$ are neglected, the bubble is assumed to remain spherical and to have negligible internal energy, the fluid is treated as incompressible, and the migration of the bubble is treated as a small correction to the motion of the bubble, gives the rate of migration of the center of the bubble as

$$\frac{dh}{dt} = \frac{3r^2}{4h^2} \frac{dr}{dt} - \frac{3}{2h^2 r^3} \int_0^t r^4 \left(\frac{dr}{d\tau} \right)^2 d\tau \quad (6)$$

where $r(t)$ is the radius at time t in the absence of the wall. In conjunction with equation (5), this equation can be separated and integrated to give the distance to the wall as a function of time. However, results obtained from doing so are known to be in poor agreement with experimental results, as this equation is very sensitive to the bubble radius versus time behavior when the bubble is near minimum radius, which is where the assumptions used in its derivation (spherical bubble with negligible internal energy, incompressible media) are least accurate [Ref. 20]. Nevertheless, this equation does contain a periodic term which changes sign at the maximum bubble radius, and a monotonic term which becomes large near the minimum radius, which again is in general agreement with the finite element results shown in Figure 28. These curves are also in qualitative agreement with results obtained by Campbell [Ref. 22] from the shallow water detonation of blasting caps near a vertical wall.

The curves in Figure 28 also show a relatively small magnitude higher frequency oscillation superimposed upon the lower frequency migration curves. We had not seen this phenomena discussed in the literature, and had not anticipated its occurrence. The primary clue to its cause is the fact that there appears to be a linear relationship between the time the high frequency oscillations begin and the standoff distance to the wall. In fact, it happens that the time the oscillations start, in milliseconds, is roughly equal to the standoff distance, in free-field radii; e.g. the oscillations start at about two milliseconds for the case where the charge center is initially two free-field radii from the wall. Using the maximum free-field radius of .7098 m and an acoustic wave velocity of 1500 m/s, the calculated time for an acoustic wave to travel from the center of the charge to the wall and back for this case is 1.89 milliseconds, which is about when the oscillations start. The higher frequency component is thus apparently due to impingement of the reflection of the initial shock wave from the boundary on the bubble.

The presence of this higher frequency component in the migration curves obtained from our finite element analysis therefore appears to be just the realization of a real, physical phenomena. The fact that the oscillation period of this high frequency component increases as the standoff distance increases can then be explained by noting that for larger standoff distances the time required for the reflected primary shock wave to reach the bubble is longer, hence the bubble has expanded to a larger radius, and so the "envelopment time" (the time required for this shock wave to transit the diameter of the bubble) is longer.

Other characteristics of the bubble can be examined in terms of the standoff distance to the rigid wall. Figure 29 shows the maximum and minimum spherical equivalent bubble radii as a function of the inverse of the standoff distance (in free-field maximum radii). The term "equivalent" is again used to indicate that these are the radii of spherical bubbles with the same volume as the actual bubbles; the plotted maximum and minimum equivalent radii are in terms of the maximum and minimum radii for the free-field bubble (70.98 cm and 22.71 cm, respectively). Note that the graphs in this figure have different vertical scales, so that while the largest reduction in the maximum equivalent radius is less than 5% of the free-field value, the largest increase in the minimum equivalent radius is over 20% of the free-field value. By analogy with the free-field case, these quantities can be viewed as being related to the energy loss of the system, a bubble with a smaller maximum radius or a larger minimum radius having less energy available for subsequent oscillations.

The displacement of the bubbles at the end of the first oscillation is another quantity of interest. The bubble pulse emitted when a bubble is near its minimum radius can be approximated as emanating from the location of the center of the bubble at this time, and if appreciable bubble migration has occurred the geometry of the bubble pulse loading problem is then changed. The top graph in Figure 30

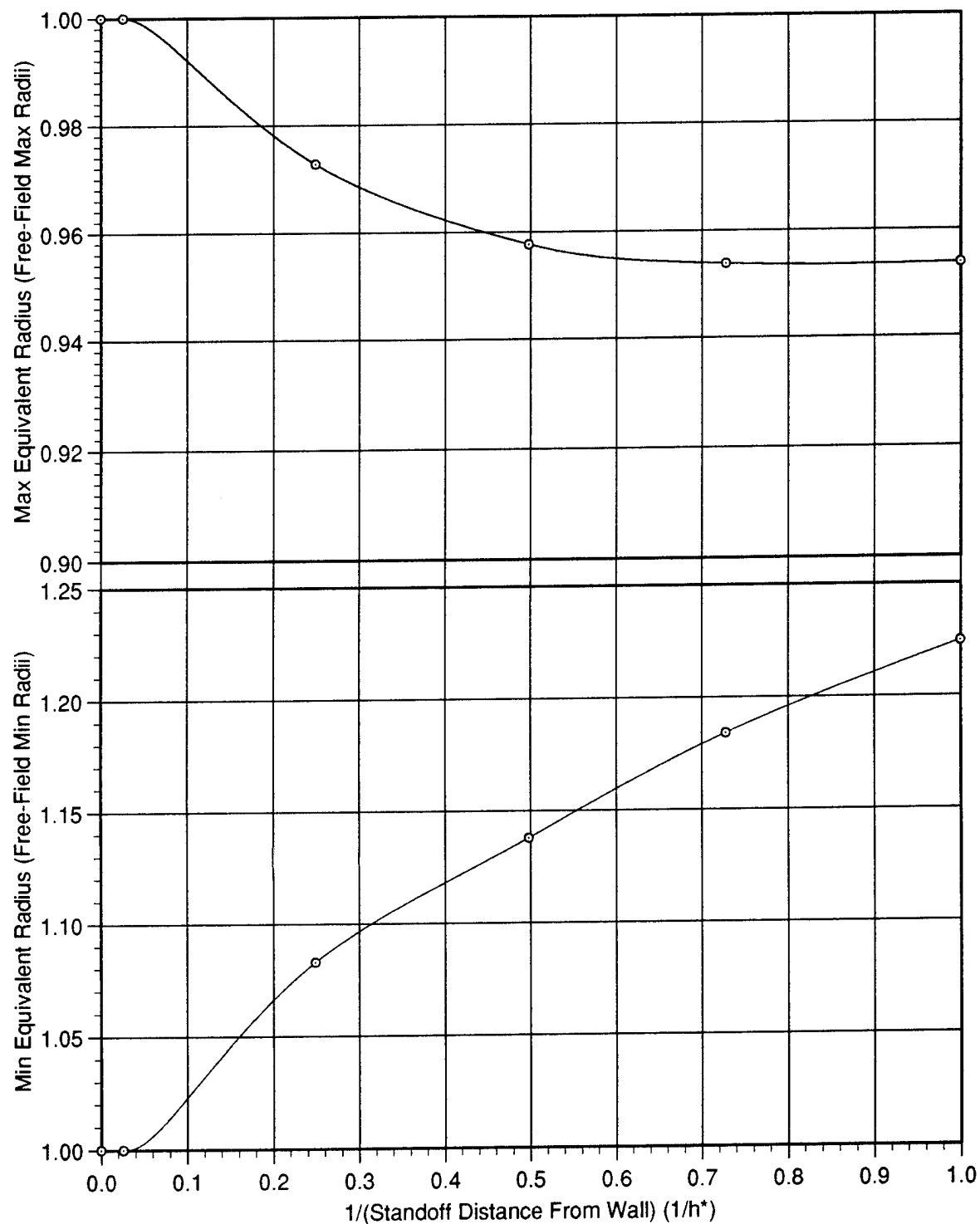


Figure 29. Displacement of Bubble Center of Mass at First Minimum and Peak Bubble Velocity Versus (Non-Dimensional Standoff Distance)⁻¹

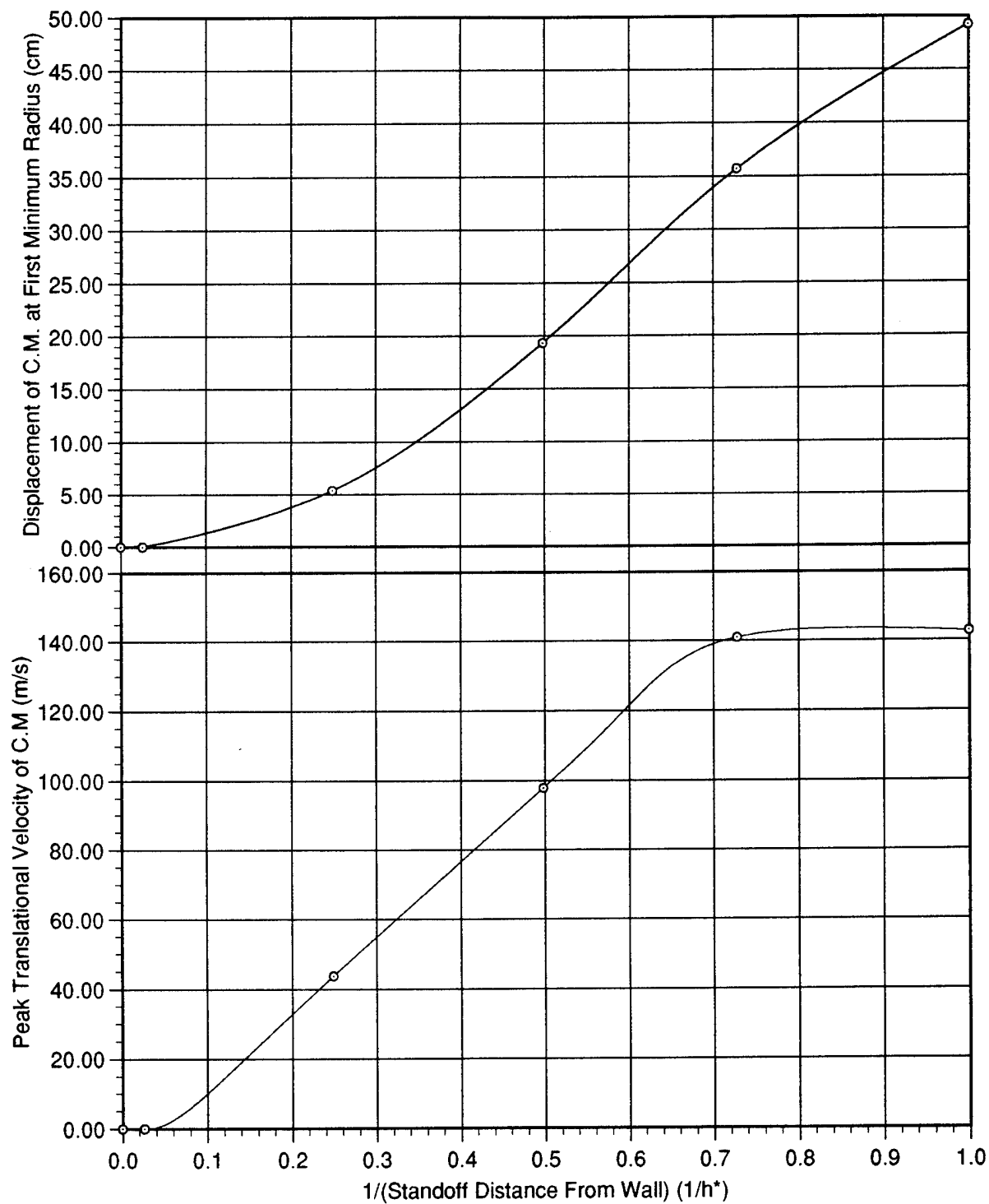


Figure 30. Maximum and Minimum Equivalent Spherical Radii Versus (Non-Dimensional Standoff Distance From Rigid Wall)⁻¹

shows, for the cases analyzed, the displacement of the center of mass of the bubbles at the the time of their first minimum radius, plotted as a function of the inverse standoff distance (in free-field maximum radii). The lower graph in this figure shows the peak velocity of the bubble center of mass, again plotted against the non-dimensional inverse standoff distance.

The shape of the bubbles for the various cases analyzed was also examined. In order to provide for meaningful comparison between the cases, the bubble shape was plotted at the same fractions of the first oscillation periods rather than at the same actual times. As the first oscillation period is different for each standoff distance, a second finite element analysis of each model was done. The first period for each case was found from the first analysis, which was then used to determine the times to ask for a complete dump of the element densities during the second analysis. Plots of the bubble shapes are provided in Appendix E, at times of 0.5, 0.8, 0.9, 0.95, 0.98, 0.99, and 1.0 first bubble periods. These plots show that for standoff distance of about two free-field radii or more, the bubble remains fairly spherical up to the time of the first minimum. In the cases for which the rigid wall is initially closer than two free-field radii, as the bubble approaches minimum volume it assumes a "kidney" shape, similar to that seen experimentally for bubbles migrating due to gravity [Ref. 23]. For the case in which the rigid wall is initially one maximum free-field radii from the center of the charge, the kidney shape evolved into a torus, indicating penetration of a wall-directed jet through the center of the bubble.

The input and postprocessing files used for the cases analyzed in this section are provided in Appendix F.

V. CONCLUSION

This report describes analysis procedures used in and results obtained by directly applying coupled Lagrangian-Eulerian and multimaterial Eulerian finite element analysis to several problems of interest in underwater shock research. The problem types analyzed encompass both classical acoustic wave-shell fluid-structure interaction and analysis of bubbles produced by the detonation of explosives underwater.

The results for the acoustic wave-shell fluid-structure interaction problems compared quite well with the analytical solutions for these problems. Results for the bubble problems analyzed were also quite satisfactory. For the one-dimensional free-field (spherical) bubble, results for the first bubble maximum radius and period were in very good agreement with results from the experiment being modeled, and the shape of the bubble radius versus time curve was similar to the theoretical result for a bubble with negligible internal energy in an incompressible media. For the other bubble problem analyzed, an explosion generated gas bubble at various distances from a rigid wall, there were fewer theoretical/experimental results available with which to make meaningful comparisons; the results obtained were in general agreement with those that were available. The large amount of data available from the analyses of a bubble at various initial standoff distances from a rigid wall provide a useful characterization of the effects of the standoff distance on the bubble.

One of the benefits of the direct finite element method used is that it does not rely on time or frequency domain approximations, so that the solution accuracy obtained is dependent only upon the fineness of the mesh used and the accuracy

with which the state equation parameters for the materials modeled are known. This method does involve a far greater number of elements than a boundary element method, however, the ever expanding capability of computers makes direct application of the finite element method using coupled Lagrangian-Eulerian and multimaterial Eulerian analysis practical for an increasing number of problems. Reasonable problem solution times can be obtained, since time-marching using an explicit finite difference technique can be very efficient even for very large problems (no eigenvalue problem need be solved).

APPENDIX A: SPHERICAL SHELL/PLANE STEP WAVE INPUT

```

$
$ MSC/DYTRAN RUN FILE : Spherical Shell/Plane Step Wave
$
START
TIME = 9999
LIMMEM = 100000
CEND
$
TITLE = Spherical Shell/Plane Step Wave
$
ENDSTEP = 99999
ENDTIME = 6.
PARAM,INISTEP,1.E-2
PARAM,MINSTEP,1.E-9
$
TYPE (NODES) = TIMEHIS
GRIDS (NODES) = 1
SET 1 = 1,37,97
GPOUT (NODES) = YVEL,ZVEL
STEPS (NODES) = 0,THRU,END,BY,1
SAVE (NODES) = 99999
$
TLOAD = 1
SPC = 1
$
BEGIN BULK
$
SET1,99,1,THRU,600
SURFACE,100,,ELEM,99
COUPLE,1,100,INSIDE,ON,ON
$
TICEUL 1
+ CYLINDER1 2 1 9. +
+ CYLINDER2 2 2 1. +
CYLINDER1 0.0 0.0 5.0 0.0 0.0 1.0 +
+ 10.0
CYLINDER2 0.0 0.0 5.0 0.0 0.0 -5.0 +
+ 10.0
$
TICVAL,1,,ZVEL,-.001,PRESSURE,.001,DENSITY,1.001
TICVAL,2,,ZVEL,0.0,PRESSURE,0.0,DENSITY,1.0
$
INCLUDE bulk.dat
$
ENDDATA
$

```

```

c
c LS-INGRID INPUT FILE : Spherical Shell/Plane Step Wave
c

c
c This file is used to create all three "parts" for this problem
c by "commenting out" 2 of the 3 parts with {curly braces} so that
c only 1 part is read in; this is repeated during execution of
c LS-INGRID for each part in turn
c

dn3d vec

mat 1 type 3 ro 1 e 1 pr .3 sigy 1 shell endmat
mat 2 type 3 ro 1 e 1 pr .3 sigy 1 endmat

c
c Part 1 : Spherical Shell
c
{
start
-1 6 -11;
-1 6 -11;
-1 6 -11;
-1 0 1
-1 0 1
-1 0 1
sfi -1 -3; -1 -3; -1 -3; sp 0 0 0 1.0
d 1 0 0 2 0 0
d 0 1 0 0 2 0
mate 1
end
}

c
c Part 2 : Dummy Elements
c
start
-1 6 -11;
-1 6 -11;
-1 6 -11;
-1 0 1
-1 0 1
-1 0 1
sfi -1 -3; -1 -3; -1 -3; sp 0 0 0 1.0
d 2 2 0 3 3 0
mate 1
end

c
c Part 3 : Fluid Elements
c
{
start
1 17 33;
1 17 33;
1 17 49 65;
0 2 4
0 2 4
-4 -2 2 4
mate 2
end
}

end

```

```

c      INGRID>NASTRAN TRANSLATION PROGRAM : Spherical Shell/Plane Step Wave
c
c      this program converts output from the preprocessor "INGRID" to
c      a MSC/NASTRAN compatible geometry data file (only one material
c      can be translated in this version)
c
      program ing2nast
      implicit double precision (a-h,o-z)
      character*5 a
      open(14,file='ingrid0',status='old')
      open(15,file='geometry.dat',status='new')
      write(*,*) 'input desired NASTRAN property number (PID):'
      read(*,*) npid
      write(*,*) 'input gridpoint numbering offset:'
      read(*,*) ngoffset
      write(*,*) 'input element numbering offset:'
      read(*,*) neoffset
      read(14,*)
      read(14,*) temp1,ngpts,nhexas,temp2,nquads
      do 100 i=1,26
         read(14,*)
100      continue
         do 200 i=1,ngpts
            read(14,991) npt,a,x,y,z
            npt = npt+ngoffset
            write(15,998) 'GRID*      ',npt,'      ',x,y,'*CONT      '
            write(15,999) '*CONT      ',z
200      continue
            if (nquads.gt.0) then
               do 300 i=1,nquads
                  read(14,993) nel,nmat,n1,n2,n3,n4
                  read(14,*)
                  nel=nel+neoffset
                  n1 = n1+ngoffset
                  n2 = n2+ngoffset
                  n3 = n3+ngoffset
                  n4 = n4+ngoffset
                  write(15,994) 'CQUAD4      ',nel,npid,n1,n2,n3,n4
300      continue
               else
                  do 400 i=1,nhexas
                     read(14,995) nel,nmat,n1,n2,n3,n4,n5,n6,n7,n8
                     nel = nel+neoffset
                     n1 = n1+ngoffset
                     n2 = n2+ngoffset
                     n3 = n3+ngoffset
                     n4 = n4+ngoffset
                     n5 = n5+ngoffset
                     n6 = n6+ngoffset
                     n7 = n7+ngoffset
                     n8 = n8+ngoffset
                     write(15,996) 'CHEXA      ',nel,npid,n1,n2,n3,n4,n5,n6,'+'
                     write(15,997) '+'      ',n7,n8
400      continue
                  endif
1991      format(i8,a5,3e20.0)
1993      format(i8,i5,4i8)
1994      format(a8,6i8)
1995      format(i8,i5,8i8)
1996      format(a8,8i8,a1)
1997      format(a8,2i8)
1998      format(a8,i16,a16,2e16.9,a8)
1999      format(a8,e16.9)
      close(14)
      close(15)
      end

```

```

!
! MSC/XL INPUT DATA STREAM : Spherical Shell/Plane Step Wave
!
Read MSCInput File="shellgeo.dat" OffsetType=None /NoExec/NoCase/Bulk
!
Select Part/1
Read MSCInput File="dummygeo.dat" OffsetType=None /NoExec/NoCase/Bulk
Refresh/Find View/1 /Erase/NoCenter/Complete/WireFrame/Undeformed/NoPlot/NoArrow
Check Grid/1t1602 Type=Duplicates View=1 PartList=0t1 Tolerance=0.005
Equivalence Grids /Update/NoExtend/NoCollapse
Define Group Name=xzsygrds Type=Grid View=1 PartList=0t1 WindowType=RubberBandWindow
CollectMode=Inside Boundary=Include RubberbandXMin=0.050091779 RubberbandXMax=1.0593952
RubberbandYMin=-0.042142798 RubberbandYMax=0.026815818
Define Group Name=yzsygrds Type=Grid View=1 PartList=0t1 WindowType=RubberBandWindow
CollectMode=Inside Boundary=Include RubberbandXMin=-0.02200132 RubberbandXMax=0.043822813
RubberbandYMin=0.036219266 RubberbandYMax=1.0455226
Define Group Name=zaxissygrds Type=Grid View=1 PartList=0t1 WindowType=RubberBandWindow
CollectMode=Inside Boundary=Include RubberbandXMin=-0.037673733 RubberbandXMax=0.059495226
RubberbandYMin=-0.051546246 RubberbandYMax=0.029950301
Edit SPC/1 GridList=xzsygrds DOF="246" /Create/Update/NoExtend/NoOverwrite
Edit SPC/1 GridList=yzsygrds DOF="156" /Create/Update/NoExtend/NoOverwrite
Edit SPC/1 GridList=zaxissygrds DOF="12456" /Create/Update/NoExtend/NoOverwrite
!
Select Part/2
Read MSCInput File="fluidgeo.dat" OffsetType=None /NoExec/NoCase/Bulk
Refresh/Find View/2 /Erase/NoCenter/Complete/WireFrame/Undeformed/NoPlot/NoArrow
Define Group Name=leftbdryels Type=Element View=2 PartList=0t2 WindowType=RubberBandWindow
CollectMode=Inside Boundary=Include RubberbandXMin=-41788.899 RubberbandXMax=-39224.691
RubberbandYMin=-0.11872614 RubberbandYMax=4.2404263
Define CFace ElementList=leftbdryels FaceNo=4 FEFaceSet=1 PartList=0t2
OutputList=1537t2560
Edit Flow/1 LoadSet=1 FEFaceSet=1 ZVel=-0.001 Pressure=1.001 Density=1.001
Edit TLoad/1 SID=1 LID=1 DynaType=Flow TableId=Blank /Create
!
Edit/Create DMatp/1 DMatRHO=7.7885 DMatE=89.097 DMatNU=0.3
Edit/Create PShell/1 MID1=1 T=0.029056
Edit/Create PShell/2 FORM=Dummy QUADPS=Gauss REF=Mid
Edit/Create EOSPol/1 EOSA1=1
Edit/Create DMat/2 DMatRHO=1 EOID=1
Edit/Create PEuler/1/3 TYPE=Hydro TICEulID=1
!
Write MSCInput File="bulk.dat" Format="Bulk" /NoExec/NoCase/Bulk

```

APPENDIX B: INFINITE CYLINDER/PLANE STEP WAVE INPUT

```
$
$ MSC/DYTRAN RUN FILE : Infinite Cylinder/Plane Step Wave
$
START
TIME = 999
CEND
$
TITLE = ELASTIC CYLINDER / STEP WAVE
$
ENDSTEP = 9999
ENDTIME = 6.
PARAM,INISTEP,1.64E-2
$
TYPE (NODES) = TIMEHIS
GRIDS (NODES) = 1
SET 1 = 1,37,73
GPOUT (NODES) = ZVEL,YVEL
STEPS (NODES) = 0,THRU,END,BY,1
SAVE (NODES) = 9999
$
TLOAD = 1
SPC = 1
$
BEGIN BULK
$
SET1,3,1,THRU,110
SURFACE,1,,ELEM,3
COUPLE,1,1,INSIDE,ON,ON
$
INCLUDE bulk.dat
$
ENDDATA
$
```

```

!
! MSC/XL INPUT FILE : Infinite Cylinder/Plane Step Wave
!
Define Point X=-0.05 Y=0 Z=1
Translate Point/1 DeltaX=0.1 DeltaY=0 DeltaZ=0 /Create
Translate Point/1t2 DeltaX=0 DeltaY=0 DeltaZ=-1 /Create
Connect Points Point1List=1 Point2List=2
Rotate Curve/1 FromX=0 FromY=0 FromZ=0 ToX=1 ToY=0 ToZ=0 Angle=-5 OffsetAngle=0 /Create
Connect Curves Curve1List=1 Curve2List=2 /Points
Rotate 35 Surface/1 FromX=0 FromY=0 FromZ=0 ToX=1 ToY=0 ToZ=0 Angle=-5 OffsetAngle=0
/Create
MeshParam Surface/1t36 Type=Quad4 U=1 V=1 Pattern=1 PID=1
Select Part/1
Connect Points Point1List=1,2 Point2List=3,4
Rotate Curve/3t4 FromX=0 FromY=0 FromZ=0 ToX=1 ToY=0 ToZ=0 Angle=-5 OffsetAngle=0 /Create
Connect Curves Curve1List=3,4 Curve2List=5,6
Rotate 35 Surface/37t38 FromX=0 FromY=0 FromZ=0 ToX=1 ToY=0 ToZ=0 Angle=-5 OffsetAngle=0
/Create
MeshParam Surface/37t108 Type=Tri3 U=1 V=1 Pattern=1 PID=2
Connect Curves Curve1List=3 Curve2List=4
Translate Surface/109 DeltaX=0 DeltaY=0 DeltaZ=-1 /Create
MeshParam Surface/109t110 Type=Quad4 U=1 V=1 Pattern=1 PID=2
Check Grid/1t368 Type=Duplicates View=1 PartList=0 Tolerance=0.005 /Update
Equivalence Grids /Update/NoExtend/NoCollapse
Renumber Grid/1t149 PartList=0 OutputList=150t225 /Update
Renumber Grid/150t225 PartList=0 OutputList=1t76 /Update
Edit SPC/1 GridList=1,2,73,74 DOF="12456" /Create
Edit SPC/1 GridList=3t72 DOF="156" /Create
Select Part/2
Define Point X=-0.05 Y=0 Z=4 CID=0
Translate Point/7 DeltaX=0 DeltaY=4 DeltaZ=0 CID=0 /Create
Connect Points Point1List=7 Point2List=8
Translate Curve/7 DeltaX=0.1 DeltaY=0 DeltaZ=0 CID=0 /Create
Connect Curves Curve1List=7 Curve2List=8 /Points
Translate Surface/111 DeltaX=0 DeltaY=0 DeltaZ=-8 CID=0 /Create
Connect Surfaces Surface1List=111 Surface2List=112
MeshParam Solid/1 Type=Hexa U=88 V=1 W=176 Pattern=1 PID=3
Define CFace ElementList=111t198 FaceNo=3 FEFaceSet=1 PartList=0t1
Define CFace ElementList=198t15598b88 FaceNo=5 FEFaceSet=2 PartList=0t1
Define CFace ElementList=15511t15598 FaceNo=6 FEFaceSet=2 PartList=0t1
Edit Flow/1 LoadSet=1 FEFaceSet=1 ZVel=-0.001 Pressure=0.001 Density=1.001 /Create
Edit Flow/2 LoadSet=1 FEFaceSet=2 /Create
Edit TLoad1/1 SID=1 LID=1 DynaType=Flow /Create
Edit TICVal/1 Name="DENSITY" Value=1 Pair=1 /Create
Edit TICVal/1 Name="ZVEL" Value=0 Pair=2 /Modify
Edit TICVal/2 Name="DENSITY" Value=1.001 Pair=1 /Create
Edit TICVal/2 Name="ZVEL" Value=-0.001 Pair=2 /Modify
Edit TICEul/1 Type=Elements TICEulList=5919t15598 MID=2 TICValId=1 Level=1 DMaterial=1
/Create
Edit TICEul/1 Type=Elements TICEulList=111t5918 MID=2 TICValId=2 Level=2 DMaterial=2
/Modify
Edit DMatE/1 DMatRHO=7.7885 DMatE=89.097 DMatNU=0.3 /Create
Edit PShell/1 MID1=1 T=0.029056 /Create
Edit Pshell1/2 FORM=Dummy QUADPS=Gauss REF=Mid /Create
Edit EOSPol/1 EOSA1=1 /Create
Edit DMat/2 DMatRHO=1 EOID=1 /Create
Edit PEuler1/3 TYPE=Hydro TICEulID=1 /Create
Write MSCInput File="bulk.dat" Format="Bulk" /NoExec/NoCase/Bulk
!

```


APPENDIX C: A POLYNOMIAL STATE EQUATION FOR SEAWATER

A straightforward process for fitting Gruneisen state equation data to the polynomial state equation usually found in most advanced finite element programs is discussed, and polynomial state equation parameters for pure water and seawater are obtained from published values of the Gruneisen state equation parameters for pure water.

GRUNEISEN EQUATION OF STATE

The Gruneisen state equation relates the pressure p_g , the condensation μ , and the specific internal energy E by:

In compression:

$$p_g(\mu, E, \gamma_0, \rho_0, C, a, S_1, S_2, S_3) := \frac{\rho_0 C^2 \mu \left[1 + \left(1 - \frac{\gamma_0}{2} \right) \mu - \frac{a}{2} \mu^2 \right]}{\left[1 - (S_1 - 1) \mu - S_2 \left(\frac{\mu^2}{\mu + 1} \right) - S_3 \left[\frac{\mu^3}{(\mu + 1)^2} \right] \right]^2} + (\gamma_0 + a\mu) \cdot E$$

In tension:

$$p_g(\mu, E, \gamma_0, \rho_0, C, a) := \rho_0 C^2 \mu + (\gamma_0 + a\mu) \cdot E$$

In these equations, p_g is the local pressure, which is a function of the condensation μ ($\mu = (\rho - \rho_0)/\rho_0$), related by the six parameters γ_0 , $\rho_0 C^2$, a , S_1 , S_2 , and S_3 , and the specific internal energy per unit volume E and condensation μ , related by the two parameters γ_0 and 'a'. Further explanation of this state equation is provided by Gurtman et al [Ref. 24] and by Hallquist and Stillman [Ref. 25].

POLYNOMIAL EQUATION OF STATE

A typical FEM program polynomial state equation is:

In compression

$$p_p(\mu, E, a_1, a_2, a_3, b_0, b_1, b_2) := a_1 \mu + a_2 \mu^2 + a_3 \mu^3 + (b_0 + b_1 \mu + b_2 \mu^2) \cdot E$$

In tension

$$p_p(\mu, E, a_1, b_0, b_1) := a_1 \mu + (b_0 + b_1 \mu) \cdot E$$

In these equations, p_p is a function of μ , related by three parameters (a_1 , a_2 , and a_3), and E and μ , related by the parameters b_0 , b_1 , and b_2 .

CURVE FITTING

The appropriate coefficients for converting Gruneisen state equation data to polynomial state equation data can be determined as follows:

Matching terms multiplying E yields:

$$b_0 = \gamma_0$$

$$b_1 = a$$

$$b_2 = 0$$

Matching the tension equations yields:

$$a_1 = \rho_0 C^2$$

The remaining polynomial coefficients a_2 and a_3 can then be found by fitting the terms not multiplying E in the Gruneisen state equation for compression with the terms in the polynomial state equation also not multiplying E, over the range for which the Gruneisen state equation is valid or the range the polynomial state equation is to be used. This procedure is carried out below for pure water.

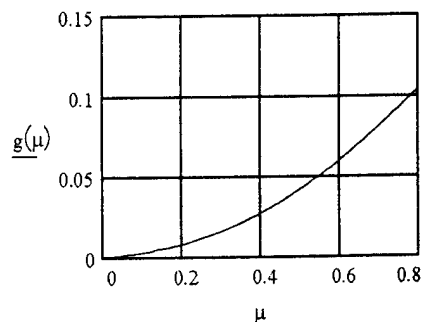
WATER EOS FOR $0 < \mu < 0.8$ ($\rho_0 < \rho < 1.8\rho_0$)

$s_1 := 2.56$	$s_2 := -1.986$	$s_3 := 0.2268$	Gruneisen Coefficients (g - cm - μ s) [Ref. 26, 27]
$a := 1.3937$	$\gamma_0 := 0.4934$		
$\rho_0 := 1.0$	$c := 0.1415$		

Then letting μ vary discretely over the range of validity of the Gruneisen state equation, and defining the function $g(\mu)$ that is to be approximated with the cubic function $h(\mu)$ (which has coefficients a_1 , a_2 , and a_3 - the terms in both state equations multiplying E are already matched), we can plot $g(\mu)$ as a function of μ .

$$\mu := 0.0, 0.01, \dots, 0.8$$

$$g(\mu) := \frac{\rho_0 \cdot C^2 \cdot \mu \cdot \left[1 + \left(1 - \frac{\gamma_0}{2} \right) \cdot \mu - \frac{a}{2} \cdot \mu^2 \right]}{\left[1 - (s_1 - 1) \cdot \mu - s_2 \cdot \left(\frac{\mu^2}{\mu + 1} \right) - s_3 \cdot \left[\frac{\mu^3}{(\mu + 1)^2} \right] \right]^2}$$



An examination of this plot shows that a cubic polynomial should do a reasonable job of approximating this function

A very simple method to determine the coefficients a_2 and a_3 (a_1 is already known) such that the cubic polynomial $h(\mu)$ approximates $g(\mu)$ in this case is to match the functions h and g at two non-zero points. The points $\mu = 0.3$ and $\mu = 0.6$ are a reasonable choice.

$$a_1 := \rho_0 \cdot C^2 \quad a_1 = 0.02002 \quad \mu_1 := 0.3 \quad \mu_2 := 0.6$$

Solving 2-equations in 2-unknowns then gives

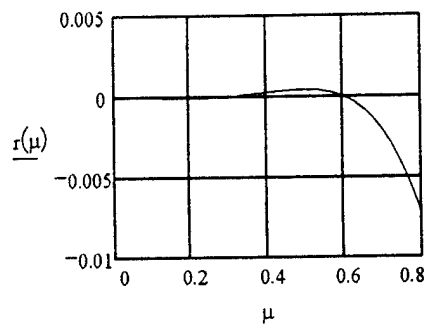
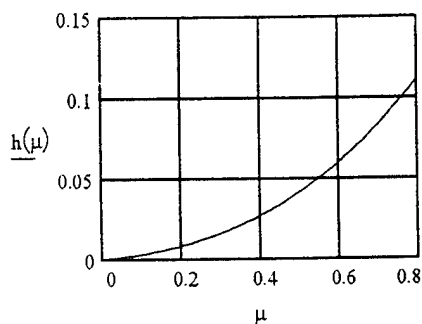
$$\begin{pmatrix} a_2 \\ a_3 \end{pmatrix} := \begin{pmatrix} \mu_1^2 & \mu_1^3 \\ \mu_2^2 & \mu_2^3 \end{pmatrix}^{-1} \cdot \begin{pmatrix} g(\mu_1) - a_1 \mu_1 \\ g(\mu_2) - a_1 \mu_2 \end{pmatrix} \quad \begin{pmatrix} a_2 \\ a_3 \end{pmatrix} = \begin{pmatrix} 0.08432 \\ 0.08014 \end{pmatrix}$$

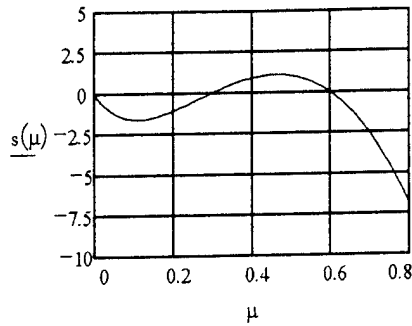
We can then plot $h(\mu)$, the residual error, and the % conversion error:

$$h(\mu) := a_1 \mu + a_2 \mu^2 + a_3 \mu^3$$

$$\text{residual: } r(\mu) := g(\mu) - h(\mu)$$

$$\% \text{ error: } s(\mu) := 100 \cdot \frac{r(\mu)}{g(\mu)}$$





Examining these plots, we see that this is a reasonably good conversion of the Gruneisen state equation to a polynomial equation of state, particularly for typical condensation values of less than 0.5. It could obviously be "tuned" for less error over a smaller condensation range of interest. In addition, a more sophisticated procedure for finding the best values for a_2 and a_3 could be used, i.e. minimize the square of the residual error over the condensation range of interest formally. In this case, the small difference between the two state equations obtained is probably already within the margin of uncertainty which results from the uncertainty with which the parameters in the Gruneisen state equation are known, so further refinement was not carried out.

SEAWATER EOS FOR $0 < \mu < 0.8$ ($\rho_0 < \rho < 1.8\rho_0$)

To extend the above polynomial state equation for use with seawater, the density and acoustic wave velocity of seawater were used in place of the density and acoustic wave velocity of pure water. Taking these as 1.025 g/cm^3 and $0.1500 \text{ cm}/\mu\text{s}$, the a_1 coefficient becomes

$$a_1 := 0.02306$$

The remaining constants determined above for pure water were used for seawater; this polynomial EOS is thus a first-order correction to the pure water polynomial EOS.

APPENDIX D: DEEP SPHERICAL BUBBLE INPUT

```
$
$ MSC/DYTRAN RUN FILE : Deep Spherical Bubble
$
START
TIME = 999
CEND
$
TITLE = SPHERICAL BUBBLE
$
ENDSTEP = 99999
ENDTIME = 0.05
PARAM,INISTEP,5.E-7
PARAM,RHOCUT,1.E-6
PARAM,ROHYDRO,1.E-6
PARAM,ROMULTI,1.E-6
$
TYPE (MATHIS) = TIMEHIS
MATS (MATHIS) = 1
SET 1 = 1
MATOUT (MATHIS) = VOLUME
STEPS (MATHIS) = 0,THRU,END,BY,10
SAVE (MATHIS) = 99999
$
BEGIN BULK
$
INCLUDE bulk.dat
$
ENDDATA
$
```

```

!
! MSC/XL INPUT FILE : Deep Spherical Bubble
!
Edit ApplicationTable DuplicateElementTolerance=0.0001
Edit ApplicationTable DuplicateGridTolerance=0.0001
Edit ApplicationTable DuplicateFEFaceTolerance=0.0001
Edit ApplicationTable DegenerateElementTolerance=0.0001
Define Point X=0.03526 Y=-0.001763 Z=-0.001763 CID=0
Translate Point/1 DeltaX=0 DeltaY=0.003526 DeltaZ=0 CID=0 /Create
Connect Points Point1List=1 Point2List=2
Translate Curve/1 DeltaX=0 DeltaY=0 DeltaZ=0.003526 CID=0 /Points/Create
Connect Curves Curve1List=1 Curve2List=2 /Points
Translate Surface/1 DeltaX=-0.01175333 DeltaY=0 DeltaZ=0 CID=0 /Points/Create
Connect Surfaces Surface1List=2 Surface2List=1 /Points
MeshParam Solid/1 Type=Hexa U=1 V=1 W=3 Pattern=1 PID=1
Define Point X=352.6 Y=-17.63 Z=-17.63 CID=0
Translate Point/9 DeltaX=0 DeltaY=35.26 DeltaZ=0 CID=0 /Create
Connect Points Point1List=9 Point2List=10
Translate Curve/3 DeltaX=0 DeltaY=0 DeltaZ=35.26 CID=0 /Points/Create
Connect Curves Curve1List=3 Curve2List=4 /Points
Connect Surfaces Surface1List=1 Surface2List=3 /Points
MeshParam Solid/2 Type=Hexa U=1 V=1 W=996 Pattern=1 PID=1 WSpace=500
Check Grid/1t100000 Type=Duplicates View=1 PartList=0 Tolerance=0.0001 /Update
Equivalence Grids /Update/NoExtend/NoCollapse
Edit EOSJWL/1 EOSA=3.712e+11 EOSB=3.231e+09 EOSR1=4.15 EOSR2=0.95 EOSOmega=0.3 /Create
Edit DetSph/1 MID=1 DetX=0 DetY=0 DetZ=0 DetVel=6390 DetTime=0 /Create
Edit EOSPol/2 EOSA1=2.306e+09 EOSA2=8.432e+09 EOSA3=8.014e+09 EOSB0=0.4934 EOSB1=1.3937
EOSB2=0 EOSB3=Blank /Create
Edit DMat/1 DMatRHO=1630 EOID=1 /Create
Edit DMat/2 DMatRHO=1025 EOID=2 /Create
Edit TICVal/1 Name="DENSITY" Value=1630 Pair=1 /Create
Edit TICVal/1 Name="SIE" Value=4290000 Pair=2 /Modify
Edit TICVal/2 Name="DENSITY" Value=1025 Pair=1 /Create
Edit TICVal/2 Name="SIE" Value=3750.4 Pair=2 /Modify
Edit TICEul/1 Type=Elements TICEulList=1t3 MID=1 TICValId=1 Level=9 DMaterial=1 /Create
Edit TICEul/1 Type=Elements TICEulList=4t999 MID=2 TICValId=2 Level=1 DMaterial=2 /Modify
Edit PEuler1/1 TYPE=MMHydro TICEulID=1 /Create
Write MSCInput File="bulk.dat" Format="Bulk" /NoExec/NoCase/Bulk
!

```

```

c      VOLUME TO RADIUS CONVERSION PROGRAM : Deep Spherical Bubble
c
c      program to convert volume of a 1-D wedge to spherical radius
c
      program vol2rad
      open(14,file='th_volume_g11.ext',status='old')
      open(15,file='r_vs_t.ext',status='new')
      do 100 i=1,9
        read(14,*)
100    continue
        write(*,*) '# of lines in volume time history file?'
        read(*,*) n
        n = n-9
        do 200 i=1,n
          read(14,*) t,v
          t = t * 1000
          r = ((300.*v)**(1./3.))*100
200    write(15,*) t,r
        continue
      close(14)
      close(15)
      end

```


APPENDIX E: BUBBLES NEAR RIGID BOUNDARIES-SHAPES

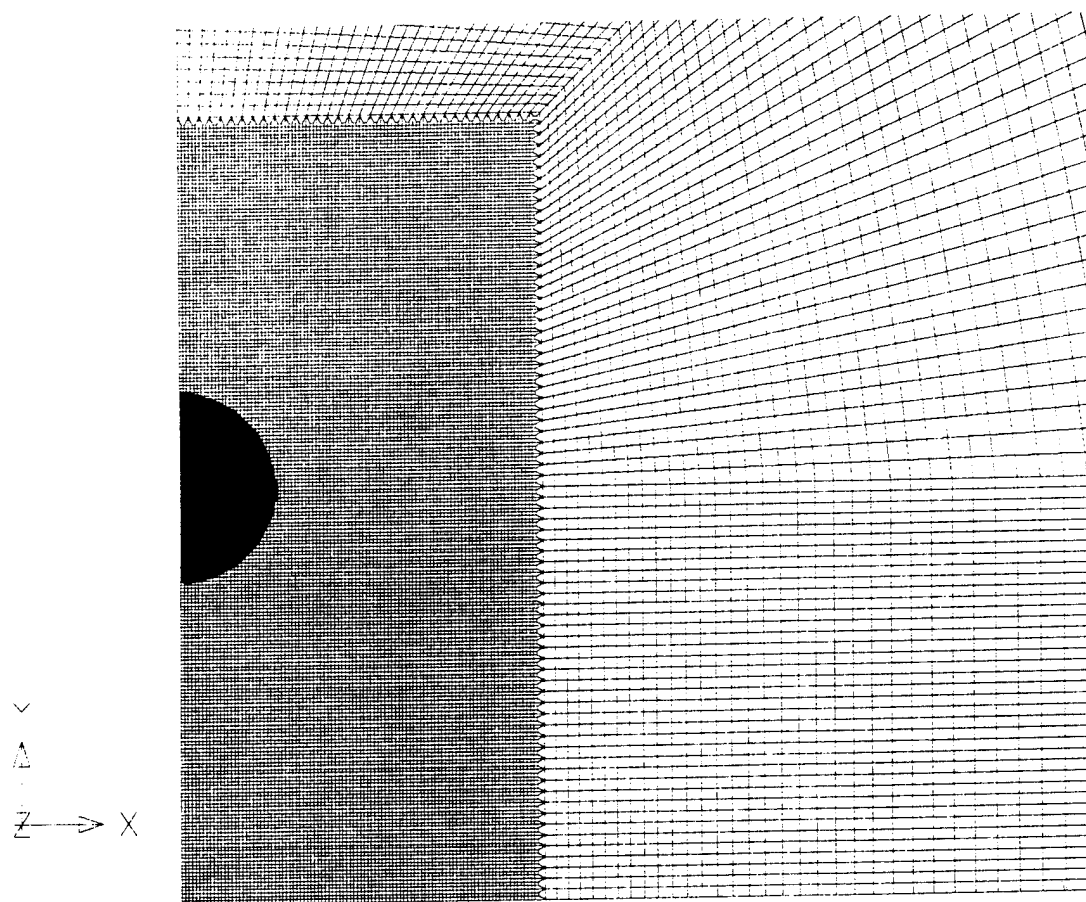


Figure 31. Bubble Shape for Rigid Wall at $h^*=4.015$ at Time $t=0.50T$

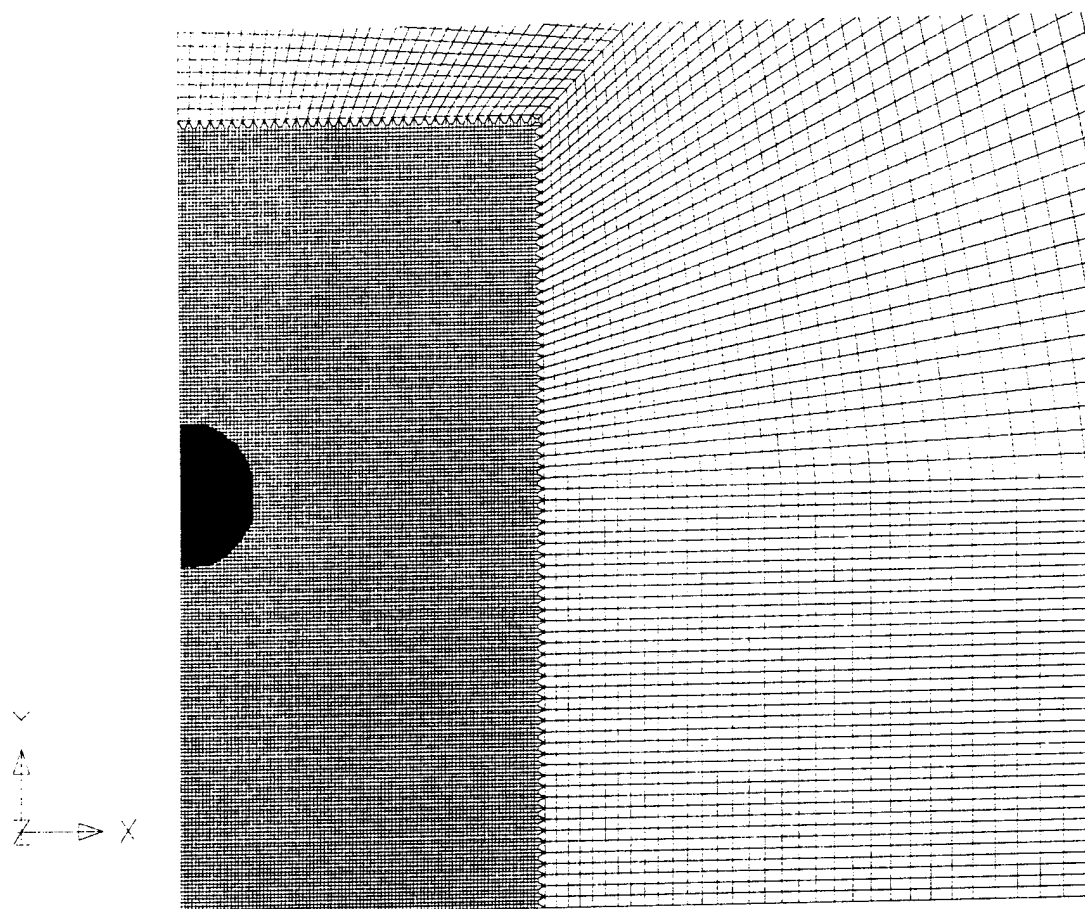


Figure 32. Bubble Shape for Rigid Wall at $h^*=4.015$ at Time $t=0.80T$

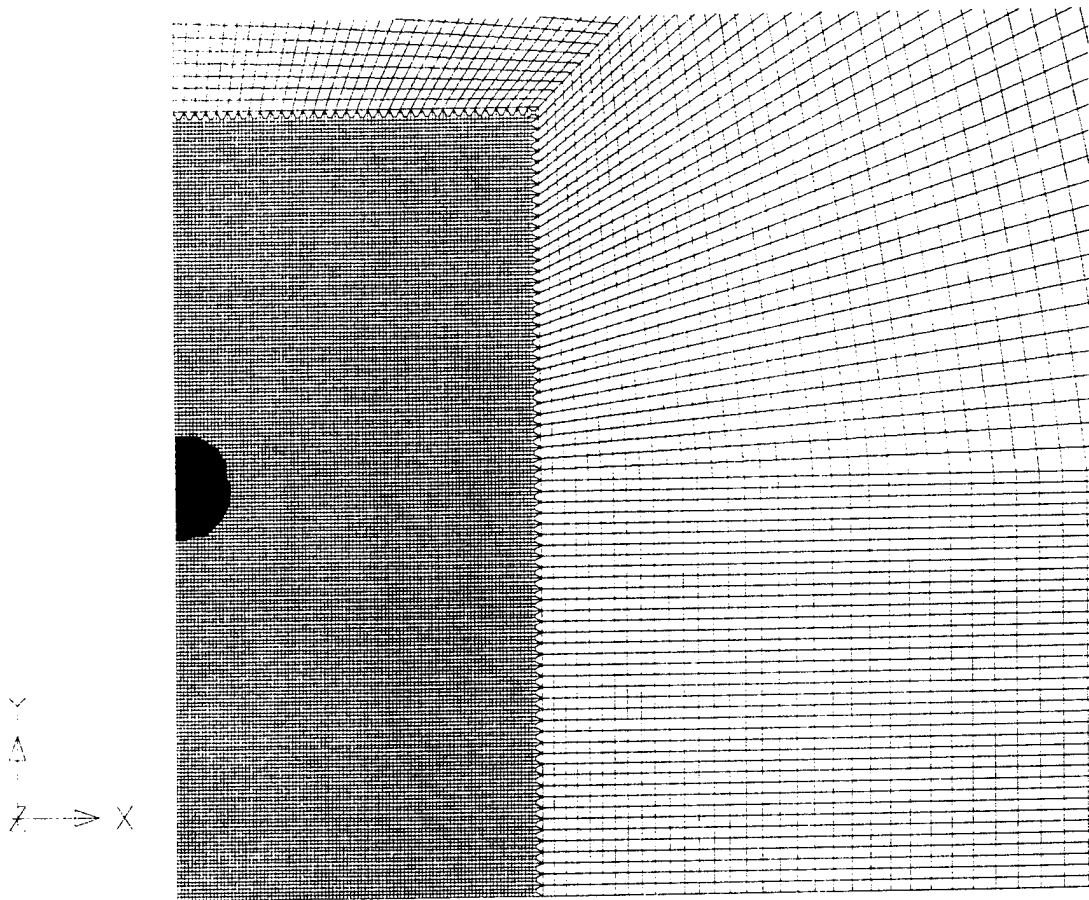


Figure 33. Bubble Shape for Rigid Wall at $h^*=4.015$ at Time $t=0.90T$

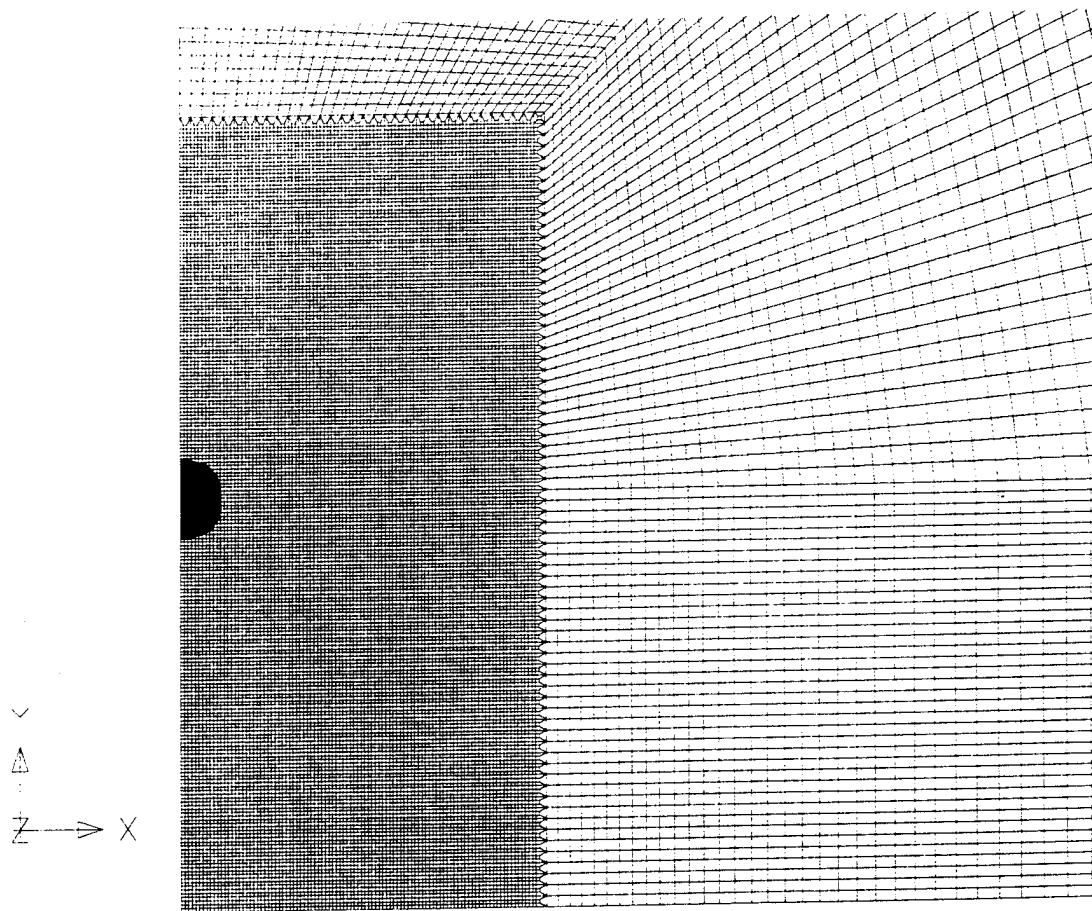


Figure 34. Bubble Shape for Rigid Wall at $h^*=4.015$ at Time $t=0.95T$

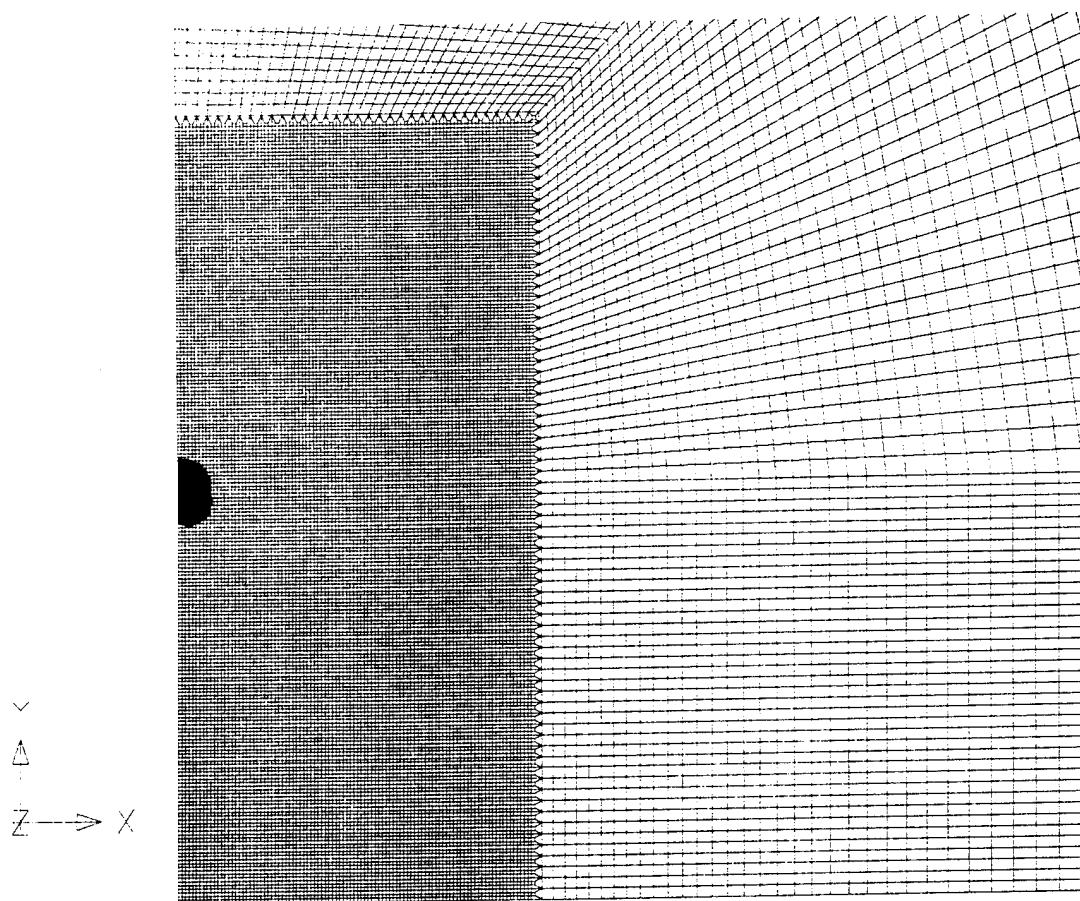


Figure 35. Bubble Shape for Rigid Wall at $h^*=4.015$ at Time $t=0.98T$

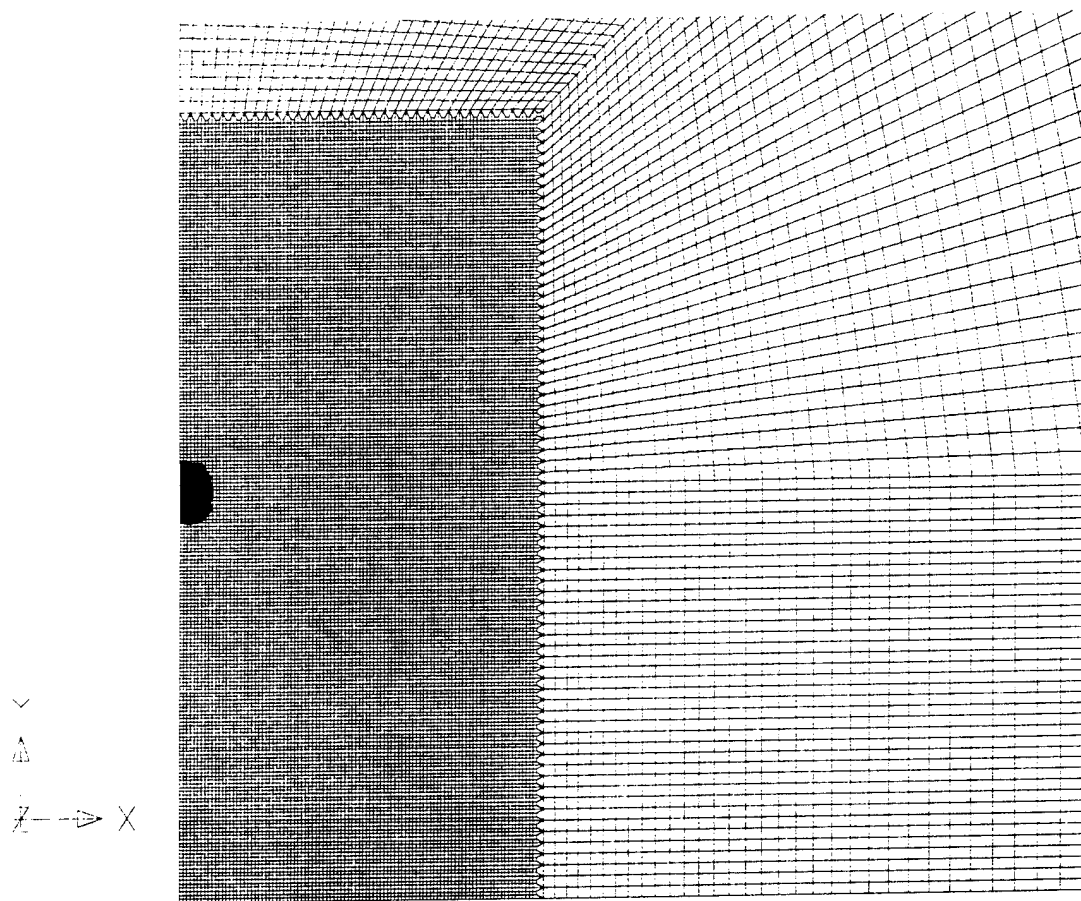


Figure 36. Bubble Shape for Rigid Wall at $h^*=4.015$ at Time $t=0.99T$

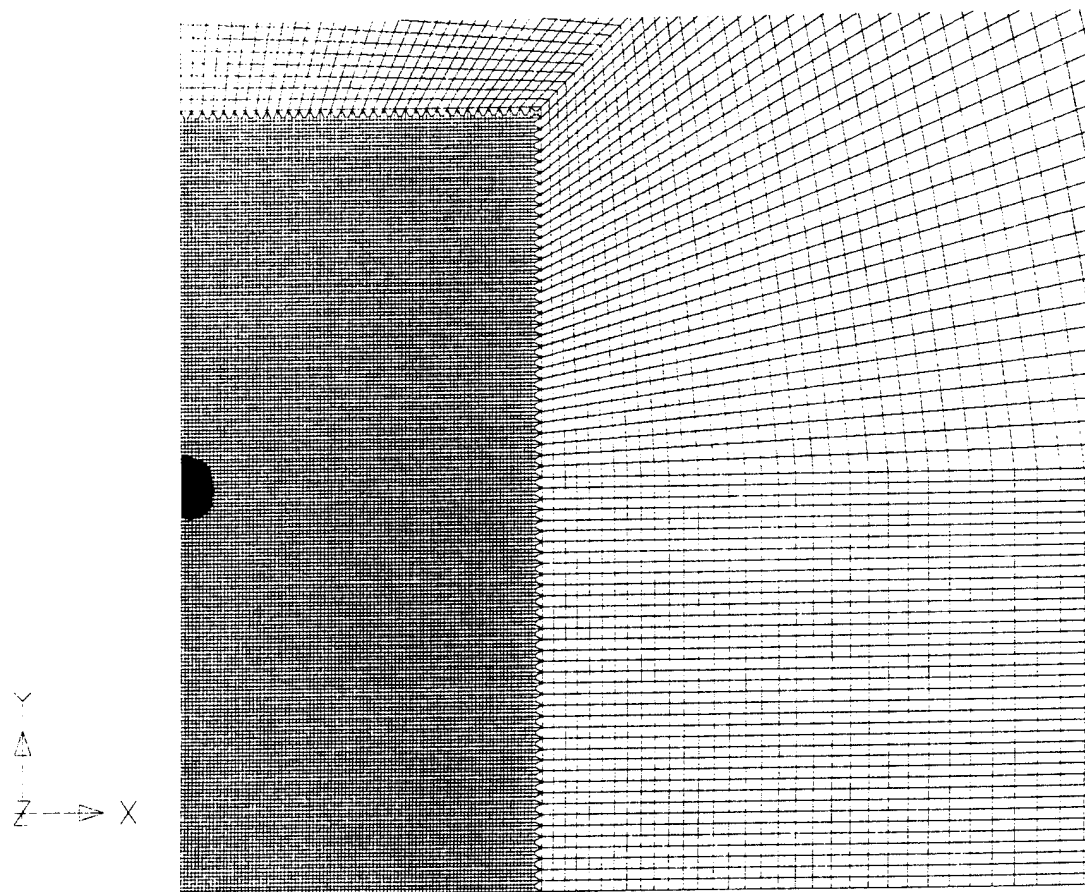


Figure 37. Bubble Shape for Rigid Wall at $h^*=4.015$ at Time $t=1.00T$

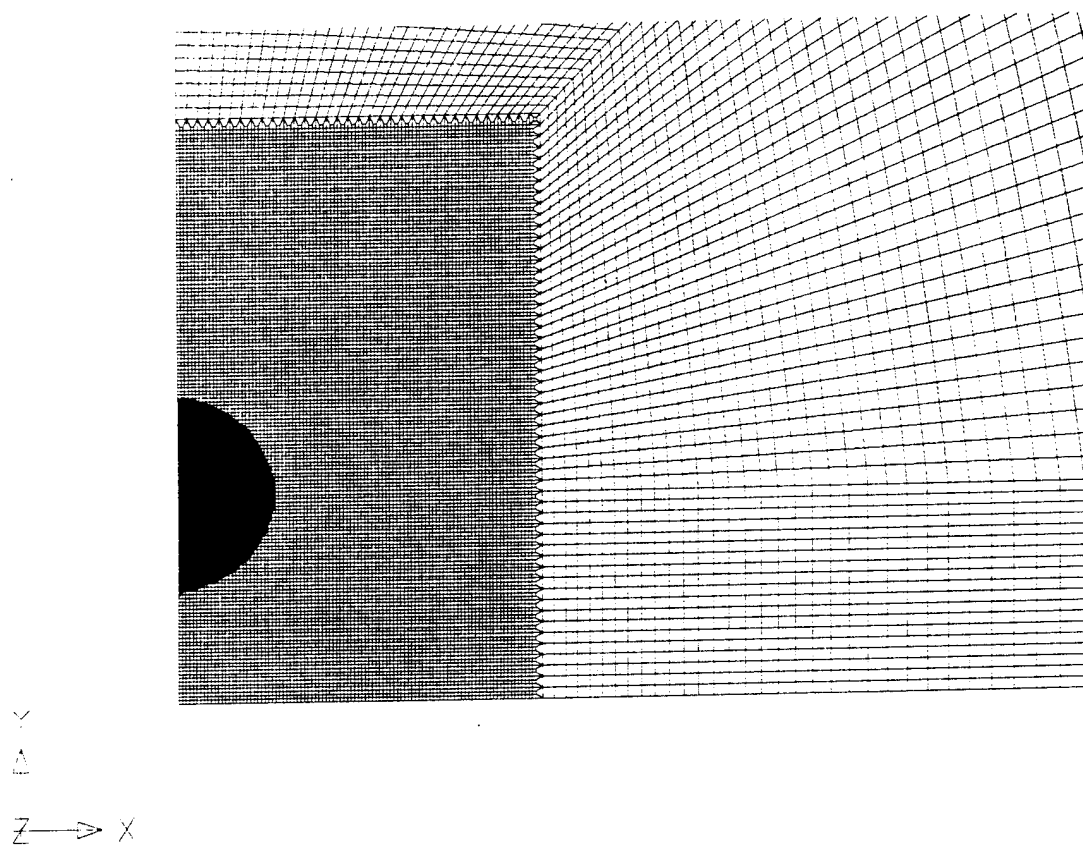


Figure 38. Bubble Shape for Rigid Wall at $h^*=2.008$ at Time $t=0.50T$

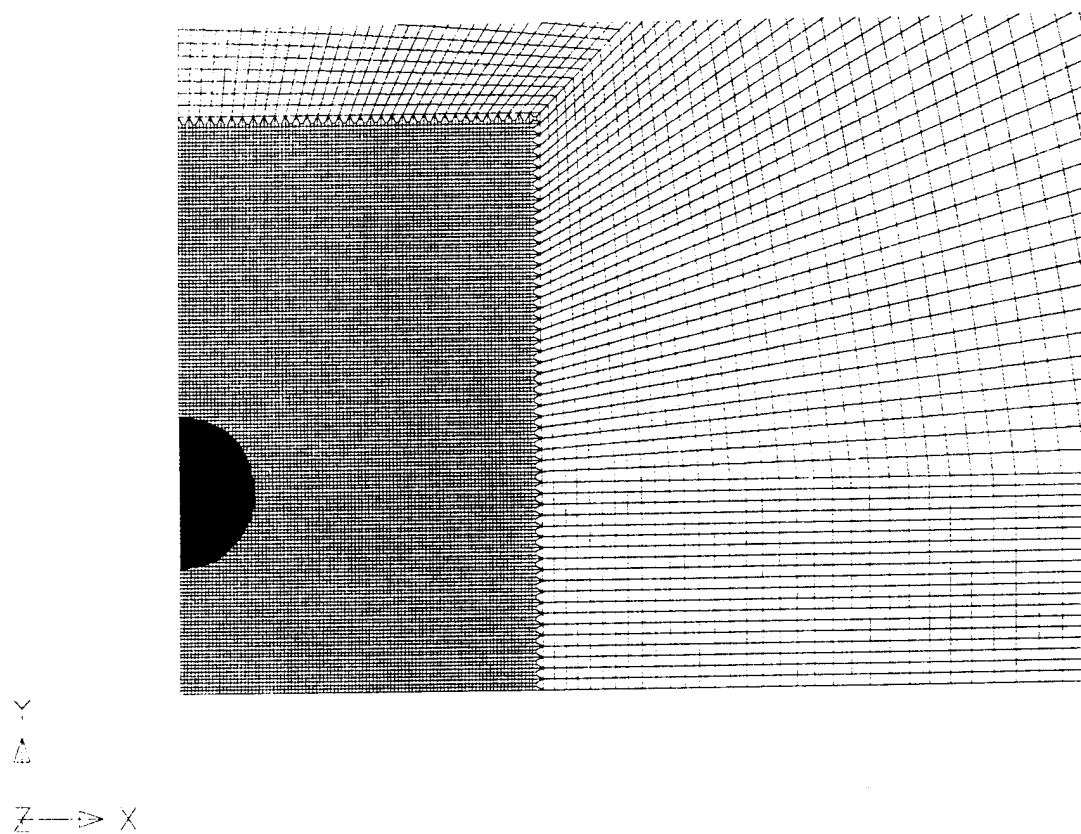


Figure 39. Bubble Shape for Rigid Wall at $h^*=2.008$ at Time $t=0.80T$

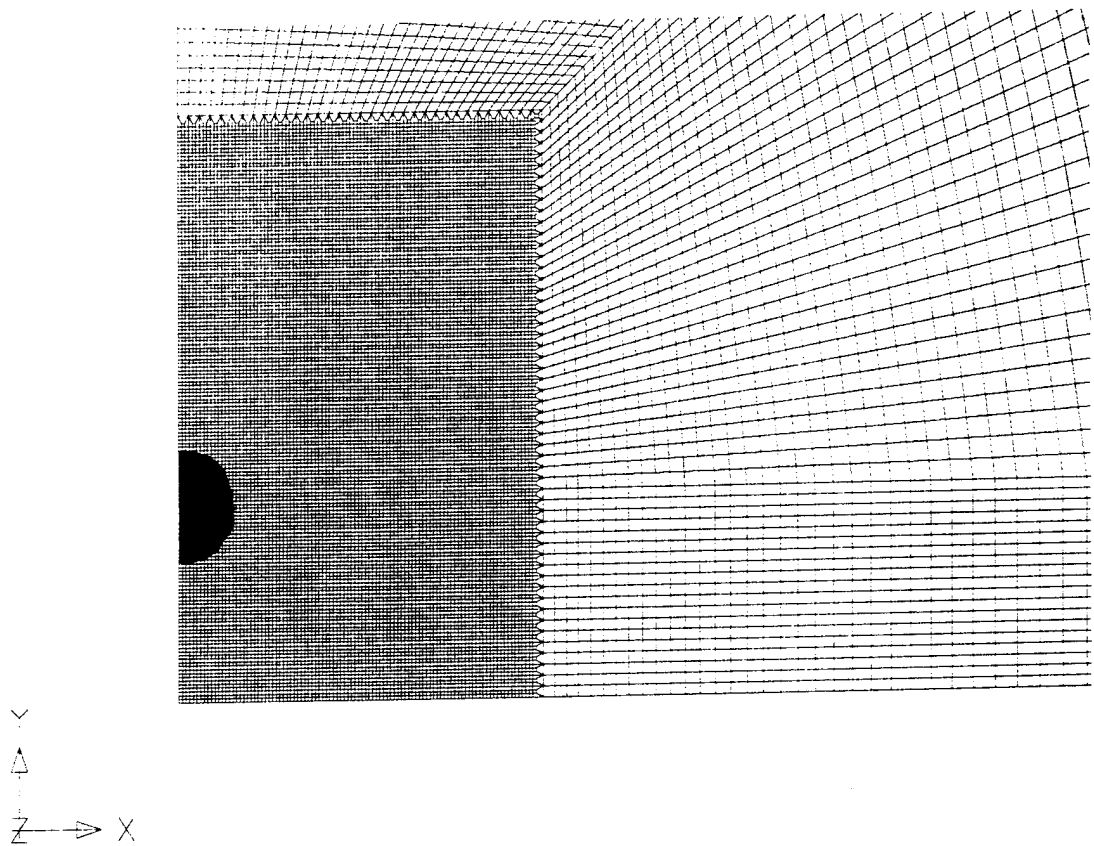


Figure 40. Bubble Shape for Rigid Wall at $h^*=2.008$ at Time $t=0.90T$

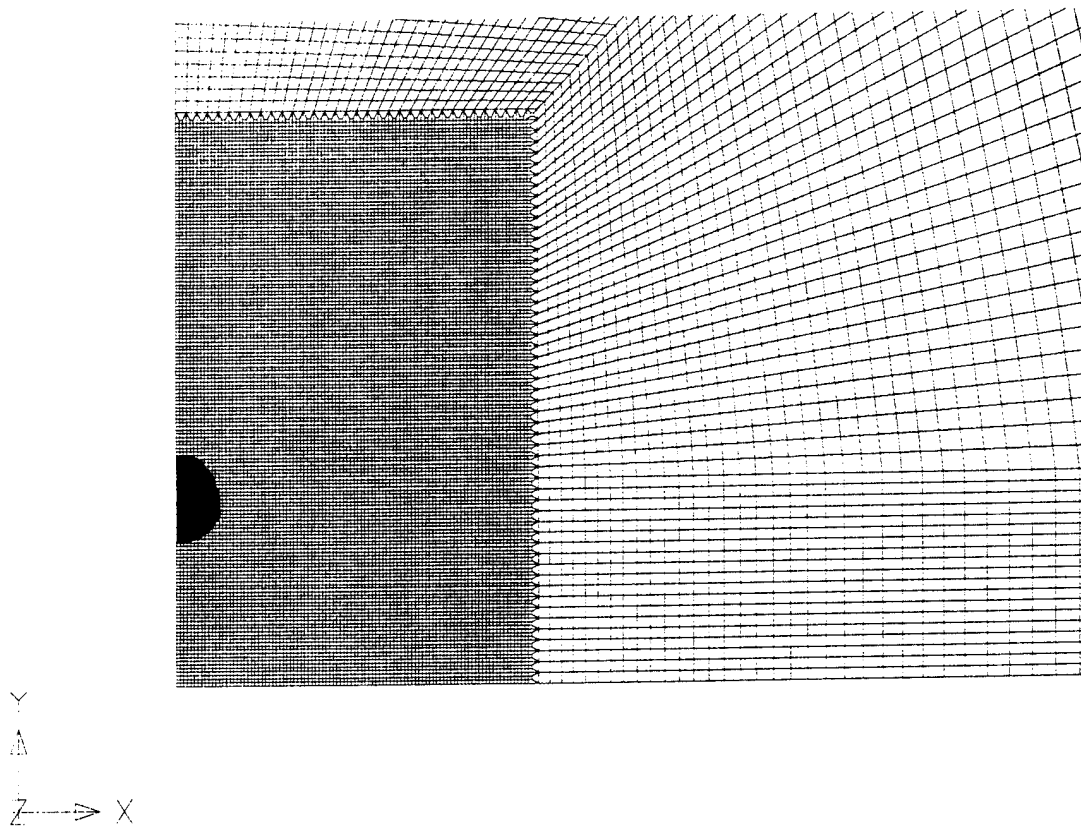


Figure 41. Bubble Shape for Rigid Wall at $h^*=2.008$ at Time $t=0.95T$

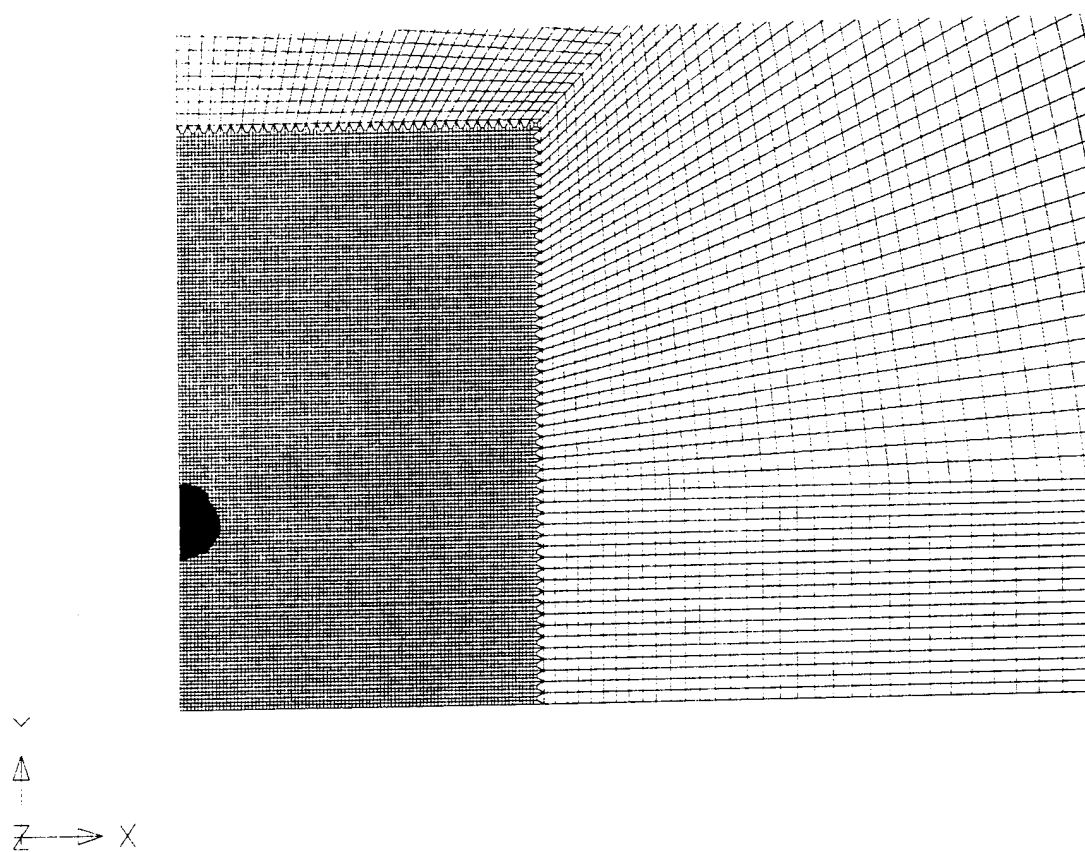


Figure 42. Bubble Shape for Rigid Wall at $h^*=2.008$ at Time $t=0.98T$

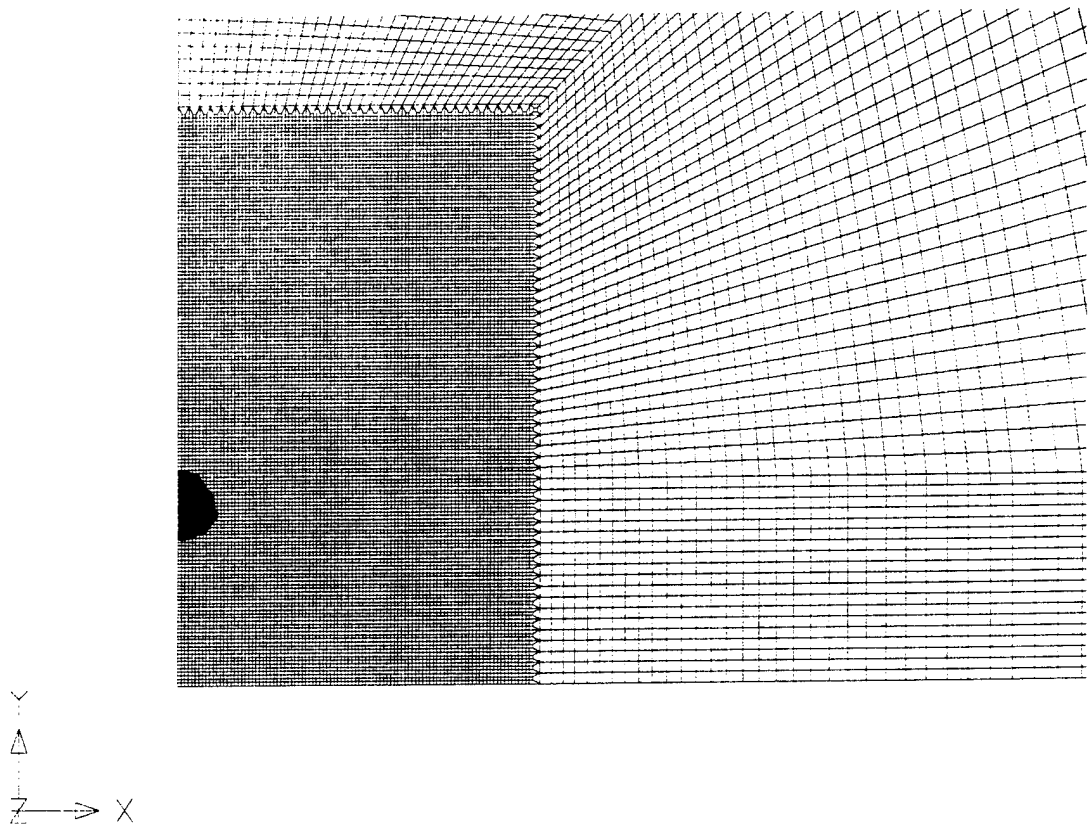


Figure 43. Bubble Shape for Rigid Wall at $h^*=2.008$ at Time $t=0.99T$

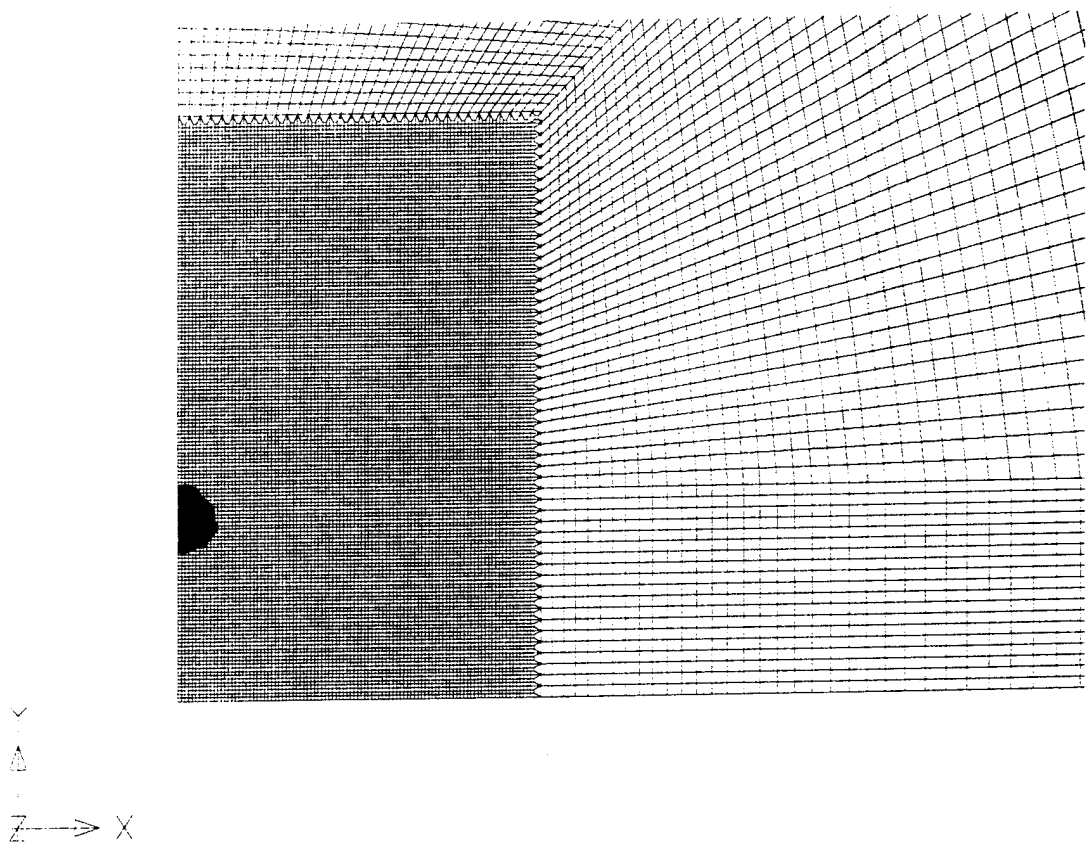


Figure 44. Bubble Shape for Rigid Wall at $h^*=2.008$ at Time $t=1.00T$

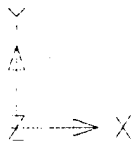
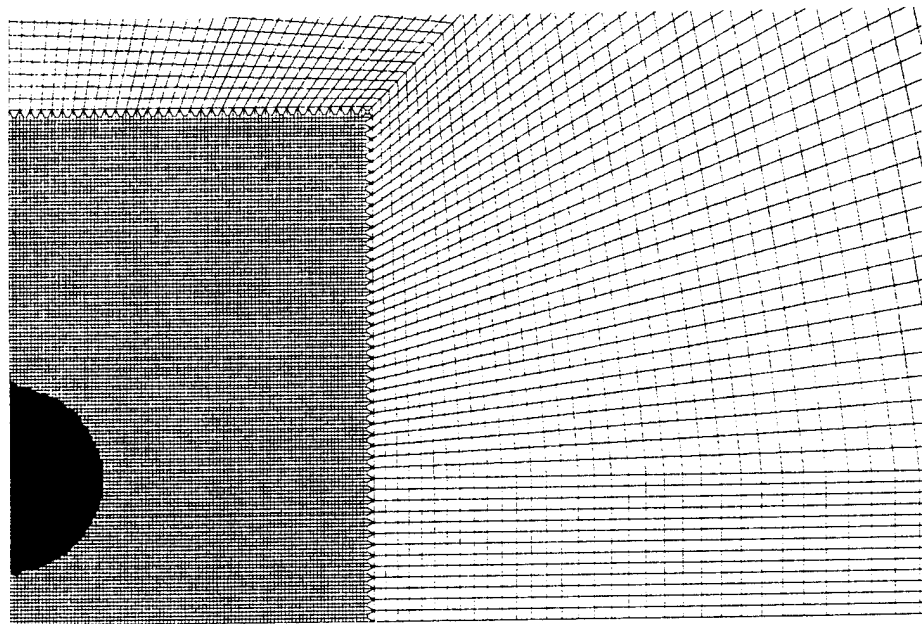


Figure 45. Bubble Shape for Rigid Wall at $h^*=1.374$ at Time $t=0.50T$

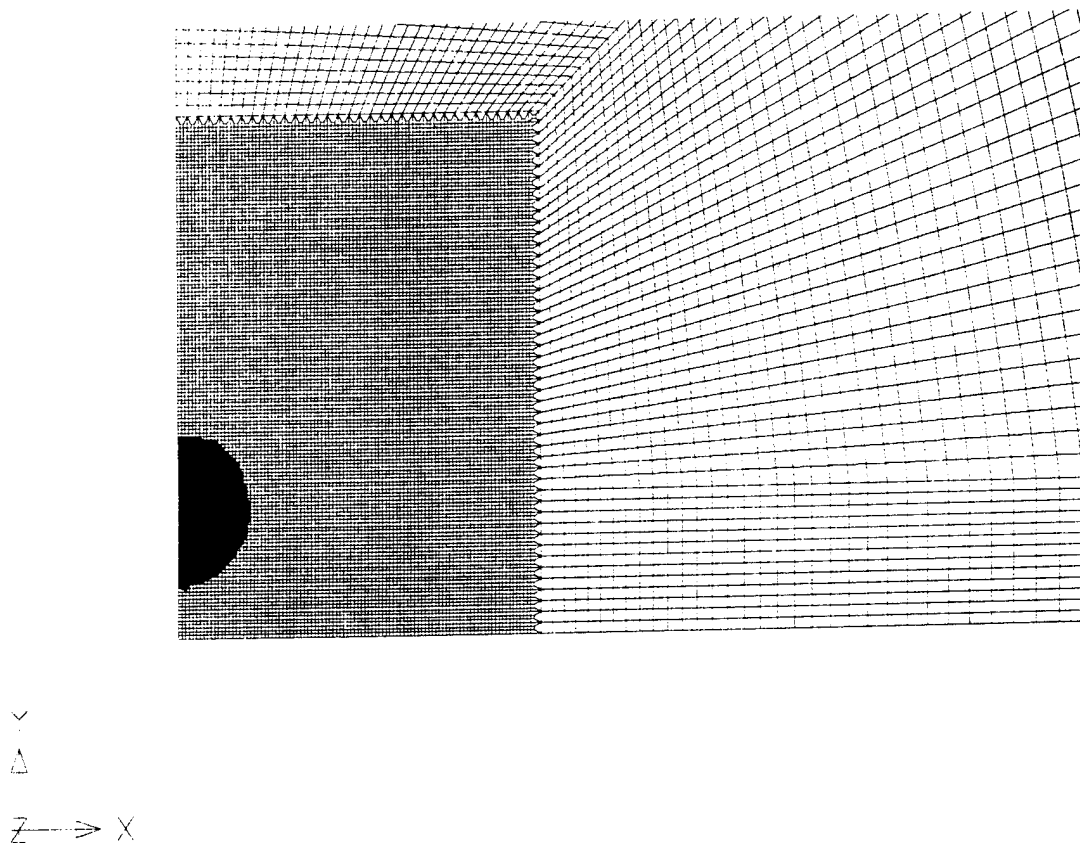


Figure 46. Bubble Shape for Rigid Wall at $h^*=1.374$ at Time $t=0.80T$

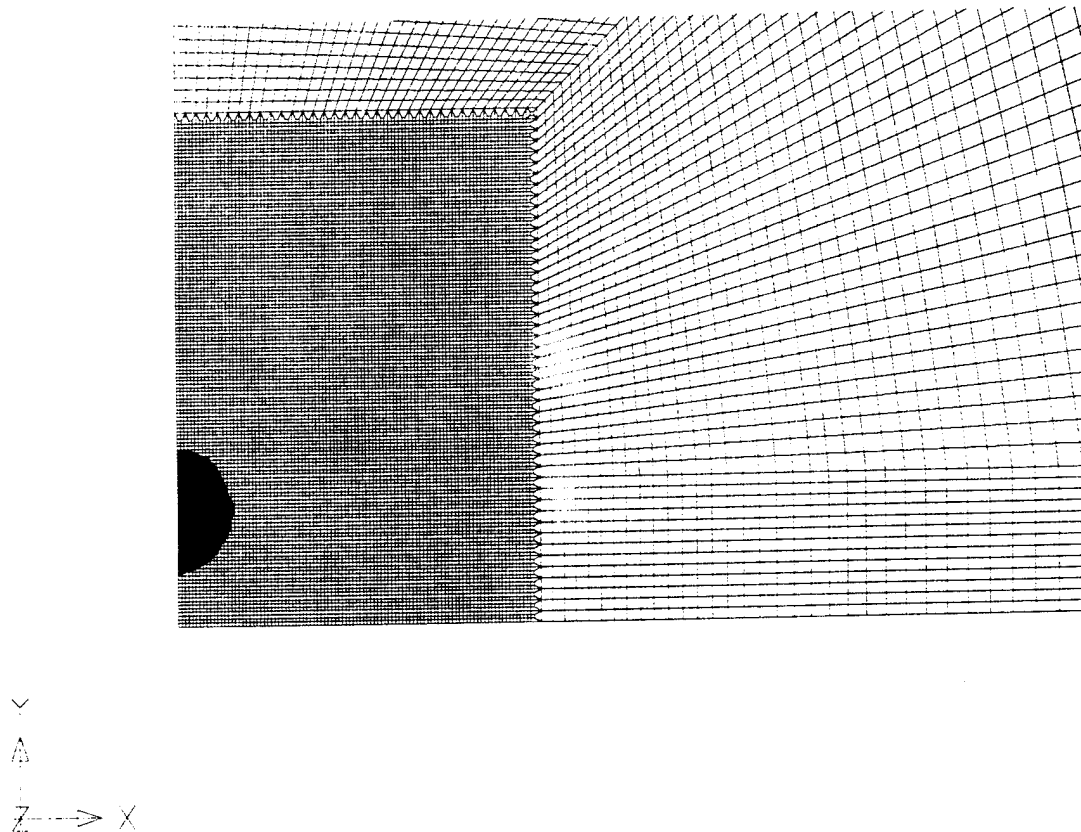


Figure 47. Bubble Shape for Rigid Wall at $h^*=1.374$ at Time $t=0.90T$

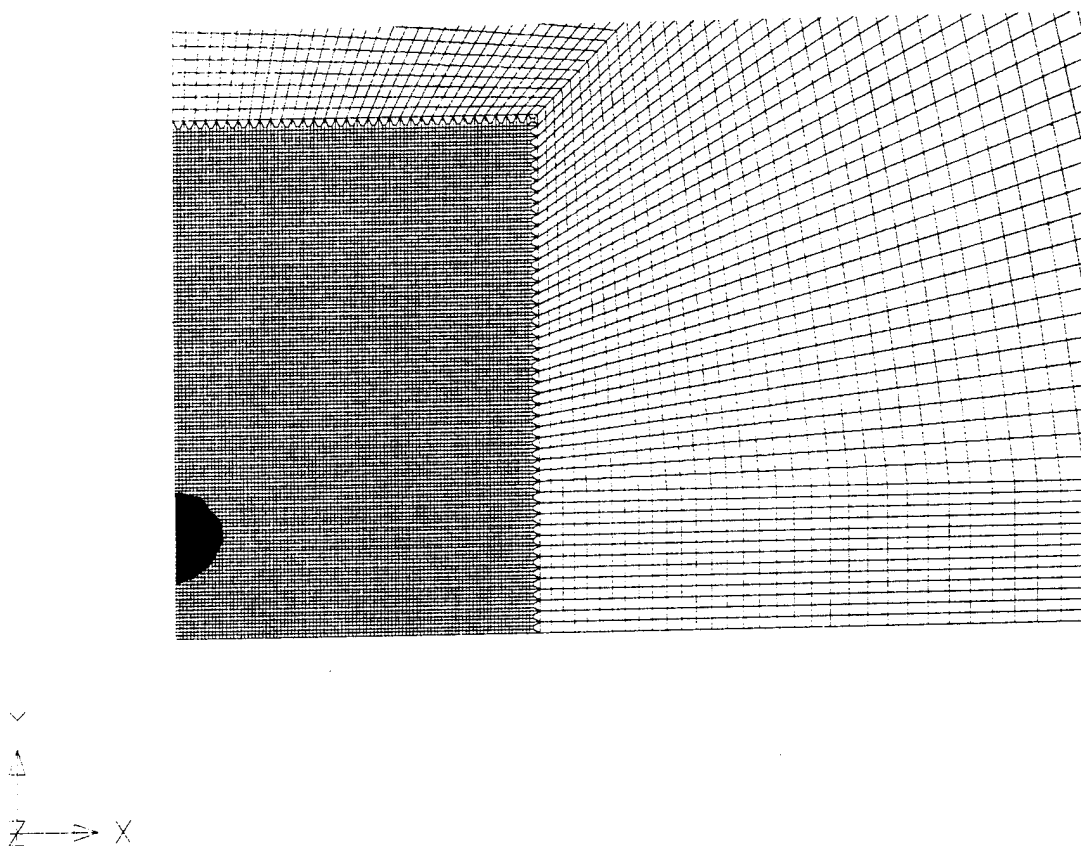


Figure 48. Bubble Shape for Rigid Wall at $h^*=1.374$ at Time $t=0.95T$

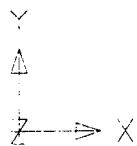
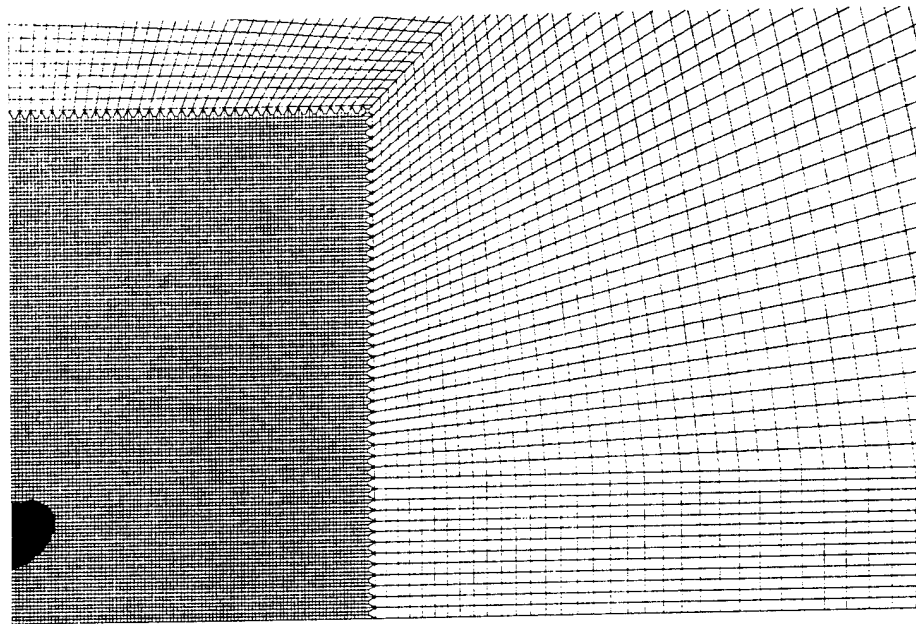


Figure 49. Bubble Shape for Rigid Wall at $h^*=1.374$ at Time $t=0.98T$

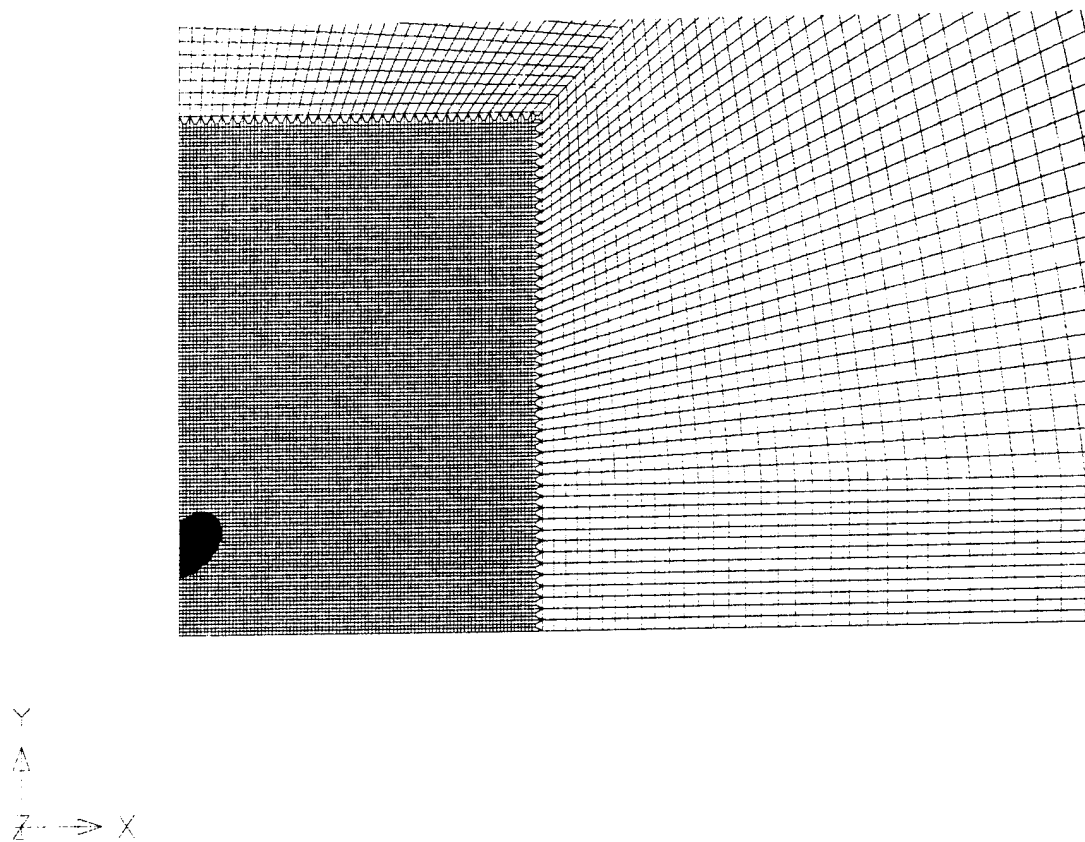


Figure 50. Bubble Shape for Rigid Wall at $h^*=1.374$ at Time $t=0.99T$

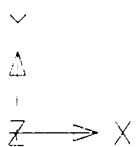
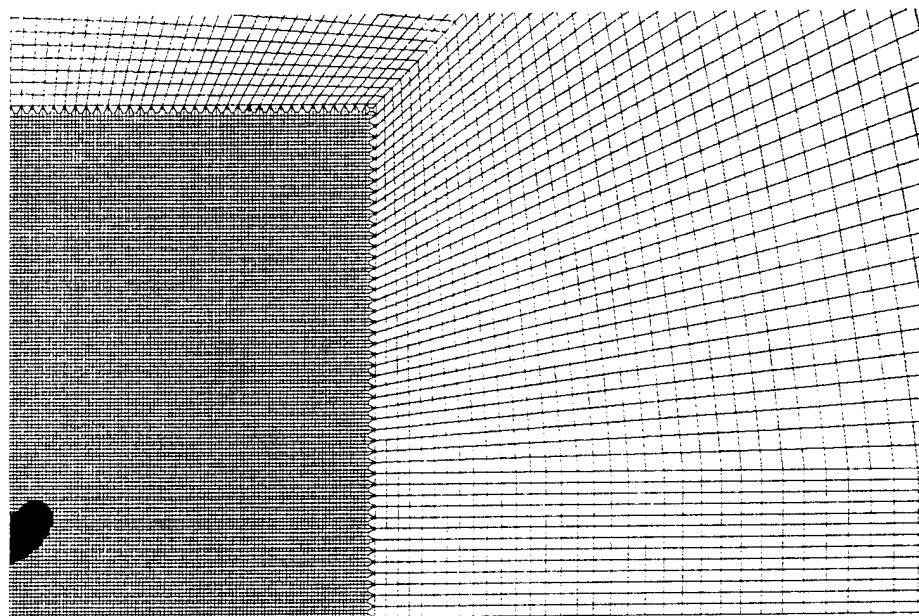


Figure 51. Bubble Shape for Rigid Wall at $h^*=1.374$ at Time $t=1.00T$

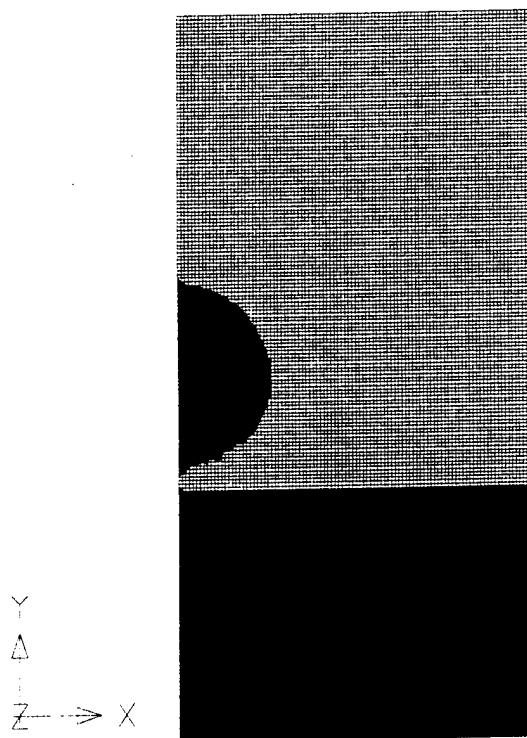


Figure 52. Bubble Shape for Rigid Wall at $h^*=1.000$ at Time $t=0.50T$

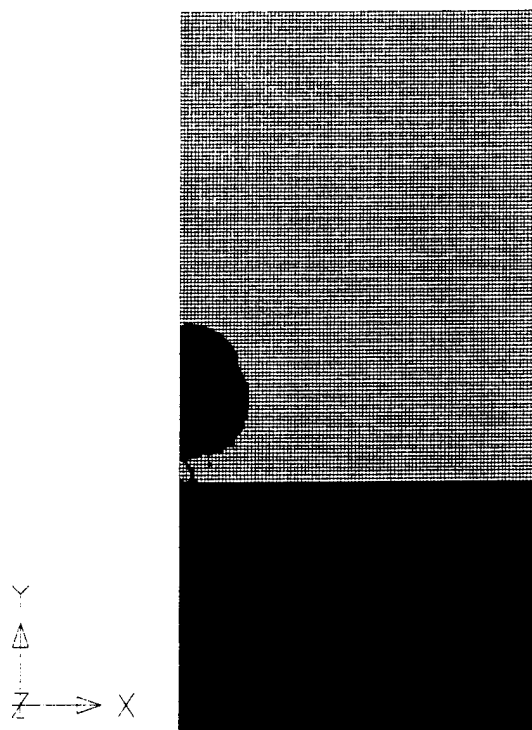


Figure 53. Bubble Shape for Rigid Wall at $h^*=1.000$ at Time $t=0.80T$

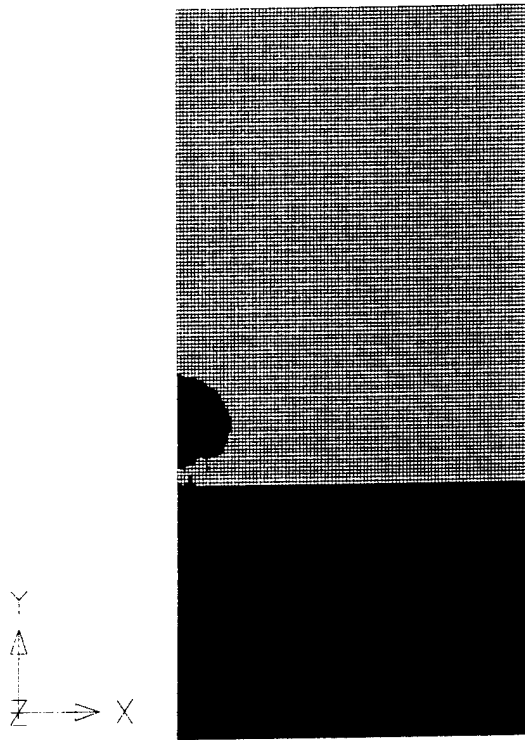


Figure 54. Bubble Shape for Rigid Wall at $h^*=1.000$ at Time $t=0.90T$

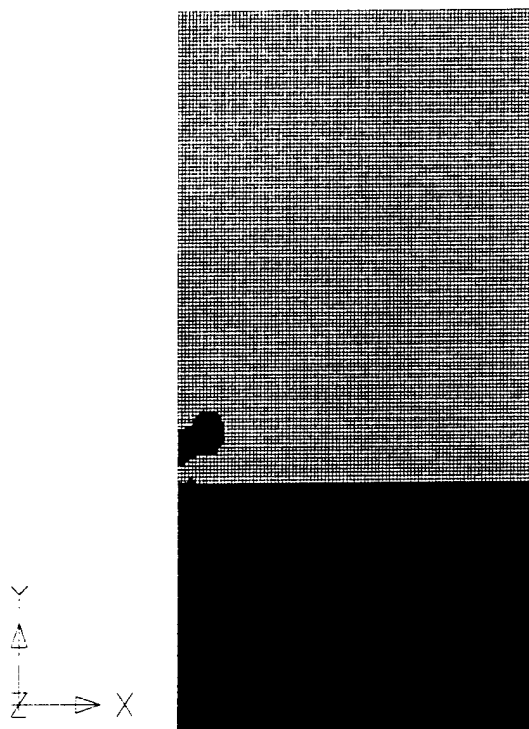


Figure 55. Bubble Shape for Rigid Wall at $h^*=1.000$ at Time $t=0.95T$

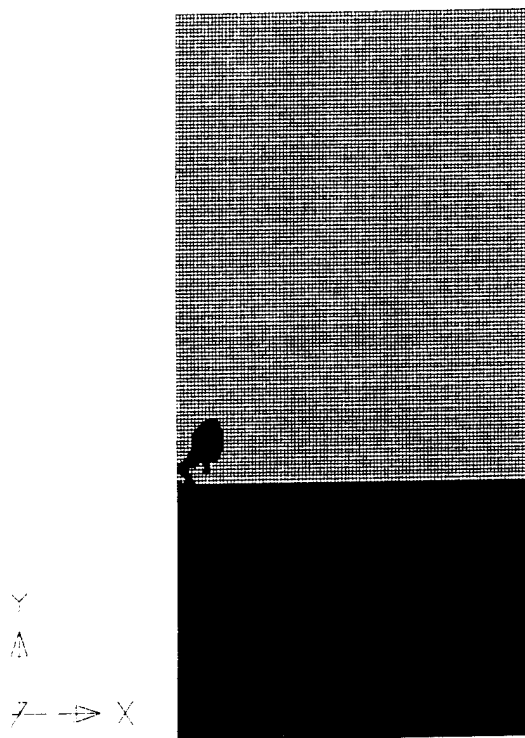


Figure 56. Bubble Shape for Rigid Wall at $h^*=1.000$ at Time $t=0.98T$

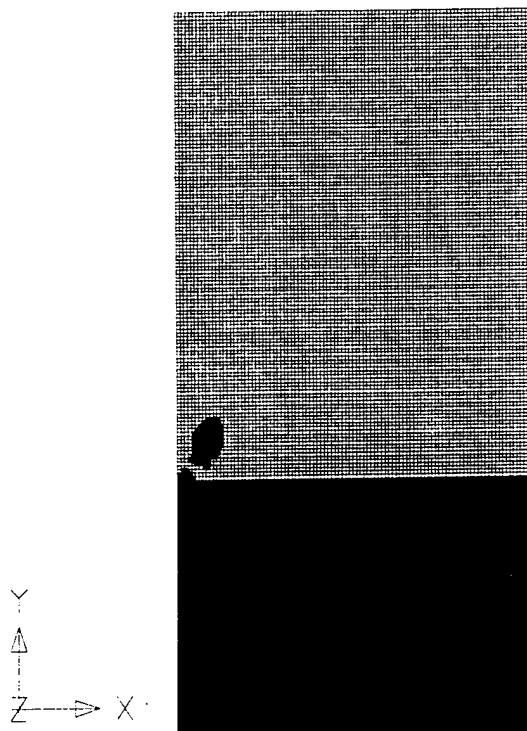


Figure 57. Bubble Shape for Rigid Wall at $h^*=1.000$ at Time $t=0.99T$

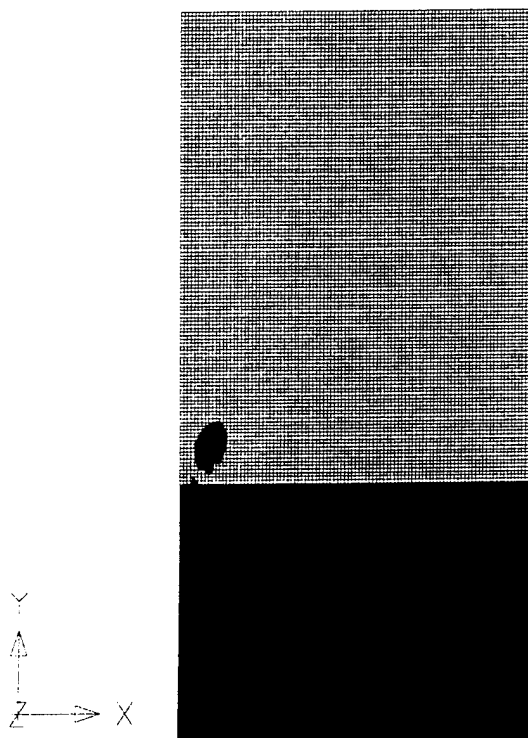


Figure 58. Bubble Shape for Rigid Wall at $h^*=1.000$ at Time $t=1.00T$

APPENDIX F: BUBBLES NEAR RIGID BOUNDARIES-INPUT

```

$
$ MSC/DYTRAN RUN FILE : Bubble Near Rigid Wall (Free-Field Case)
$
START
TIME = 999
CEND
$
TITLE = BUBBLE NEAR WALL
$
ENDSTEP = 99999
ENDTIME = 17.995E-3
PARAM, INISTEP, 0.2E-5
PARAM, MINSTEP, 0.2E-11
PARAM, STEPPCT, 19.0717446865
PARAM, DELCLUMP, 0.1
PARAM, RHOCUT, 1.E-4
PARAM, ROHYDRO, 1.E-4
PARAM, ROMULTI, 1.E-4
$
TYPE (MATHIS) = TIMEHIS
MATS (MATHIS) = 1
SET 1 = 1
MATOUT (MATHIS) = VOLUME
STEPS (MATHIS) = 0, THRU, END, BY, 1
SAVE (MATHIS) = 99999
$
TYPE (DENS) = ARCHIVE
ELEMENTS (DENS) = 2
SET 2 = 1t9801
ELOUT (DENS) = DENSITY
TIMES (DENS) = 0, THRU, END, BY, 0.005
$
BEGIN BULK
$
TICEUL 1 +
+ CYLINDER1 1 1 9. +
+ ELEM 2 2 1. +
CYLINDER1 0.0 -0.10 0.0 0.0 0.10 0.0 +
+ 0.1
SET1 2 1 THRU 23670
$
TICVAL 1 DENSITY 1630. SIE 4290000.
TICVAL 2 DENSITY 1025. SIE 20076.
$
INCLUDE bulk.dat
$
ENDDATA
$

```

```

!
! MSC/XL INPUT FILE : Bubble Near Rigid Wall (Free-Field Case) (1/2)
!
Edit ApplicationTable DuplicateElementTolerance=5e-06
Edit ApplicationTable DuplicateGridTolerance=5e-06
Edit ApplicationTable DuplicateFEFaceTolerance=5e-06
Edit ApplicationTable DegenerateElementTolerance=5e-06
Define Point X=0 Y=0 Z=0 CID=0 OutputList=1
Translate Point/1 DeltaX=2.475 DeltaY=0 DeltaZ=0 CID=0 OutputList=2 /Create
Connect Points Point1List=1 Point2List=2 OutputList=1
Translate Curve/1 DeltaX=0 DeltaY=2.475 DeltaZ=0 CID=0 OutputList=2 /Create/Points
Connect Curves Curve1List=1 Curve2List=2 OutputList=1 /Points
Define Point X=0.025 Y=0 Z=0 CID=0 OutputList=5
Define Point X=0.05 Y=0 Z=0 CID=0 OutputList=6
Define Point X=0.075 Y=0 Z=0 CID=0 OutputList=7
Translate Point/1,7 DeltaX=0 DeltaY=0.075 DeltaZ=0 CID=0 OutputList=8t9 /Create
Translate Point/5t6 DeltaX=0 DeltaY=0.025 DeltaZ=0 CID=0 OutputList=10t11 /Create
Connect Points Point1List=8 Point2List=1 OutputList=3
Connect Points Point1List=10 Point2List=5 OutputList=4
Connect Points Point1List=11 Point2List=6 OutputList=5
Connect Points Point1List=9 Point2List=7 OutputList=6
Connect Points Point1List=8 Point2List=9 OutputList=7
Connect Points Point1List=10 Point2List=11 OutputList=8
Connect Curves Curve1List=3 Curve2List=4 OutputList=2 /Points
Connect Curves Curve1List=4 Curve2List=5 OutputList=3 /Points
Connect Curves Curve1List=8 Curve2List=7 OutputList=4 /Points
Connect Curves Curve1List=5 Curve2List=6 OutputList=5 /Points
Translate 32 Surface/2t5 DeltaX=0.075 DeltaY=0 DeltaZ=0 CID=0 /Create/NoPoints
Translate 1 Surface/2t133 DeltaX=0 DeltaY=2.475 DeltaZ=0 CID=0 /Create/NoPoints
Rotate Surface/2t133 FromX=2.475 FromY=0 FromZ=0 ToX=2.475 ToY=0 ToZ=1 Angle=90
OffsetAngle=0 CID=0 OutputList=434t441 /Modify/NoPoints
Translate 3 Point/4 DeltaX=0.025 DeltaY=0 DeltaZ=0 CID=0 OutputList=12t14 /Create
Translate 3 Point/4,12t14 DeltaX=0 DeltaY=0.025 DeltaZ=0 CID=0 OutputList=15t26 /Create
Connect Points Point1List=4 Point2List=23 OutputList=9
Connect Points Point1List=16 Point2List=20 OutputList=10
Connect Points Point1List=17 Point2List=21 OutputList=11
Connect Points Point1List=14 Point2List=26 OutputList=12
Connect Points Point1List=23 Point2List=26 OutputList=13
Connect Points Point1List=20 Point2List=21 OutputList=14
Connect Points Point1List=16 Point2List=17 OutputList=15
Connect Points Point1List=4 Point2List=14 OutputList=16
Connect Curves Curve1List=9 Curve2List=10 OutputList=266 /Points
Connect Curves Curve1List=13 Curve2List=14 OutputList=267 /Points
Connect Curves Curve1List=14 Curve2List=15 OutputList=268 /Points
Connect Curves Curve1List=15 Curve2List=16 OutputList=269 /Points
Connect Curves Curve1List=11 Curve2List=12 OutputList=270 /Points
Translate Point/2 DeltaX=0.075 DeltaY=0 DeltaZ=0 CID=0 OutputList=27 /Create
Translate Point/3 DeltaX=0 DeltaY=0.075 DeltaZ=0 CID=0 OutputList=28 /Create
Connect Points Point1List=28 Point2List=26 OutputList=17
Connect Points Point1List=26 Point2List=27 OutputList=18
Define Point X=0 Y=400 Z=0 CID=0 OutputList=29
Sweep 2 Point/29 FromX=0 FromY=0 FromZ=0 ToX=0 ToY=0 ToZ=1 Angle=-45 OffsetAngle=0 CID=0
OutputList=19t20 /Points
Connect Curves Curve1List=17t18 Curve2List=19t20 OutputList=271t272 /Points
Translate Surface/1t272 DeltaX=0 DeltaY=0 DeltaZ=-5e-6 CID=0 /Modify/NoPoints
Translate Surface/1t272 DeltaX=0 DeltaY=0 DeltaZ=10e-6 CID=0 /Create/NoPoints
Rotate Surface/1t272 FromX=0 FromY=0 FromZ=0 ToX=0 ToY=1 ToZ=0 Angle=1 OffsetAngle=0 CID=0
/Modify/NoPoints
Rotate Surface/273t544 FromX=0 FromY=0 FromZ=0 ToX=0 ToY=1 ToZ=0 Angle=-1 OffsetAngle=0
CID=0 /Modify/NoPoints
Connect Surfaces Surface1List=1t272 Surface2List=273t544

```

```

!
! MSC/XL INPUT FILE : Bubble Near Rigid Wall (Free-Field Case) (2/2)
!
MeshParam Solid/1 Type=Hexa U=99 V=99 W=1 Pattern=1 PID=1 USpace=1 VSpace=1 WSpace=1
ResultingGridList=1t20000 OutputList=1t9801 /Extend/Update/NoOverwrite/NoMidNode
Select Part/1
MeshParam Solid/2t270 Type=Hexa U=1 V=1 W=1 Pattern=1 PID=1 USpace=1 VSpace=1 WSpace=1
ResultingGridList=20001t22152 OutputList=9802t10070 /Extend/Update/NoOverwrite/NoMidNode
MeshParam Solid/271t272 Type=Hexa U=34 V=200 W=1 Pattern=1 PID=1 USpace=1 VSpace=120
WSpace=1 ResultingGridList=22153t50292 OutputList=10071t23670
/Extend/Update/NoOverwrite/NoMidNode
!
Edit EOSJWL/1 EOSA=3.712e+11 EOSB=3.231e+09 EOSR1=4.15 EOSR2=0.95 EOSOmega=0.3 /Create
Edit DetSph/1 MID=1 DetX=0 DetY=0 DetZ=0 DetVel=6390 DetTime=0 /Create
Edit EOSPol/2 EOSA1=2.306e+09 EOSA2=8.432e+09 EOSA3=8.014e+09 EOSB0=0.4934 EOSB1=1.3937
EOSB2=0 EOSB3=Blank /Create
Edit DMat/1 DMatRHO=1630 EOID=1 /Create
Edit DMat/2 DMatRHO=1025 EOID=2 /Create
Edit PEuler1/1 TYPE=MMHydro TICEulID=1 /Create
!
Check Grid/1t50292 Type=Duplicates View=1 PartList=0t1 Tolerance=5e-06 /Update/NoExtend
Check Grid/1t50292 Type=Duplicates View=1 PartList=0t1 Tolerance=5e-06 /Update/NoExtend
Equivalence Grids /Update/NoExtend/NoCollapse
Write MSCInput File="bulk.dat" Format="Bulk" /NoExec/NoCase/Bulk
!

```

```

$
$ MSC/DYTRAN RUN FILE : Bubble Near Rigid Wall (h*=4.015)
$
START
TIME = 999
CEND
$
TITLE = BUBBLE NEAR WALL
$
ENDSTEP = 9999
ENDTIME = 17.995E-3
PARAM,INISTEP,0.2E-5
PARAM,MINSTEP,0.2E-11
PARAM,STEPFCT,19.0717446865
PARAM,DELCLUMP,0.1
PARAM,RHOCUT,1.E-4
PARAM,ROHYDRO,1.E-4
PARAM,ROMULTI,1.E-4
$
TYPE (MATHIS) = TIMEHIS
MATS (MATHIS) = 1
SET 1 = 1
MATOUT (MATHIS) = VOLUME,YMOM
STEPS (MATHIS) = 0,THRU,END,BY,1
SAVE (MATHIS) = 99999
$
TYPE (DENS) = ARCHIVE
ELEMENTS (DENS) = 2
SET 2 = 1t21087
ELOUT (DENS) = DENSITY
TIMES (DENS)= 0.,.007431,.011890,.013376,.014119,.014565,.014713,.014862
$
BEGIN BULK
$
TICEUL 1
+ CYLINDER1 1 1 9.
+ ELEM 2 2 2 1.
CYLINDER1 0.0 -0.10 0.0 0.0 0.10 0.0
+ 0.1
SET1 2 1 THRU 42708
$
TICVAL 1 DENSITY 1630. SIE 4290000.
TICVAL 2 DENSITY 1025. SIE 20076.
$
INCLUDE bulk.dat
$
ENDDATA
$

```



```

!
! MSC/XL INPUT FILE : Bubble Near Rigid Wall (h*=4.015) (1/2)
!
Edit ApplicationTable DuplicateElementTolerance=5e-06
Edit ApplicationTable DuplicateGridTolerance=5e-06
Edit ApplicationTable DuplicateFEFaceTolerance=5e-06
Edit ApplicationTable DegenerateElementTolerance=5e-06
Define Point X=0 Y=0 Z=0 CID=0 OutputList=1
Translate Point/1 DeltaX=2.475 DeltaY=0 DeltaZ=0 CID=0 OutputList=2 /Create
Connect Points Point1List=1 Point2List=2 OutputList=1
Translate Curve/1 DeltaX=0 DeltaY=2.475 DeltaZ=0 CID=0 OutputList=2 /Create/Points
Connect Curves Curve1List=1 Curve2List=2 OutputList=1 /Points
Define Point X=0.025 Y=0 Z=0 CID=0 OutputList=5
Define Point X=0.05 Y=0 Z=0 CID=0 OutputList=6
Define Point X=0.075 Y=0 Z=0 CID=0 OutputList=7
Translate Point/1,7 DeltaX=0 DeltaY=0.075 DeltaZ=0 CID=0 OutputList=8t9 /Create
Translate Point/5t6 DeltaX=0 DeltaY=0.025 DeltaZ=0 CID=0 OutputList=10t11 /Create
Connect Points Point1List=8 Point2List=1 OutputList=3
Connect Points Point1List=10 Point2List=5 OutputList=4
Connect Points Point1List=11 Point2List=6 OutputList=5
Connect Points Point1List=9 Point2List=7 OutputList=6
Connect Points Point1List=8 Point2List=9 OutputList=7
Connect Points Point1List=10 Point2List=11 OutputList=8
Connect Curves Curve1List=3 Curve2List=4 OutputList=2 /Points
Connect Curves Curve1List=4 Curve2List=5 OutputList=3 /Points
Connect Curves Curve1List=8 Curve2List=7 OutputList=4 /Points
Connect Curves Curve1List=5 Curve2List=6 OutputList=5 /Points
Translate 32 Surface/2t5 DeltaX=0.075 DeltaY=0 DeltaZ=0 CID=0 /Create/NoPoints
Translate 1 Surface/2t133 DeltaX=0 DeltaY=2.475 DeltaZ=0 CID=0 /Create/NoPoints
Rotate Surface/2t133 FromX=2.475 FromY=0 FromZ=0 ToX=2.475 ToY=0 ToZ=1 Angle=-90
OffsetAngle=0 CID=0 OutputList=434t441 /Modify/NoPoints
Translate 3 Point/4 DeltaX=0.025 DeltaY=0 DeltaZ=0 CID=0 OutputList=12t14 /Create
Translate 3 Point/4,12t14 DeltaX=0 DeltaY=0.025 DeltaZ=0 CID=0 OutputList=15t26 /Create
Connect Points Point1List=4 Point2List=23 OutputList=9
Connect Points Point1List=16 Point2List=20 OutputList=10
Connect Points Point1List=17 Point2List=21 OutputList=11
Connect Points Point1List=14 Point2List=26 OutputList=12
Connect Points Point1List=23 Point2List=26 OutputList=13
Connect Points Point1List=20 Point2List=21 OutputList=14
Connect Points Point1List=16 Point2List=17 OutputList=15
Connect Points Point1List=4 Point2List=14 OutputList=16
Connect Curves Curve1List=9 Curve2List=10 OutputList=266 /Points
Connect Curves Curve1List=13 Curve2List=14 OutputList=267 /Points
Connect Curves Curve1List=14 Curve2List=15 OutputList=268 /Points
Connect Curves Curve1List=15 Curve2List=16 OutputList=269 /Points
Connect Curves Curve1List=11 Curve2List=12 OutputList=270 /Points
Translate Point/2 DeltaX=0.075 DeltaY=0 DeltaZ=0 CID=0 OutputList=27 /Create
Translate Point/3 DeltaX=0 DeltaY=0.075 DeltaZ=0 CID=0 OutputList=28 /Create
Connect Points Point1List=28 Point2List=26 OutputList=17
Connect Points Point1List=26 Point2List=27 OutputList=18
Define Point X=0 Y=400 Z=0 CID=0 OutputList=29
Sweep 2 Point/29 FromX=0 FromY=0 FromZ=0 ToX=0 ToY=0 ToZ=1 Angle=-45 OffsetAngle=0 CID=0
OutputList=19t20 /Points
Connect Curves Curve1List=17t18 Curve2List=19t20 OutputList=271t272 /Points
Translate Surface/1t272 DeltaX=0 DeltaY=0 DeltaZ=-5e-6 CID=0 /Modify/NoPoints
Translate Surface/1t272 DeltaX=0 DeltaY=0 DeltaZ=10e-6 CID=0 /Create/NoPoints
Rotate Surface/1t272 FromX=0 FromY=0 FromZ=0 ToX=0 ToY=1 ToZ=0 Angle=1 OffsetAngle=0 CID=0
/Modify/NoPoints
Rotate Surface/273t544 FromX=0 FromY=0 FromZ=0 ToX=0 ToY=1 ToZ=0 Angle=-1 OffsetAngle=0
CID=0 /Modify/NoPoints
Connect Surfaces Surface1List=1t272 Surface2List=273t544

```

```

!
! MSC/XL INPUT FILE : Bubble Near Rigid Wall (h*=4.015) (2/2)
!
Edit EOSJWL/1 EOSA=3.712e+11 EOSB=3.231e+09 EOSR1=4.15 EOSR2=0.95 EOSOmega=0.3 /Create
Edit DetSph/1 MID=1 DetX=0 DetY=0 DetZ=0 DetVel=6390 DetTime=0 /Create
Edit EOSPol/2 EOSA1=2.306e+09 EOSA2=8.432e+09 EOSA3=8.014e+09 EOSB0=0.4934 EOSB1=1.3937
EOSB2=0 EOSB3=Blank /Create
Edit DMat/1 DMatRHO=1630 EOID=1 /Create
Edit DMat/2 DMatRHO=1025 EOID=2 /Create
Edit PEuler1/1 TYPE=MMHydro TICEulID=1 /Create
!
Define Point X=0 Y=-2.85 Z=0 CID=0 OutputList=32
Translate Point/32 DeltaX=2.475 DeltaY=0 DeltaZ=0 CID=0 OutputList=33 /Create
Connect Points Point1List=32 Point2List=33 OutputList=21
Translate Curve/21 DeltaX=0 DeltaY=2.85 DeltaZ=0 CID=0 OutputList=22 /Points/Create
Connect Curves Curve1List=21 Curve2List=22 OutputList=545 /Points
Translate Surface/545 DeltaX=0 DeltaY=0 DeltaZ=-5e-06 CID=0 OutputList=545 /Points/Modify
Translate Surface/545 DeltaX=0 DeltaY=0 DeltaZ=1e-05 CID=0 OutputList=546 /Points/Create
Rotate Surface/545 FromX=0 FromY=0 FromZ=0 ToX=0 ToY=1 ToZ=0 Angle=1 OffsetAngle=0 CID=0
OutputList=545 /Points/Modify
Rotate Surface/546 FromX=0 FromY=0 FromZ=0 ToX=0 ToY=1 ToZ=0 Angle=-1 OffsetAngle=0 CID=0
OutputList=546 /Points/Modify
Connect Surfaces Surface1List=545 Surface2List=546 Weight1=1 Weight2=1 OutputList=273
/Points
Translate 38 Solid/130t133 DeltaX=0 DeltaY=-0.075 DeltaZ=0 CID=0 OutputList=274t425
/Points/Create
Define Point X=400 Y=0 Z=0 CID=0 OutputList=494
Translate Point/494 DeltaX=0 DeltaY=0 DeltaZ=-5e-06 CID=0 OutputList=495 /Create
Translate Point/495 DeltaX=0 DeltaY=0 DeltaZ=1e-05 CID=0 OutputList=496 /Create
Rotate Point/495 FromX=0 FromY=0 FromZ=0 ToX=0 ToY=1 ToZ=0 Angle=1 OffsetAngle=0 CID=0
OutputList=497 /Create
Rotate Point/496 FromX=0 FromY=0 FromZ=0 ToX=0 ToY=1 ToZ=0 Angle=-1 OffsetAngle=0 CID=0
OutputList=498 /Create
Translate Point/497t498 DeltaX=0 DeltaY=-2.85 DeltaZ=0 CID=0 OutputList=499t500 /Create
MeshParam Solid/1 Type=Hexa U=99 V=99 W=1 Pattern=1 PID=1 USpace=1 VSpace=1 WSpace=1
ResultingGridList=1t20000 OutputList=1t9801
MeshParam Solid/273 Type=Hexa U=99 V=114 W=1 Pattern=1 PID=1 USpace=1 VSpace=1 WSpace=1
ResultingGridList=20001t43000 OutputList=9802t21087
MeshParam Solid/2t270 Type=Hexa U=1 V=1 W=1 Pattern=1 PID=1 USpace=1 VSpace=1 WSpace=1
ResultingGridList=43001t45152 OutputList=21088t21356
MeshParam Solid/274t425 Type=Hexa U=1 V=1 W=1 Pattern=1 PID=1 USpace=1 VSpace=1 WSpace=1
ResultingGridList=45153t46368 OutputList=21357t21508
MeshParam Solid/271t272 Type=Hexa U=34 V=200 W=1 Pattern=1 PID=1 USpace=1 VSpace=120
WSpace=1 ResultingGridList=46369t74508 OutputList=21509t35108
Connect Points Point1List=38 Point2List=41 OutputList=27 /Update/NoOverwrite/Extend
Connect Points Point1List=492 Point2List=493 OutputList=28 /Update/NoOverwrite/Extend
Connect Points Point1List=497 Point2List=498 OutputList=29 /Update/NoOverwrite/Extend
Connect Points Point1List=499 Point2List=500 OutputList=30 /Update/NoOverwrite/Extend
Connect Curves Curve1List=27 Curve2List=28 OutputList=549
/Update/NoOverwrite/Align/Extend/Points
Connect Curves Curve1List=29 Curve2List=30 OutputList=550
/Update/NoOverwrite/Align/Extend/Points
Connect Surfaces Surface1List=549 Surface2List=550 Weight1=1 Weight2=1 OutputList=426
/Update/NoOverwrite/Align/Extend/Points
MeshParam Solid/426 Type=Hexa U=1 V=38 W=200 Pattern=1 PID=1 USpace=1 VSpace=1 WSpace=120
ResultingGridList=74509t90186 OutputList=35109t42708 /Extend/Update/NoOverwrite/NoMidNode
Check Grid/1t90186 Type=Duplicates View=1 PartList=0t1 Tolerance=5e-06 /Update/NoExtend
Equivalence Grids /Update/NoExtend/NoCollapse
Check Grid/1t90186 Type=Duplicates View=1 PartList=0t1 Tolerance=5e-06 /Update/NoExtend
Equivalence Grids /Update/NoExtend/NoCollapse
Write MSCInput File="bulk.dat" Format="Bulk" /NoExec/NoCase/Bulk

```

```

$
$ MSC/DYTRAN RUN FILE: Bubble Near Rigid Wall (h*=2.008)
$
START
TIME = 999
CEND
$
TITLE = BUBBLE NEAR WALL
$
ENDSTEP = 9999
ENDTIME = 17.995E-3
PARAM,INISTEP,0.2E-5
PARAM,MINSTEP,0.2E-11
PARAM,STPEPCT,19.0717446865
PARAM,DELCLUMP,0.1
PARAM,RHOCUT,1.E-4
PARAM,ROHYDRO,1.E-4
PARAM,ROMULTI,1.E-4
$
TYPE (MATHIS) = TIMEHIS
MATS (MATHIS) = 1
SET 1 = 1
MATOUT (MATHIS) = VOLUME, YMOM
STEPS (MATHIS) = 0, THRU, END, BY, 1
SAVE (MATHIS) = 9999
$
TYPE (DENS) = ARCHIVE
ELEMENTS (DENS) = 2
SET 2 = 1t15444
ELOUT (DENS) = DENSITY
TIMES (DENS) = .00776, .012418, .013971, .014747, .015057, .015213, .015368, .015523
$
BEGIN BULK
$
TICEUL 1
+ CYLINDER1 1 1 9.
+ ELEM 2 2 1.
CYLINDER1 0.0 -0.10 0.0 0.0 0.10 0.0
+ 0.1
SET1 2 1 THRU 33189
$
TICVAL 1 DENSITY 1630. SIE 4290000.
TICVAL 2 DENSITY 1025. SIE 20076.
$
INCLUDE bulk.dat
$
ENDDATA
$

```

```

!
! MSC/XL INPUT FILE : Bubble Near Rigid Wall (h*=2.008) (1/2)
!
Edit ApplicationTable DuplicateElementTolerance=5e-06
Edit ApplicationTable DuplicateGridTolerance=5e-06
Edit ApplicationTable DuplicateFEFaceTolerance=5e-06
Edit ApplicationTable DegenerateElementTolerance=5e-06
Define Point X=0 Y=0 Z=0 CID=0 OutputList=1
Translate Point/1 DeltaX=2.475 DeltaY=0 DeltaZ=0 CID=0 OutputList=2 /Create
Connect Points Point1List=1 Point2List=2 OutputList=1
Translate Curve/1 DeltaX=0 DeltaY=2.475 DeltaZ=0 CID=0 OutputList=2 /Create/Points
Connect Curves Curve1List=1 Curve2List=2 OutputList=1 /Points
Define Point X=0.025 Y=0 Z=0 CID=0 OutputList=5
Define Point X=0.05 Y=0 Z=0 CID=0 OutputList=6
Define Point X=0.075 Y=0 Z=0 CID=0 OutputList=7
Translate Point/1,7 DeltaX=0 DeltaY=0.075 DeltaZ=0 CID=0 OutputList=8t9 /Create
Translate Point/5t6 DeltaX=0 DeltaY=0.025 DeltaZ=0 CID=0 OutputList=10t11 /Create
Connect Points Point1List=8 Point2List=1 OutputList=3
Connect Points Point1List=10 Point2List=5 OutputList=4
Connect Points Point1List=11 Point2List=6 OutputList=5
Connect Points Point1List=9 Point2List=7 OutputList=6
Connect Points Point1List=8 Point2List=9 OutputList=7
Connect Points Point1List=10 Point2List=11 OutputList=8
Connect Curves Curve1List=3 Curve2List=4 OutputList=2 /Points
Connect Curves Curve1List=4 Curve2List=5 OutputList=3 /Points
Connect Curves Curve1List=8 Curve2List=7 OutputList=4 /Points
Connect Curves Curve1List=5 Curve2List=6 OutputList=5 /Points
Translate 32 Surface/2t5 DeltaX=0.075 DeltaY=0 DeltaZ=0 CID=0 /Create/NoPoints
Translate 1 Surface/2t133 DeltaX=0 DeltaY=2.475 DeltaZ=0 CID=0 /Create/NoPoints
Rotate Surface/2t133 FromX=2.475 FromY=0 FromZ=0 ToX=2.475 ToY=0 ToZ=1 Angle=-90
OffsetAngle=0 CID=0 OutputList=434t441 /Modify/NoPoints
Translate 3 Point/4 DeltaX=0.025 DeltaY=0 DeltaZ=0 CID=0 OutputList=12t14 /Create
Translate 3 Point/4,12t14 DeltaX=0 DeltaY=0.025 DeltaZ=0 CID=0 OutputList=15t26 /Create
Connect Points Point1List=4 Point2List=23 OutputList=9
Connect Points Point1List=16 Point2List=20 OutputList=10
Connect Points Point1List=17 Point2List=21 OutputList=11
Connect Points Point1List=14 Point2List=26 OutputList=12
Connect Points Point1List=23 Point2List=26 OutputList=13
Connect Points Point1List=20 Point2List=21 OutputList=14
Connect Points Point1List=16 Point2List=17 OutputList=15
Connect Points Point1List=4 Point2List=14 OutputList=16
Connect Curves Curve1List=9 Curve2List=10 OutputList=266 /Points
Connect Curves Curve1List=13 Curve2List=14 OutputList=267 /Points
Connect Curves Curve1List=14 Curve2List=15 OutputList=268 /Points
Connect Curves Curve1List=15 Curve2List=16 OutputList=269 /Points
Connect Curves Curve1List=11 Curve2List=12 OutputList=270 /Points
Translate Point/2 DeltaX=0.075 DeltaY=0 DeltaZ=0 CID=0 OutputList=27 /Create
Translate Point/3 DeltaX=0 DeltaY=0.075 DeltaZ=0 CID=0 OutputList=28 /Create
Connect Points Point1List=28 Point2List=26 OutputList=17
Connect Points Point1List=26 Point2List=27 OutputList=18
Define Point X=0 Y=400 Z=0 CID=0 OutputList=29
Sweep 2 Point/29 FromX=0 FromY=0 FromZ=0 ToX=0 ToY=0 ToZ=1 Angle=-45 OffsetAngle=0 CID=0
OutputList=19t20 /Points
Connect Curves Curve1List=17t18 Curve2List=19t20 OutputList=271t272 /Points
Translate Surface/1t272 DeltaX=0 DeltaY=0 DeltaZ=-5e-6 CID=0 /Modify/NoPoints
Translate Surface/1t272 DeltaX=0 DeltaY=0 DeltaZ=10e-6 CID=0 /Create/NoPoints
Rotate Surface/1t272 FromX=0 FromY=0 FromZ=0 ToX=0 ToY=1 ToZ=0 Angle=1 OffsetAngle=0 CID=0
/Modify/NoPoints
Rotate Surface/273t544 FromX=0 FromY=0 FromZ=0 ToX=0 ToY=1 ToZ=0 Angle=-1 OffsetAngle=0
CID=0 /Modify/NoPoints
Connect Surfaces Surface1List=1t272 Surface2List=273t544

```

```

!
! MSC/XL INPUT FILE : Bubble Near Rigid Wall (h*=2.008) (2/2)
!
Edit EOSJWL/1 EOSA=3.712e+11 EOSB=3.231e+09 EOSR1=4.15 EOSR2=0.95 EOSOmega=0.3 /Create
Edit DetSph/1 MID=1 DetX=0 DetY=0 DetZ=0 DetVel=6390 DetTime=0 /Create
Edit EOSPol/2 EOSA1=2.306e+09 EOSA2=8.432e+09 EOSA3=8.014e+09 EOSB0=0.4934 EOSB1=1.3937
EOSB2=0 EOSB3=Blank /Create
Edit DMat/1 DMatRHO=1630 EOID=1 /Create
Edit DMat/2 DMatRHO=1025 EOID=2 /Create
Edit PEuler1/1 TYPE=MMHydro TICEulID=1 /Create
!
Define Point X=0 Y=-1.425 Z=0 CID=0 OutputList=32
Translate Point/32 DeltaX=2.475 DeltaY=0 DeltaZ=0 CID=0 OutputList=33 /Create
Connect Points Point1List=32 Point2List=33 OutputList=21
Translate Curve/21 DeltaX=0 DeltaY=1.425 DeltaZ=0 CID=0 OutputList=22 /Points/Create
Connect Curves Curve1List=21 Curve2List=22 OutputList=545 /Points
Translate Surface/545 DeltaX=0 DeltaY=0 DeltaZ=-5e-06 CID=0 OutputList=545 /Points/Modify
Translate Surface/545 DeltaX=0 DeltaY=0 DeltaZ=1e-05 CID=0 OutputList=546 /Points/Create
Rotate Surface/545 FromX=0 FromY=0 FromZ=0 ToX=0 ToY=1 ToZ=0 Angle=1 OffsetAngle=0 CID=0
OutputList=545 /Points/Modify
Rotate Surface/546 FromX=0 FromY=0 FromZ=0 ToX=0 ToY=1 ToZ=0 Angle=-1 OffsetAngle=0 CID=0
OutputList=546 /Points/Modify
Connect Surfaces Surface1List=545 Surface2List=546 Weight1=1 Weight2=1 OutputList=273
/Points
Translate 19 Solid/130t133 DeltaX=0 DeltaY=-0.075 DeltaZ=0 CID=0 OutputList=274t349
/Points/Create
Define Point X=400 Y=0 Z=0 CID=0 OutputList=494
Translate Point/494 DeltaX=0 DeltaY=0 DeltaZ=-5e-06 CID=0 OutputList=495 /Create
Translate Point/495 DeltaX=0 DeltaY=0 DeltaZ=1e-05 CID=0 OutputList=496 /Create
Rotate Point/495 FromX=0 FromY=0 FromZ=0 ToX=0 ToY=1 ToZ=0 Angle=1 OffsetAngle=0 CID=0
OutputList=497 /Create
Rotate Point/496 FromX=0 FromY=0 FromZ=0 ToX=0 ToY=1 ToZ=0 Angle=-1 OffsetAngle=0 CID=0
OutputList=498 /Create
Translate Point/497t498 DeltaX=0 DeltaY=-1.425 DeltaZ=0 CID=0 OutputList=499t500 /Create
MeshParam Solid/1 Type=Hexa U=99 V=99 W=1 Pattern=1 PID=1 USpace=1 VSpace=1 WSpace=1
MeshParam Solid/273 Type=Hexa U=99 V=57 W=1 Pattern=1 PID=1 USpace=1 VSpace=1 WSpace=1
Select Part/1
MeshParam Solid/2t270 Type=Hexa U=1 V=1 W=1 Pattern=1 PID=1 USpace=1 VSpace=1 WSpace=1
MeshParam Solid/274t349 Type=Hexa U=1 V=1 W=1 Pattern=1 PID=1 USpace=1 VSpace=1 WSpace=1
MeshParam Solid/271t272 Type=Hexa U=34 V=200 W=1 Pattern=1 PID=1 USpace=1 VSpace=120
WSpace=1
Connect Points Point1List=38 Point2List=41 OutputList=27
Connect Points Point1List=264 Point2List=265 OutputList=28
Connect Points Point1List=497 Point2List=498 OutputList=29
Connect Points Point1List=499 Point2List=500 OutputList=30
Connect Curves Curve1List=27 Curve2List=28 OutputList=549 /Points
Connect Curves Curve1List=29 Curve2List=30 OutputList=550 /Points
Connect Surfaces Surface1List=549 Surface2List=550 Weight1=1 Weight2=1 OutputList=426
MeshParam Solid/426 Type=Hexa U=1 V=19 W=200 Pattern=1 PID=1 USpace=1 VSpace=1 WSpace=120
Check Grid/1t99999 Type=Duplicates View=1 PartList=0t1 Tolerance=5e-06 /Update/NoExtend
Equivalence Grids /Update/NoExtend/NoCollapse
Write MSCInput File="bulk.dat" Format="Bulk" /NoExec/NoCase/Bulk
!

```

```

$
$ MSC/DYTRAN RUN FILE: Bubble Near Rigid Wall (h*=1.374)
$
START
TIME = 999
CEND
$
TITLE = BUBBLE NEAR WALL
$
ENDSTEP = 9999
ENDTIME = 17.995E-3
PARAM,INISTEP,0.2E-5
PARAM,MINSTEP,0.2E-11
PARAM,STEPFCT,19.0717446865
PARAM,DELCLUMP,0.1
PARAM,RHOCUT,1.E-4
PARAM,ROHYDRO,1.E-4
PARAM,ROMULTI,1.E-4
$
TYPE (MATHIS) = TIMEHIS
MATS (MATHIS) = 1
SET 1 = 1
MATOUT (MATHIS) = VOLUME,YMOM
STEPS (MATHIS) = 0,THRU,END,BY,1
SAVE (MATHIS) = 9999
$
TYPE (DENS) = ARCHIVE
ELEMENTS (DENS) = 2
SET 2 = 1t13662
ELOUT (DENS) = DENSITY
TIMES (DENS) = .008071,.012914,.014528,.015335,.015758,.015819,.015981,.016142
$
BEGIN BULK
$
TICEUL 1
+ CYLINDER1 1 1 9.
+ ELEM 2 2 1.
CYLINDER1 0.0 -0.10 0.0 0.0 0.10 0.0
+ 0.1
SET1 2 1 THRU 30183
$
TICVAL 1 DENSITY 1630. SIE 4290000.
TICVAL 2 DENSITY 1025. SIE 20076.
$
INCLUDE bulk.dat
$
ENDDATA
$

```

```

!
! MSC/XL INPUT FILE : Bubble Near Rigid Wall (h*=1.374) (1/2)
!
Edit ApplicationTable DuplicateElementTolerance=5e-06
Edit ApplicationTable DuplicateGridTolerance=5e-06
Edit ApplicationTable DuplicateFEFaceTolerance=5e-06
Edit ApplicationTable DegenerateElementTolerance=5e-06
Define Point X=0 Y=0 Z=0 CID=0 OutputList=1
Translate Point/1 DeltaX=2.475 DeltaY=0 DeltaZ=0 CID=0 OutputList=2 /Create
Connect Points Point1List=1 Point2List=2 OutputList=1
Translate Curve/1 DeltaX=0 DeltaY=2.475 DeltaZ=0 CID=0 OutputList=2 /Create/Points
Connect Curves Curve1List=1 Curve2List=2 OutputList=1 /Points
Define Point X=0.025 Y=0 Z=0 CID=0 OutputList=5
Define Point X=0.05 Y=0 Z=0 CID=0 OutputList=6
Define Point X=0.075 Y=0 Z=0 CID=0 OutputList=7
Translate Point/1,7 DeltaX=0 DeltaY=0.075 DeltaZ=0 CID=0 OutputList=8t9 /Create
Translate Point/5t6 DeltaX=0 DeltaY=0.025 DeltaZ=0 CID=0 OutputList=10t11 /Create
Connect Points Point1List=8 Point2List=1 OutputList=3
Connect Points Point1List=10 Point2List=5 OutputList=4
Connect Points Point1List=11 Point2List=6 OutputList=5
Connect Points Point1List=9 Point2List=7 OutputList=6
Connect Points Point1List=8 Point2List=9 OutputList=7
Connect Points Point1List=10 Point2List=11 OutputList=8
Connect Curves Curve1List=3 Curve2List=4 OutputList=2 /Points
Connect Curves Curve1List=4 Curve2List=5 OutputList=3 /Points
Connect Curves Curve1List=8 Curve2List=7 OutputList=4 /Points
Connect Curves Curve1List=5 Curve2List=6 OutputList=5 /Points
Translate 32 Surface/2t5 DeltaX=0.075 DeltaY=0 DeltaZ=0 CID=0 /Create/NoPoints
Translate 1 Surface/2t133 DeltaX=0 DeltaY=2.475 DeltaZ=0 CID=0 /Create/NoPoints
Rotate Surface/2t133 FromX=2.475 FromY=0 FromZ=0 ToX=2.475 ToY=0 ToZ=1 Angle=-90
OffsetAngle=0 CID=0 OutputList=434t441 /Modify/NoPoints
Translate 3 Point/4 DeltaX=0.025 DeltaY=0 DeltaZ=0 CID=0 OutputList=12t14 /Create
Translate 3 Point/4,12t14 DeltaX=0 DeltaY=0.025 DeltaZ=0 CID=0 OutputList=15t26 /Create
Connect Points Point1List=4 Point2List=23 OutputList=9
Connect Points Point1List=16 Point2List=20 OutputList=10
Connect Points Point1List=17 Point2List=21 OutputList=11
Connect Points Point1List=14 Point2List=26 OutputList=12
Connect Points Point1List=23 Point2List=26 OutputList=13
Connect Points Point1List=20 Point2List=21 OutputList=14
Connect Points Point1List=16 Point2List=17 OutputList=15
Connect Points Point1List=4 Point2List=14 OutputList=16
Connect Curves Curve1List=9 Curve2List=10 OutputList=266 /Points
Connect Curves Curve1List=13 Curve2List=14 OutputList=267 /Points
Connect Curves Curve1List=14 Curve2List=15 OutputList=268 /Points
Connect Curves Curve1List=15 Curve2List=16 OutputList=269 /Points
Connect Curves Curve1List=11 Curve2List=12 OutputList=270 /Points
Translate Point/2 DeltaX=0.075 DeltaY=0 DeltaZ=0 CID=0 OutputList=27 /Create
Translate Point/3 DeltaX=0 DeltaY=0.075 DeltaZ=0 CID=0 OutputList=28 /Create
Connect Points Point1List=28 Point2List=26 OutputList=17
Connect Points Point1List=26 Point2List=27 OutputList=18
Define Point X=0 Y=400 Z=0 CID=0 OutputList=29
Sweep 2 Point/29 FromX=0 FromY=0 FromZ=0 ToX=0 ToY=0 ToZ=1 Angle=-45 OffsetAngle=0 CID=0
OutputList=19t20 /Points
Connect Curves Curve1List=17t18 Curve2List=19t20 OutputList=271t272 /Points
Translate Surface/1t272 DeltaX=0 DeltaY=0 DeltaZ=-5e-6 CID=0 /Modify/NoPoints
Translate Surface/1t272 DeltaX=0 DeltaY=0 DeltaZ=10e-6 CID=0 /Create/NoPoints
Rotate Surface/1t272 FromX=0 FromY=0 FromZ=0 ToX=0 ToY=1 ToZ=0 Angle=1 OffsetAngle=0 CID=0
/Modify/NoPoints
Rotate Surface/273t544 FromX=0 FromY=0 FromZ=0 ToX=0 ToY=1 ToZ=0 Angle=-1 OffsetAngle=0
CID=0 /Modify/NoPoints
Connect Surfaces Surface1List=1t272 Surface2List=273t544

```

```

!
! MSC/XL INPUT FILE : Bubble Near Rigid Wall (h*=1.374) (2/2)
!
Edit EOSJWL/1 EOSA=3.712e+11 EOSB=3.231e+09 EOSR1=4.15 EOSR2=0.95 EOSOmega=0.3 /Create
Edit DetSph/1 MID=1 DetX=0 DetY=0 DetZ=0 DetVel=6390 DetTime=0 /Create
Edit EOSPol/2 EOSA1=2.306e+09 EOSA2=8.432e+09 EOSA3=8.014e+09 EOSB0=0.4934 EOSB1=1.3937
EOSB2=0 EOSB3=Blank /Create
Edit DMat/1 DMatRHO=1630 EOID=1 /Create
Edit DMat/2 DMatRHO=1025 EOID=2 /Create
Edit PEuler1/1 TYPE=MMHydro TICEulID=1 /Create
!
Define Point X=0 Y=-0.975 Z=0 CID=0 OutputList=32
Translate Point/32 DeltaX=2.475 DeltaY=0 DeltaZ=0 CID=0 OutputList=33 /Create
Connect Points Point1List=32 Point2List=33 OutputList=21
Translate Curve/21 DeltaX=0 DeltaY=0.975 DeltaZ=0 CID=0 OutputList=22 /Points/Create
Connect Curves Curve1List=21 Curve2List=22 OutputList=545 /Points
Translate Surface/545 DeltaX=0 DeltaY=0 DeltaZ=-5e-06 CID=0 OutputList=545 /Points/Modify
Translate Surface/545 DeltaX=0 DeltaY=0 DeltaZ=1e-05 CID=0 OutputList=546 /Points/Create
Rotate Surface/545 FromX=0 FromY=0 FromZ=0 ToX=0 ToY=1 ToZ=0 Angle=1 OffsetAngle=0 CID=0
OutputList=545 /Points/Modify
Rotate Surface/546 FromX=0 FromY=0 FromZ=0 ToX=0 ToY=1 ToZ=0 Angle=-1 OffsetAngle=0 CID=0
OutputList=546 /Points/Modify
Connect Surfaces Surface1List=545 Surface2List=546 Weight1=1 Weight2=1 OutputList=273
/Points
Translate 13 Solid/130t133 DeltaX=0 DeltaY=-0.075 DeltaZ=0 CID=0 OutputList=274t349
/Points/Create
Define Point X=400 Y=0 Z=0 CID=0 OutputList=494
Translate Point/494 DeltaX=0 DeltaY=0 DeltaZ=-5e-06 CID=0 OutputList=495 /Create
Translate Point/495 DeltaX=0 DeltaY=0 DeltaZ=1e-05 CID=0 OutputList=496 /Create
Rotate Point/495 FromX=0 FromY=0 FromZ=0 ToX=0 ToY=1 ToZ=0 Angle=1 OffsetAngle=0 CID=0
OutputList=497 /Create
Rotate Point/496 FromX=0 FromY=0 FromZ=0 ToX=0 ToY=1 ToZ=0 Angle=-1 OffsetAngle=0 CID=0
OutputList=498 /Create
Translate Point/497t498 DeltaX=0 DeltaY=-1.425 DeltaZ=0 CID=0 OutputList=499t500 /Create
MeshParam Solid/1 Type=Hexa U=99 V=99 W=1 Pattern=1 PID=1 USpace=1 VSpace=1 WSpace=1
MeshParam Solid/273 Type=Hexa U=99 V=39 W=1 Pattern=1 PID=1 USpace=1 VSpace=1 WSpace=1
Select Part/1
MeshParam Solid/2t270 Type=Hexa U=1 V=1 W=1 Pattern=1 PID=1 USpace=1 VSpace=1 WSpace=1
MeshParam Solid/274t349 Type=Hexa U=1 V=1 W=1 Pattern=1 PID=1 USpace=1 VSpace=1 WSpace=1
MeshParam Solid/271t272 Type=Hexa U=34 V=200 W=1 Pattern=1 PID=1 USpace=1 VSpace=120
WSpace=1
Connect Points Point1List=38 Point2List=41 OutputList=27
Connect Points Point1List=192 Point2List=193 OutputList=28
Connect Points Point1List=497 Point2List=498 OutputList=29
Connect Points Point1List=499 Point2List=500 OutputList=30
Connect Curves Curve1List=27 Curve2List=28 OutputList=549 /Points
Connect Curves Curve1List=29 Curve2List=30 OutputList=550 /Points
Connect Surfaces Surface1List=549 Surface2List=550 Weight1=1 Weight2=1 OutputList=426
MeshParam Solid/426 Type=Hexa U=1 V=13 W=200 Pattern=1 PID=1 USpace=1 VSpace=1 WSpace=120
Check Grid/1t99999 Type=Duplicates View=1 PartList=0t1 Tolerance=5e-06 /Update/NoExtend
Equivalence Grids /Update/NoExtend/NoCollapse
Write MSCInput File="bulk.dat" Format="Bulk" /NoExec/NoCase/Bulk
!

```



```

$
$ MSC/DYTRAN RUN FILE: Bubble Near Rigid Wall (h*=1.000)
$
START
TIME = 999
CEND
$
TITLE = BUBBLE NEAR WALL
$
ENDSTEP = 9999
ENDTIME = 17.995E-3
PARAM, INISTEP, 0.2E-5
PARAM, MINSTEP, 0.2E-11
PARAM, STEPFCT, 19.0717446865
PARAM, DELCLUMP, 0.1
PARAM, RHOCUT, 1.E-4
PARAM, ROHYDRO, 1.E-4
PARAM, ROMULTI, 1.E-4
$
TYPE (MATHIS) = TIMEHIS
MATS (MATHIS) = 1
SET 1 = 1
MATOUT (MATHIS) = VOLUME, YMOM
STEPS (MATHIS) = 0, THRU, END, BY, 1
SAVE (MATHIS) = 9999
$
TYPE (DENS) = ARCHIVE
ELEMENTS (DENS) = 2
SET 2 = 1t19602
ELOUT (DENS) = DENSITY
TIMES (DENS) = .008522, .013636, .015340, .016193, .016704, .016875, .017045
$
SPC=1
$
BEGIN BULK
$
TICEUL 1
+ CYLINDER1 1 1 9. +
+ ELEM 2 2 2 1. +
CYLINDER1 0.0 -0.10 0.0 0.0 0.10 0.0 +
+ 0.1
SET1 2 1 THRU 47340
$
TICVAL 1 DENSITY 1630. SIE 4290000.
TICVAL 2 DENSITY 1025. SIE 20076.
$
INCLUDE bulk.dat
INCLUDE wall.dat
$
ENDDATA
$

```

```

$
$ MSC/DYTRAN DATA FILE "wall.dat": Bubble Near Rigid Wall (h*=1.000)
$
BEGIN BULK
$
$ THIS SECTION CONTAINS BULK DATA
$
$
GRID    100585      -.025  -.7098  -200.
GRID    100586      400.025 -.7098  -200.
GRID    100587      -.025  -.7098   200.
GRID    100588      400.025 -.7098   200.
GRID    100589      -.025  -400.71 -200.
GRID    100590      400.025 -400.71 -200.
GRID    100591      -.025  -400.71  200.
GRID    100592      400.025 -400.71  200.
$
CHEXA   47341    3      100585  100589  100590  100586  100587  100591  +
+      100592  100588
$
$ THIS SECTION CONTAINS THE LOADS, CONSTRAINTS, AND CONTROL BULK DATA ENTRIES
$
$
SPC     1      100585  123456
SPC     1      100586  123456
SPC     1      100587  123456
SPC     1      100588  123456
SPC     1      100589  123456
SPC     1      100590  123456
SPC     1      100591  123456
SPC     1      100592  123456
$
$
$ THIS SECTION CONTAINS THE DEFINED FEFACES OF ELEMENTS
$
$
CFACE   1      2      47341  1
CFACE   2      2      47341  2
CFACE   3      2      47341  3
CFACE   4      2      47341  4
CFACE   5      2      47341  5
CFACE   6      2      47341  6
$
PSOLID  3      3
$
DMATEL  3      7890.  1.95+11 .28
$
SURFACE 1      SEG      2
$
COUPLE  1      1      Inside On      On
ENDDATA

```

```

!
! MSC/XL INPUT FILE : Bubble Near Rigid Wall (h*=1.000) (1/2)
!
Edit ApplicationTable DuplicateElementTolerance=5e-06
Edit ApplicationTable DuplicateGridTolerance=5e-06
Edit ApplicationTable DuplicateFEFaceTolerance=5e-06
Edit ApplicationTable DegenerateElementTolerance=5e-06
Define Point X=0 Y=0 Z=0 CID=0 OutputList=1
Translate Point/1 DeltaX=2.475 DeltaY=0 DeltaZ=0 CID=0 OutputList=2 /Create
Connect Points Point1List=1 Point2List=2 OutputList=1
Translate Curve/1 DeltaX=0 DeltaY=2.475 DeltaZ=0 CID=0 OutputList=2 /Create/Points
Connect Curves Curve1List=1 Curve2List=2 OutputList=1 /Points
Define Point X=0.025 Y=0 Z=0 CID=0 OutputList=5
Define Point X=0.05 Y=0 Z=0 CID=0 OutputList=6
Define Point X=0.075 Y=0 Z=0 CID=0 OutputList=7
Translate Point/1,7 DeltaX=0 DeltaY=0.075 DeltaZ=0 CID=0 OutputList=8t9 /Create
Translate Point/5t6 DeltaX=0 DeltaY=0.025 DeltaZ=0 CID=0 OutputList=10t11 /Create
Connect Points Point1List=8 Point2List=1 OutputList=3
Connect Points Point1List=10 Point2List=5 OutputList=4
Connect Points Point1List=11 Point2List=6 OutputList=5
Connect Points Point1List=9 Point2List=7 OutputList=6
Connect Points Point1List=8 Point2List=9 OutputList=7
Connect Points Point1List=10 Point2List=11 OutputList=8
Connect Curves Curve1List=3 Curve2List=4 OutputList=2 /Points
Connect Curves Curve1List=4 Curve2List=5 OutputList=3 /Points
Connect Curves Curve1List=8 Curve2List=7 OutputList=4 /Points
Connect Curves Curve1List=5 Curve2List=6 OutputList=5 /Points
Translate 32 Surface/2t5 DeltaX=0.075 DeltaY=0 DeltaZ=0 CID=0 /Create/NoPoints
Translate 1 Surface/2t133 DeltaX=0 DeltaY=2.475 DeltaZ=0 CID=0 /Create/NoPoints
Rotate Surface/2t133 FromX=2.475 FromY=0 FromZ=0 ToX=2.475 ToY=0 ToZ=1 Angle=-90
OffsetAngle=0 CID=0 OutputList=434t441 /Modify/NoPoints
Translate 3 Point/4 DeltaX=0.025 DeltaY=0 DeltaZ=0 CID=0 OutputList=12t14 /Create
Translate 3 Point/4,12t14 DeltaX=0 DeltaY=0.025 DeltaZ=0 CID=0 OutputList=15t26 /Create
Connect Points Point1List=4 Point2List=23 OutputList=9
Connect Points Point1List=16 Point2List=20 OutputList=10
Connect Points Point1List=17 Point2List=21 OutputList=11
Connect Points Point1List=14 Point2List=26 OutputList=12
Connect Points Point1List=23 Point2List=26 OutputList=13
Connect Points Point1List=20 Point2List=21 OutputList=14
Connect Points Point1List=16 Point2List=17 OutputList=15
Connect Points Point1List=4 Point2List=14 OutputList=16
Connect Curves Curve1List=9 Curve2List=10 OutputList=266 /Points
Connect Curves Curve1List=13 Curve2List=14 OutputList=267 /Points
Connect Curves Curve1List=14 Curve2List=15 OutputList=268 /Points
Connect Curves Curve1List=15 Curve2List=16 OutputList=269 /Points
Connect Curves Curve1List=11 Curve2List=12 OutputList=270 /Points
Translate Point/2 DeltaX=0.075 DeltaY=0 DeltaZ=0 CID=0 OutputList=27 /Create
Translate Point/3 DeltaX=0 DeltaY=0.075 DeltaZ=0 CID=0 OutputList=28 /Create
Connect Points Point1List=28 Point2List=26 OutputList=17
Connect Points Point1List=26 Point2List=27 OutputList=18
Define Point X=0 Y=400 Z=0 CID=0 OutputList=29
Sweep 2 Point/29 FromX=0 FromY=0 FromZ=0 ToX=0 ToY=0 ToZ=1 Angle=-45 OffsetAngle=0 CID=0
OutputList=19t20 /Points
Connect Curves Curve1List=17t18 Curve2List=19t20 OutputList=271t272 /Points
Translate Surface/1t272 DeltaX=0 DeltaY=0 DeltaZ=-5e-6 CID=0 /Modify/NoPoints
Translate Surface/1t272 DeltaX=0 DeltaY=0 DeltaZ=10e-6 CID=0 /Create/NoPoints
Rotate Surface/1t272 FromX=0 FromY=0 FromZ=0 ToX=0 ToY=1 ToZ=0 Angle=1 OffsetAngle=0 CID=0
/Modify/NoPoints
Rotate Surface/273t544 FromX=0 FromY=0 FromZ=0 ToX=0 ToY=1 ToZ=0 Angle=-1 OffsetAngle=0
CID=0 /Modify/NoPoints
Connect Surfaces Surface1List=1t272 Surface2List=273t544

```

```

!
! MSC/XL INPUT FILE : Bubble Near Rigid Wall (h*=1.000) (2/2)
!
Reflect/NoOverwrite/Extend/Update/Create Solid/1t272 FromX=0 FromY=0 FromZ=0 ToX=0 ToY=1
ToZ=0 CID=0 OutputList=273t544 /NoPoints/NoFlip
MeshParam Solid/1,273 Type=Hexa U=99 V=99 W=1 Pattern=1 PID=1 USpace=1 VSpace=1 WSpace=1
ResultingGridList=1t40000 OutputList=1t19602 /Extend/Update/NoOverwrite/NoMidNode
Select Part/1
MeshParam Solid/2t270,274t542 Type=Hexa U=1 V=1 W=1 Pattern=1 PID=1 USpace=1 VSpace=1
WSpace=1 ResultingGridList=40001t44304 OutputList=19603t20140
/Extend/Update/NoOverwrite/NoMidNode
MeshParam Solid/271,272,543,544 Type=Hexa U=34 V=200 W=1 Pattern=1 PID=1 USpace=1
VSpace=120 WSpace=1 ResultingGridList=44305t100584 OutputList=20141t47340
/Extend/Update/NoOverwrite/NoMidNode
Check Grid/1t100584 Type=Duplicates View=1 PartList=0t1 Tolerance=5e-06 /Update/NoExtend
Equivalence Grids /Update/NoExtend/NoCollapse
Check Grid/1t100583 Type=Duplicates View=1 PartList=0t1 Tolerance=5e-06 /Update/NoExtend
Equivalence Grids /Update/NoExtend/NoCollapse
!
Edit EOSJWL/1 EOSA=3.712e+11 EOSB=3.231e+09 EOSR1=4.15 EOSR2=0.95 EOSOmega=0.3 /Create
Edit DetSph/1 MID=1 DetX=0 DetY=0 DetZ=0 DetVel=6390 DetTime=0 /Create
Edit EOSPol/2 EOSA1=2.306e+09 EOSA2=8.432e+09 EOSA3=8.014e+09 EOSB0=0.4934 EOSB1=1.3937
EOSB2=0 EOSB3=Blank /Create
Edit DMat/1 DMatRHO=1630 EOID=1 /Create
Edit DMat/2 DMatRHO=1025 EOID=2 /Create
Edit PEuler1/1 TYPE=MMHydro TICEulID=1 /Create
Write MSCInput File="bulk.dat" Format="Bulk" /NoExec/NoCase/Bulk
!

```

```

c
c
c
c
VOLUME TO RADIUS CONVERSION PROGRAM : Bubble Near Rigid Wall
                                         (axisymmetric 1/2 model)

program vol2rad
open(14,file='th_volume_g11.ext',status='old')
open(15,file='r_vs_t.ext',status='new')
do 100 i=1,9
  read(14,*)
100  continue
  write(*,*) '# of lines in volume time history file?'
  read(*,*) n
  n = n-9
  do 200 i=1,n
    read(14,*) t,v
    t = t * 1000
    r = ((0.5*85.94367*v)**(1./3.))*100
    write(15,*) t,r
200  continue
  close(14)
  close(15)
end

```

```

c      C.M. DISPLACEMENT CALCULATION PROGRAM: Bubble Near Rigid Wall
c
c      program ydisp
c      implicit double precision(a-h,o-z)
c      open(14,file='th_ymom_gll.ext',status='old')
c      open(15,file='ydisp_vs_t.ext',status='new')
c      do 100 i=1,9
c         read(14,*)
100      continue
c         write(*,*) '# of lines in momentum time history file?'
c         read(*,*) n
c         n = n-9
c         w = 10.2415920507/180.0
c         sum = 0.0
c         read(14,*) t1,ymom1
c         write(15,*) sum,sum
c         do 200 i=1,n-1
c            read(14,*) t2,ymom2
c            sum = sum+(t2-t1)*0.5*(ymom2+ymom1)
c            t = t1+0.5*(t2-t1)
c            y = sum/w
c            write(15,*) t*1000,y*100
c            t1 = t2
c            ymom1 = ymom2
200      continue
c         close(14)
c         close(15)
c      end

```

LIST OF REFERENCES

1. Jones, R. A. and Shin, Y. S., *The Response and Failure Mechanisms of Circular Metal and Composite Plates Subjected to Underwater Shock Loading*, Report NPS-69-90-02, Naval Postgraduate School, Monterey, CA, February 1992.
2. Fox, P. K., Kwon, Y. W. and Shin, Y. S., *Nonlinear Response of Cylindrical Shells to Underwater Explosion: Testing and Numerical Prediction Using VEC/DYNA3D*, Report NPS-ME-92-002, Naval Postgraduate School, Monterey, CA, March 1992.
3. Nelson, K. W., Shin, Y. S. and Kwon, Y. W., "Failure of Aluminum Cylinder from Underwater Shock Effects," *63rd Shock and Vibration Symposium*, pp. 83-95, Las Crusas, NM, October 1992.
4. Kwon, Y. W., Bergersen, J. K. and Shin, Y. S., "Effect of Surface Coatings on Cylinders Subjected to Underwater Shock," *Shock and Vibration*, Vol. 1, No. 3, pp. 253-265, 1994.
5. Chisum, J. E., *Response Predictions for Double Hull Cylinders Subjected to Underwater Shock Loading*, Masters Thesis, Naval Postgraduate School, Monterey, CA, 1992.
6. Chisum, J. E. and Shin, Y. S., "Coupled Lagrangian-Eulerian and Multimaterial Eulerian Analysis in Underwater Shock Research," *Structures Under Extreme Loading Conditions*, PVP-Vol. 299, The American Society of Mechanical Engineers, New York, 1995.
7. *MSC/DYTRAN Users Manual: MSC/DYTRAN Version 2.2*, The MacNeal-Schwendler Corporation, Los Angeles, 1994.
8. *MSC/DYNA*, The MacNeal-Schwendler Corporation, Los Angeles.
9. *MSC/Pisces-2DELK*, The MacNeal-Schwendler Corporation, Los Angeles.

10. Huang, H., "Transient Interaction of Plane Acoustic Waves With a Spherical Elastic Shell," *Journal of the Acoustical Society of America*, Vol. 45, pp. 661-670, 1969.
11. Huang, H., "An Exact Analysis of the Transient Interaction of Acoustic Plane Waves With a Cylindrical Elastic Shell," *Journal of Applied Mechanics*, Vol. 37, pp. 1091-1099, 1970.
12. Stillman, D. W. and Hallquist, J. O., *LS-INGRID: A Pre-Processor and Three-Dimensional Mesh Generator for the Programs LS-DYNA3D, LS-NIKE3D, and TOPAZ-3D, Version 3.0*, Livermore Software Technology Corporation Report 1019, June 1991.
13. *MSC/XL User's Manual*, Version 3B, The MacNeal-Schwendler Corporation, Los Angeles.
14. Huang, H., Private Communication, February 24, 1995.
15. Cole, R. H., *Underwater Explosions*, Princeton University Press, Princeton, NJ, 1948.
16. Swift, E. and Decius, J. C., "Measurement of Bubble Phenomena III: Radius and Period Studies," *Underwater Explosion Research: A Compendium of British and American Reports*, Vol. 2, pp. 553-599, Office of Naval Research, Department of the Navy, Washington, D.C., 1950.
17. Dobratz, B. M., *LLNL Explosives Handbook*, UCRL-52997, pp. 8-21 - 8-23, Lawrence Livermore National Laboratory, Livermore, CA, 1981.
18. *MATHCAD 5.0 User's Guide*, Mathsoft Inc., Cambridge, MA, 1994.
19. Herring, C., "Theory of the Pulsations of the Gas Bubble Produced by an Underwater Explosion," NDRC Report C4-sr20-010, 1941.
20. Hicks, A. N., "Effect of Bubble Migration on Explosion-Induced Whipping of Ships," NSRDC Report 3301, 1971.

21. Herring, C., "Theory of the Pulsations of the Gas Bubble Produced by an Underwater Explosion," *Underwater Explosion Research: A Compendium of British and American Reports*, Vol. 2, pp. 35-130, Office of Naval Research, Department of the Navy, Washington, D.C., 1950.
22. Campbell, D. C., "Motion of a Pulsating Gas Globe Under Water - A Photographic Study," TMB Report 512, Bureau of Ships, United States Navy, Washington, D. C., 1943.
23. Bryant, A. R., "Photographic Measurements of the Size, Shape and Movement of the Bubble Produced by 1-OZ. Charges of Polar Ammon Gelignite Detonated Underwater at a Depth of 3 Feet," *Underwater Explosion Research: A Compendium of British and American Reports*, Vol. 2, pp. 505-523, Office of Naval Research, Department of the Navy, Washington, D.C., 1950.
24. Gurtman, G. A., Kirsch, J. W. and Hastings, C. R., "Analytical Equation of State for Water Compressed to 300 Kbar," *Journal of Applied Physics*, Vol. 42, pp. 851-857, 1971.
25. Hallquist, J. O., and Stillman, D. W., *LS-DYNA3D Course Notes*, Livermore Software Technology Corporation Report 1009, Sec. 12-6, 1991.
26. Steinberg, D. J., *Spherical Explosions and the Equation of State of Water*, Report UCID-20974, Lawrence Livermore National Laboratory, Livermore, CA, 1987.
27. Miller, W. E., *Simulation of the Underwater Nuclear Explosion and its Effects*, Master's Thesis, Naval Postgraduate School, Monterey, CA, June 1992.

INITIAL DISTRIBUTION LIST

		No. Copies
1.	Defense Technical Information Center Cameron Station Alexandria, Virginia 22304-6145	2
2.	Library, Code 052 Naval Postgraduate School Monterey, California 93943-5002	2
3.	Professor Young S. Shin, Code ME/Sg Department of Mechanical Engineering Naval Postgraduate School Monterey, California 93943	5
4.	LCDR James E. Chisum, USN Department of Mechanical Engineering Naval Postgraduate School Monterey, California 93943	5
5.	Defense Nuclear Agency 6801 Telegraph Road Alexandria, Virginia 22310-3398	
	Douglas Bruder	2
	M. Giltrud	1
	Kent Goering	1
6.	Carderock Division, Naval Surface Warfare Center Indian Head Division, White Oak Detachment (Explosion Damage Division, Code 460) Silver Spring, MD 20903-5640	
	Hanson Huang Code 460	1
	Hans Mair Code 460	1

7. Carderock Division, Naval Surface Warfare Center
9500 MacArthur Blvd.
Bethesda, Maryland 20084-5000

Ib. S. Hansen	Code 67	1
Benjamin Whang	Code 671	1
Charles Milligan	Code 6711	1
Stephen Zilliacus	Code 6711	1
Frances F. Rasmussen	Code 6712	1
Young G. Sohn	Code 6712	1
William R. Conley	Code 672	1
David C. Bond	Code 6721	1
Mark W. Hoffman	Code 6721	1
Cuong Q. Nguyen	Code 6721	1
George V. Waldo	Code 6721	1
Harry P. Gray	Code 673	1
Stephen Poy	Code 6733	1
Erik A. Rasmussen	Code 1720.4	1
Gordon C. Everstine	Code 204	1
J. Corrado		1
B. Douglas		1

8. Carderock Division, Naval Surface Warfare Center
Underwater Explosion Research Division (UERD)
Norfolk Naval Shipyard
Portsmouth, Virginia 23709-5000

Fred Costanzo	Code 177.1	1
Michael Riley	Code 177.1	1

9. Naval Sea Systems Command
2531 Jefferson Davis Highway
Arlington, VA 22242-5160

Peter Czapiewski	Code 03D53	1
Victor Dirienzo	Code 06K213	1
Dan Dozier	Code PEO-SUB-R	1
Dana Johansen	Code 03P	1
Mark McLean	Code 06K213	1
Philip Wu	Code 03P	1

15. A&T Engineering Tech. Center
240 Oral School Road, Suite 105
Mystic, CT 06355-1208

T. Littlewood
V. Godino

1
1

16. NKF Engineering
4200 Wilson Blvd., Suite 900
Arlington, VA 22203-1800

George Amir
Jerry Hill

1
1

17. Weidlinger Associates
333 Seventh Ave.
New York, NY 10001

R. Atkatsh
M. Baron
R. Daddazio
I. Sandler
R. Smilowitz

1
1
1
1
1

18. General Dynamics
Electric Boat Division
Dept. 457
Eastern Point Road
Groton, CT 06340

Austin Alvarez
Steve Gordon

1
1

19. J. Baum
SAIC
1710 Goodridge Drive
McLean, VA 22102

1

20. Peter Mendoza
The MacNeal-Schwendler Corporation
815 Colorado Blvd
Los Angeles, CA 90041-1777

3